TECHNISCHE MECHANIK

since 1980

Editor:
Magdeburger Verein für Technische Mechanik e.V.
und Otto-von-Guericke-Universität Magdeburg

Volume 39 Issue 2 (2019)

ISSN 0232-3869 (print)
ISSN 2199-9244 (online)

TECHNISCHE MECHANIK

Wissenschaftliche Zeitschrift für Grundlagen und Anwendungen der Technischen Mechanik
Scientific Journal for Fundamentals and Applications of Engineering Mechanics

The journal **Technische Mechanik** publishes refereed original articles on Engineering Mechanics in its broadest sense. It is intended to provide a forum for a rapid transfer of research results to industry and science. In that sense contributions are encouraged which demonstrate the practical application of new results and scientific findings.

In der **Technischen Mechanik** werden begutachtete Beiträge aus allen Gebieten der Mechanik publiziert. Ein Hauptanliegen besteht in der raschen Verfügbarmachung von Forschungsergebnissen für Industrie und Wissenschaft. In diesem Sinne werden vor allem auch solche Beiträge bevorzugt, die neben neuen Ergebnissen und Erkenntnissen auch deren praktische Anwendung beinhalten.

Redaktion/Editorial Office
W. Lenz (Chefredakteur)

Bezugsmöglichkeiten

Die Zeitschrift Technische Mechanik erscheint ab dem Jahr 2019 ausschließlich in elektronischer Form. Die Zeitschrift Technische Mechanik ist ein Open Access Journal. Alle Artikel können kostenfrei von unserer Webseite herunter geladen werden.
Für Veröffentlichungen fallen für die Autoren keine Kosten an. Alle Artikel werden einem standardmäßigen Begutachtungsprozess unterzogen.

The journal Technische Mechanik is distributed only electronically with the beginning of 2019. The journal Technische Mechanik is an Open Access journal. All papers are available free of charge for download. Publishing of papers is free of any costs for the authors. Each submitted paper runs through a standard peer review process.

Anschrift der Redaktion/Editorial Office
Redaktion Technische Mechanik
Institut für Mechanik
Otto-von-Guericke-Universität
Postfach 4120
D-39016 Magdeburg
Telefon: +49 391 67–52 459
Telefax: +49 391 67–12 439/–12 863
e-mail: Technische.Mechanik@ovgu.de
http://www.ovgu.de/techmech/

Herausgeber/Publisher
Magdeburger Verein für Technische Mechanik e.V.
und Otto-von-Guericke-Universität Magdeburg
Geschäftsführender Herausgeber: D. Juhre
Stellvertr. geschäftsführender Herausgeber: E. Woschke

Inhalt / Contents

ISSN 0232-3869 (print)
ISSN 2199-9244 (online)

DOI: 10.24352/UB.OVGU-2019-016 TECHNISCHE MECHANIK, 39, 2, (2019), 175 - 185
submitted: October 19, 2018

Pulsed Laser Heating of a Thermoelastic Medium with Two-temperature under Three-phase-lag Model

M. I. A. Othman, N. T. Mansour

In this paper, the problem of the generalized thermoelastic medium for three different theories under the effect of a laser pulse and two-temperature is investigated. The Lord–Shulman (L-S), Green-Naghdi of type III (G-N III) and three-phase-lag (3PHL) theories are discussed with two-temperature. The normal mode analysis is used to obtain the analytical expressions of the displacement components, force stress, thermodynamic temperature and conductive temperature. The numerical results are given and presented graphically and the thermal force was applied. Comparisons are made with the results predicted by (3PHL), (G-N III) and (L-S) in the presence and absence of two-temperature. The boundary plane surface is heated by a non-Gaussian laser beam.

Nomenclature

σ_{ij} Components of stress tensor	T_0 Reference temperature $\left\|(T-T_0)/T_0\right\|<1$
e_{ij} Components of strain tensor	ϕ Conductive temperature
$e=e_{kk}$ Cubic dilatation	λ,μ Lame' constants
u,v Displacement vectors	δ_{ij} Kronecker's delta
T Thermodynamic temperature	c_e Specific heat at constant strain
α_t Coefficient of linear thermal expansion	ρ Density
K Coefficient of thermal conductivity	K^* Material characteristic of the theory
τ_T Phase lag of temperature gradient	τ_q Phase lag of heat flux
τ_v Phase lag of thermal displacement gradient	

1 Introduction

The generalized theory of thermoelasticity is one of the modified versions of classical uncoupled and coupled theory of thermoelasticity and has been developed in order to remove the paradox of physical impossible phenomena of infinite velocity of thermal signals in the classical coupled thermoelasticity. The thermoelasticity with finite wave speeds was investigated by (Ignaczak and Ostoja-Starzewski, 2010). Five generalizations of the coupled theory of thermoelasticity were explained by (Hetnarski and Ignaczak, 1999). The first generalization formulates the generalized thermoelasticity theory involving one thermal relaxation time by (Lord and Shulman, 1967). The temperature rate-dependent thermoelasticity is developed where includes two thermal relaxation times and does not violate the second law of thermodynamics of heat conduction, when the body under consideration has a center of symmetry by (Green and Lindsay, 1972). The influence of magnetic field on generalized piezo-thermoelastic rotating medium with two relaxation times was studied by (Othman et al., 2017). Hetnarski and Ignaczak (1996) were reviewed and presentation of generalized theories of thermoelasticity. The wave propagation in anisotropic solids in generalized theories of thermoelasticity was investigated by many authors (Marin, et al. 2014; Sharma and Marin, 2013; Sharma and Singh, 1985; Othman, et al. 2018; Tzou, 1995, Sangwan, et al. 2018). The third generalization of the coupled theory of thermoelasticity is developed by Hetnarski and Ignaczak and is known as low-temperature thermoelasticity. The fourth generalization to the coupled theory of thermoelasticity introduced by Green and Naghdi and this theory is concerned with the thermoelasticity theory without energy dissipation, referred to as (G-N II) in which the classical Fourier law is replaced by a heat flux rate-temperature gradient relation and Green and Naghdi with energy dissipation referred to as (G-N III). The fifth generalization of the coupled theory of thermo-elasticity is referred to the dual-phase-lag thermoelasticity as in (Othman and Abd-Elaziz, 2015; Othman and Atwa, 2013). Recently the (3PHL),

heat conduction equation in which the Fourier law of heat conduction is replaced by an approximation to a modification of the Fourier law with the introduction of three different phases-lags for the heat flux vector, the temperature gradient and the thermal displacement gradient by (Roy Choudhuri, 2007). Quintanilla and Racke (2008) discussed the stability of the (3PHL), the heat conduction equation. Subsequently, this theory has employed of thermoelasticity with (3PHL) to discuss a problem of generalized magneto-thermoelastic half-space with diffusion under initial stress by Othman and Eraki (2017).

The two-temperature theory of thermoelasticity was introduced by many works (Chen and Gurtin, 1968; Khamis, et al. 2017), in which the classical Clausius-Duhem inequality was replaced by another one depending on two-temperatures; the conductive temperature and the thermo-dynamic temperature, the first is due to the thermal processes, and the second is due to the mechanical processes inherent between the particles and the layers of elastic material, this theory was also investigated by Ieşan (1970). The two-temperature model was underrated and unnoticed for many years thereafter. Only in the last decade has the theory been noticed, developed in many works, and find its applications, mainly in the problems in which the discontinuities of stresses have no physical interpretations. Among Quintanilla (2004) who contributes to develop this theory, it has studied existence, structural stability, convergence and spatial behavior of this theory, it was introduced the generalized Fourier law to the field equations of the two-temperature theory of thermoelasticity and proved the uniqueness of the solution for homogeneous isotropic material by Youssef (2006), the propagation of harmonic plane waves studied by Puri and Jordan (2006). Recently, authors have studied the uniqueness and growth solutions by Magaña and Quintanilla (2009), for the model proposed by (Youssef, 2006).

The so-called ultra-short lasers are those with pulse duration ranging from nano-seconds to femtoseconds. In the case of ultra-short-pulsed laser heating, the high-intensity energy flux and ultra-short duration laser beam have introduced situations where very large thermal gradients or an ultra-high heating rate may exist on the boundaries by Sun et al. (2008). Researchers have proposed several models to describe the mechanism of heat conduction during short-pulse laser heating. It has been found that usually the microscopic two-step models, that is, parabolic and hyperbolic are useful for modification material as thin films. When a metal film is heated by a laser pulse, a thermoelastic wave is generated due to thermal expansion near the surface. The effect of magnetic field on a rotating thermoelastic medium with voids under thermal loading due to laser pulse with energy dissipation has investigated by Othman et al. (2018).

In this paper, the generalized thermoelastic theory is applied to study the effect of two-temperature on thermoelastic medium due to laser pulse using three-phase-lag model. The (L-S), (G-N III) and (3PHL) theories are discussed with two-temperatures. The normal mode analysis is used to obtain the exact solution of the physical quantities. The effect of laser pulse as well as two-temperature are discussed numerically and illustrated graphically.

2 Basic Equations

The governing equations for an isotropic, homogeneous elastic solid with the generalized thermoelastic medium in the absence of body forces using (3PHL) model are:

The constitutive equations

$$\sigma_{ij} = 2\mu e_{ij} + \delta_{ij}[\lambda e - \gamma(T - T_0)], \tag{1}$$

$$e_{ij} = \frac{1}{2}(u_{i,j} + u_{j,i}). \tag{2}$$

The equation of motion

$$\rho \ddot{u}_i = 2\mu e_{ij,j} + [\lambda e_{,j} - \gamma T_{,j}]\delta_{ij}. \tag{3}$$

The equation of heat conduction

$$K^* \nabla^2 \phi + \tau_v^* \nabla^2 \dot{\phi} + K\tau_t \nabla^2 \ddot{\phi} = (1 + \tau_q \frac{\partial}{\partial t} + \frac{\tau_q^2}{2!}\frac{\partial^2}{\partial t^2})[\rho c_e \ddot{T} + \gamma T_0 \ddot{e} - \rho \dot{Q}]. \tag{4}$$

Where, $\tau_v^* = (K + K^* \tau_v)$, $\gamma = (3\lambda + 2\mu)\alpha_t$.

The equation of two-temperatures

$$T = (1 - b\nabla^2)\phi. \tag{5}$$

Where, the list of symbols is given in the nomenclature.

The plate surface is illuminated by laser pulse given by the heat input

$$Q = I_0 \frac{t}{t_0^2}\exp(\frac{-t}{t_0}).\frac{1}{2\pi r^2}\exp(\frac{-x^2}{r^2})\,\gamma e^{-\gamma y}. \tag{6}$$

where, I_0 is the energy absorbed, t_0 is the pulse rise time, r is the beam radius, y is a function of the depth of the heat deposition due to the laser pulse is assumed to decay exponentially within the solid.

3 Formulation of the Problem

We consider an isotropic, homogeneous elastic solid with the generalized thermo-elastic medium. All quantities are considered are functions of the time variable t and of the coordinates x and y. We consider the normal source acting on the plane surface of generalized thermoelastic half-space under the effect of two-temperatures, we assume $\boldsymbol{u} = (u, v, 0)$.

The equation of motion in the absence of body force

$$\rho\ddot{u} = \mu\nabla^2 u + (\lambda+\mu)e_{,x} - \gamma(1-b\nabla^2)\phi_{,x}, \tag{7}$$

$$\rho\ddot{v} = \mu\nabla^2 v + (\lambda+\mu)e_{,y} - \gamma(1-b\nabla^2)\phi_{,y}, \tag{8}$$

$$K^*\nabla^2\phi + \tau_v^*\nabla^2\frac{\partial\phi}{\partial t} + K\tau_t\nabla^2\frac{\partial^2\phi}{\partial t^2} = (1+\tau_q\frac{\partial}{\partial t}+\frac{\tau_q^2}{2!}\frac{\partial^2}{\partial t^2})[(\rho c_e(1-b\nabla^2)\ddot{\phi} + \gamma T_0\frac{\partial^2 e}{\partial t^2} - \rho\dot{Q}]. \tag{9}$$

To facilitate the solution, the following dimensions quantities are introduced

$$(x', y') = c\eta(x, y), \qquad (u', v') = c\eta(u, v), \qquad \{t', \tau', \tau_T', \tau_q', \tau_v'\} = c^2\eta\{t, \tau, \tau_T, \tau_q, \tau_v\},$$

$$(T', \phi') = \frac{\gamma}{(\lambda+2\mu)}(T, \phi), \quad \sigma_{ij}' = \frac{\sigma_{ij}}{(\lambda+2\mu)}, \quad Q' = \frac{\gamma}{c_e\eta c_1^2(\lambda+2\mu)}Q, \quad \eta = \rho c_e / K,$$

$$\nabla^2 = \frac{\partial^2}{\partial x^2}+\frac{\partial^2}{\partial y^2}+\frac{\partial^2}{\partial z^2} \text{ and } c^2 = (\lambda+2\mu)/\rho. \tag{10}$$

The displacement components $u(x, y, t)$ and $v(x, y, t)$ may be written in terms of potential functions $q(x, y, t)$ and $\Psi(x, y, t)$ as

$$u = q_{,x} - \Psi_{,y}, \qquad v = q_{,y} + \Psi_{,x}. \tag{11}$$

Using Eqs. (10) and (11), in the Eqs. (7)-(9) become in the following form (after suppressing the primes)

$$\nabla^2 q - (1-b\nabla^2)\phi = \ddot{q}, \tag{12}$$

$$\nabla^2\Psi = \beta^2\frac{\partial^2}{\partial t^2}\Psi, \tag{13}$$

$$\varepsilon_1\nabla^2\phi + \varepsilon_2\nabla^2\dot{\phi} + \tau_t\nabla^2\ddot{\phi} = (1+\tau_q\frac{\partial}{\partial t}+\frac{\tau_q^2}{2!}\frac{\partial^2}{\partial t^2})[(1-b^*\nabla^2)\ddot{\phi} + \varepsilon_3\ddot{q} - \dot{Q}]. \tag{14}$$

Where $\beta^2 = \frac{\lambda+2\mu}{\mu}$, $\varepsilon_1 = \frac{k^*}{\rho c_e c_0^2}$, $\varepsilon_2 = 1+\varepsilon_1\tau_v$, $\varepsilon_3 = \frac{\gamma^2 T_0}{\rho c_e(\lambda+2\mu)}$, $b^* = b\,c^2\eta^2$.

Also, by using Eqs. (1) and (10)-(11), we obtain the components of stress in the form

$$\sigma_{xx} = u_{,x} + (1-\frac{2}{\beta^2})v_{,y} - T, \tag{15}$$

$$\sigma_{yy} = (1-\frac{2}{\beta^2})u_{,x} + v_{,y} - T, \tag{16}$$

$$\sigma_{xy} = \frac{1}{\beta^2}(u_{,y} + v_{,x}). \tag{17}$$

The solution of the considered physical variables can be decomposed in terms of normal modes in the form

$$[u, v, e, \phi, \Psi, q, T](x, y, t) = [u^*, v^*, e^*, \phi^*, \Psi^*, q^*, T^*](y)\exp i(\omega t + kx), \tag{18}$$

Where ω is the complex time constant (frequency), i is the imaginary unit, k is the wave number in the $x-$direction and $[u^*, v^*, e^*, \phi^*, \Psi^*, q^*, T^*]$ are the amplitudes of the functions.

Using equation (18), equations (12)-(14) become respectively

$$(\mathrm{D}^2 - A_1)q^* + (b^*\mathrm{D}^2 - A_2)\phi^* = 0, \tag{19}$$

$$(\mathrm{D}^2 - A_3)\Psi^* = 0, \tag{20}$$

$$(\mathrm{A}_4\mathrm{D}^2 - A_5)\phi^* + (A_6\mathrm{D}^2 - A_7)q^* = -Q_0 f(x,t)e^{-\gamma y}. \tag{21}$$

Where $A_1 = k^2 - \omega^2, \quad \mathrm{A}_2 = 1 + b^* k^2, \quad A_3 = k^2 - \beta^2\omega^2,$

$$A_4 = \varepsilon_1 + i\varepsilon_2\omega - \tau_t\omega^2 - b^*\omega^2[1 + i\tau_q\omega - \frac{\tau_q^2}{2!}\omega^2],$$

$$A_5 = (\varepsilon_1 k^2 + i\varepsilon_2\omega k^2 - \tau_t\omega^2 k^2) + (\omega^2 + k^2\omega^2\,\mathrm{b}^*)[1 + i\tau_q\omega - \frac{\tau_q^2}{2!}\omega^2],$$

$$A_6 = \varepsilon_3\omega^2[1 + \mathrm{i}\tau_q\omega - \frac{\tau_q^2}{2!}\omega^2], \qquad A_7 = \varepsilon_3\omega^2 k^2[1 + i\tau_q\omega - \frac{\tau_q^2}{2!}\omega^2], \qquad Q_0 = \frac{I_0\gamma}{2\pi r^2 t_0^2},$$

$$f(x,t) = [(1 - \frac{t}{t_0}) + \tau_q(\frac{-2}{t_0} + \frac{t}{t_0^2}) + \frac{\tau_q^2}{2}(\frac{3}{t_0^2} - \frac{t}{t_0^3})]\exp(-\frac{x^2}{r^2} - \frac{t}{t_0} - i\omega t - ikx), \quad \mathrm{D} = \frac{\mathrm{d}}{\mathrm{d}y}.$$

Eliminating ϕ^* and q^* among Eqs. (19) and (21) respectively, we obtain the following differential equations

$$\{\mathrm{D}^4 - A\mathrm{D}^2 + B\}q^* = -Q_0 N_1 f(x,t)e^{-\gamma y}, \tag{22}$$

$$\{\mathrm{D}^4 - A\mathrm{D}^2 + B\}\phi^* = -Q_0 N_2 f(x,t)e^{-\gamma y}, \tag{23}$$

where, $A = \dfrac{A_2A_6 + A_7b^* - A_5 - A_1A_4}{-A_4 + A_6b^*}, \quad B = \dfrac{A_2A_7 - A_5A_1}{-A_4 + A_6b^*}, \quad N_1 = b^*\gamma^2 - A_2,$

$N_2 = \gamma^2 - A_1, \qquad \mathrm{i} = 1, 2.$

Equation (22) and (23) can be factored as

$$(\mathrm{D}^2 - k_1^2)(\mathrm{D}^2 - k_2^2)q^* = -N_1 Q_0 f(x,t)e^{-\gamma y}, \tag{24}$$

$$(\mathrm{D}^2 - k_1^2)(\mathrm{D}^2 - k_2^2)\phi^* = -N_2 Q_0 f(x,t)e^{-\gamma y}, \tag{25}$$

where $k_n^2\,(n = 1, 2)$ are the roots of the characteristic equation of Eqs. (24) and (25).

The general solutions of Eqs. (20), (22) and (23) are given by:

$$\Psi = M_3 e^{(-k_n y + i\omega t + ikx)}. \tag{26}$$

$$q = \sum_{n=1}^{2} M_n e^{(-k_n y + i\omega t + ikx)} - \ell_1 N_1 Q_0 f_1(x,t)e^{-\gamma y}, \tag{27}$$

$$\phi = \sum_{n=1}^{2} H_{1n} M_n e^{(-k_n y + i\omega t + ikx)} - \ell_1 N_2 Q_0 f_1(x,t)e^{-\gamma y}, \tag{28}$$

From Eq. (5) and (28) we obtain

$$T = \sum_{n=1}^{2} H_{2n} M_n e^{(-k_n y + i\omega t + ikx)} - \ell_1 N_2 Q_0 J(x) f_1(x,t)e^{-\gamma y}, \tag{29}$$

where, $M_n\,(n = 1, 2)$ are some constants,

$$f_1(x,t) = [(1 - \frac{t}{t_0}) + \tau_q(\frac{-2}{t_0} + \frac{t}{t_0^2}) + \frac{\tau_q^2}{2}(\frac{3}{t_0^2} - \frac{t}{t_0^3})]\exp(-\frac{x^2}{r^2} - \frac{t}{t_0}), \; \ell_1 = \frac{1}{\gamma^4 - A\gamma^2 + B},$$

$$H_{1n} = \frac{-(k_n^2 - A_1)}{b^* k_n^2 - A_2}, \qquad H_{2n} = H_{1n}[1 - b^*(k_n^2 - k^2)], \qquad J(x) = 1 - b^*\left(\frac{-2}{r^2}\left[1 - \frac{2x}{r^2}\right] + \gamma^2\right).$$

To obtain the components of the displacement vector, substituting from Eqs. (26) and (27) in Eq. (11), then

$$u = \sum_{n=1}^{2} ikM_n e^{(-k_n y + i\omega t + ikx)} + \frac{2x\ell_1}{r^2} N_1 Q_0 f_1(x,t) e^{-\gamma y} - mM_3 e^{(-m y + i\omega t + ikx)}, \tag{30}$$

$$v = \sum_{n=1}^{2} -k_n M_n e^{(-k_n y + i\omega t + ikx)} + \ell_1 N_1 \gamma Q_0 f_1(x,t) e^{-\gamma y} + ikM_3 e^{(-m y + i\omega t + ikx)}, \tag{31}$$

Substituting from Eqs. (29), (30) and (31) in Eqs. (15)-(17), we obtain the stress components as follows:

$$\sigma_{xx} = H_3 \ell_1 Q_0 f_1(x,t) e^{-\gamma y} - H_4 M_3 e^{(-m y + i\omega t + ikx)} - \sum_{n=1}^{2} H_{5n} M_n e^{(-k_n y + i\omega t + ikx)}, \tag{32}$$

$$\sigma_{yy} = H_6 \ell_1 Q_0 f_1(x,t) e^{-\gamma y} - H_7 M_3 e^{(-m y + i\omega t + ikx)} + \sum_{n=1}^{2} H_{8n} M_n e^{(-k_n y + i\omega t + ikx)}, \tag{33}$$

$$\sigma_{xy} = H_9 \ell_1 N_1 Q_0 f_1(x,t) e^{-\gamma y} + H_{10} M_3 e^{(-m y + i\omega t + ikx)} - \sum_{n=1}^{2} H_{11n} M_n e^{(-k_n y + i\omega t + ikx)}. \tag{34}$$

Where, $H_3 = \frac{2N_1}{r^2} - \frac{4x^2 N_1}{r^4} - N_1\gamma^2 + \frac{2N_1\gamma^2}{\beta^2} + N_2 J(x)$, $H_4 = m + ikm - \frac{2ikm}{\beta^2}$,

$H_{5n} = \frac{2k_n^2}{\beta^2} + H_{2n}$, $H_6 = -N_1\gamma^2 + \frac{2N_1}{r^2} - \frac{4x^2 N_1}{r^4} - \frac{2N_1}{\beta^2}\left(\frac{2}{r^2} - \frac{4x^2}{r^4}\right) + N_2 J(x)$,

$H_7 = m + ikm + \frac{2m}{\beta^2}$, $H_{8n} = \frac{2k^2}{\beta^2} - H_{2n}$, $H_9 = \frac{-4x\gamma}{r^2\beta^2}$, $H_{10} = \frac{m^2 - k^2}{\beta^2}$, $H_{11n} = \frac{2ikk_n}{\beta^2}$.

4 The Boundary Conditions

In order to determine the parameters $M_n\ (n = 1,2)$, we need to consider the boundary conditions at $y = 0$ as follows:

$$\sigma_{xx}(x,0,t) = -P(x,t) = -P^* e^{i(\omega t + kx)}, \ \sigma_{xy}(x,0,t) = 0, \ T(x,0,t) = 0. \tag{35}$$

Using the expressions of the variables considered into the above boundary conditions, we can obtain the following equations satisfied by the parameters:

$$\sum_{n=1}^{2} H_{5n} M_n + H_4 M_3 = P^*, \tag{36}$$

$$\sum_{n=1}^{2} -H_{11n} M_n + H_{10} M_3 = 0, \tag{37}$$

$$\sum_{n=1}^{2} H_{2n} M_n = 0, \tag{38}$$

Solving Eqs. (36)-(38), the constants $M_n\ (n = 1,2)$ are defined as follows:

$$M_1 = \frac{\Delta_1}{\Delta}, \qquad M_2 = \frac{\Delta_2}{\Delta}, \qquad M_3 = \frac{\Delta_3}{\Delta}. \tag{39}$$

Where, $\Delta = H_{10}(H_{52}H_{21} - H_{51}H_{22}) + H_4(-H_{111}H_{22} - H_{112}H_{21})$,

$\Delta_1 = -H_{10}H_{22}P^*$, $\Delta_2 = P^*(H_{10}H_{21})$, $\Delta_3 = P^*(H_{112}H_{21} - H_{111}H_{22})$.

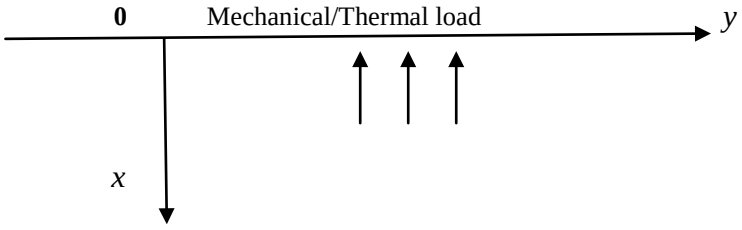

Figure 1. Geometry of the problem.

5 Numerical Results

To study the effect of time and two-temperatures, we now present some numerical results. For this purpose, copper is taken as the thermoelastic material for which we take the following values of the different physical constants as in Othman and Eraki (2017).

$\lambda = 7.7\cdot10^{10}\, N\cdot m^{-2},\ \mu = 3.86\cdot10^{10}\, kg\cdot m^{-1}\cdot s^{-2},\ K = 300\ w\cdot m^{-1}\cdot K^{-1},\ \ \alpha_t = 1.78\cdot10^{-5} K^{-1},$

$\rho = 8954 kg\cdot m^{-3},\ \ c_e = 383.1\ J\cdot kg^{-1}K^{-1},\ \ T_0 = 293K,\ \ k = 1.5,\ \omega = -0.7,\ \ x = 0.1,$

$K^* = 2.97\cdot10^{13},\ \ \ p^* = -1,\ \ \ \tau_v = 0.3,\ \ \tau_t = 0.5,\ \ \ \tau_q = 1.5.$

The laser pulse parameters are $I_0 = 10^5,\ \ r = 10^{-5} m,\ \ \gamma = 2\cdot10^{-4} m^{-1},\ \ t_0 = 0.1\cdot10^{-7}$ s.

The numerical technique, outlined above, was used for the distribution of the real part of the temperature T, the displacement components u, v and the stress components σ_{xx}, σ_{yy}, σ_{xy} for the problem. All the variables are taken in non-dimensional form the result. Figs. 2-7 depict the variety of the displacement components u, v, the temperature T, the stress components σ_{xx}, σ_{yy} and σ_{xy} in the absence and the presence of two-temperature (i.e. $b = 0, 0.1$) in the presence of the laser pulse.

Fig. 2 shows that the distribution of the displacement u, in the context of (3PHL), (L-S) and (G-N III) theories, always begins from positive values for $b = 0, 0.1$. It shows that, in the presence of two-temperature (i.e. $b = 0.1$), the values of u based on (3PHL), (L-S) and (G-N III) theories decrease in the range $0 \le y \le 5$. However, in the absence of two-temperature (i.e. $b = 0$), the values of u based on (3PHL), (L-S) and (G-N III) theories decrease in the range $0 \le y \le 1$. Fig. 3 is plotted the distribution of the displacement v with distance y. The behavior of v for both theories is almost similar for $b = 0, 0.1$. It decreases in the range $0 \le y \le 0.9$, and begin to increase in the range $1 \le y \le 9$. Even approaching the final to zero. The change in the temperature distribution T with the distance y represents in Fig. 4. The temperature distribution is exhibiting the similar trend for both theories for $b = 0, 0.1$. It is an increasing function in the domain $0 \le y \le 0.8$ and a decreasing function in the domain $0.8 \le y \le 4$, at $b = 0$. It is an increasing function in the domain $0 \le y \le 0.8$ and a decreasing function in the domain $0.8 \le y \le 4$, for $b = 0$. It is noticed that the temperature distribution is strongly affected by the presence of two-temperature because for $b = 0.1$, temperature distribution increases in the range $0 \le y \le 1$, while decreases in the range $1 \le y \le 6$. The variation of the stress component σ_{xx} with distance y has shown in Fig. 5. The behavior of σ_{xx} for both theories is alike. It satisfied the boundary conditions and decreasing in the range $0 \le y \le 6$ for $b = 0,\ 0.1$ and finally decays to zero. Fig. 6 shows the variation of the stress component σ_{yy} with distance y. The behavior of σ_{yy} for $b = 0.1$ begins to decrease, then smooth decreases and takes the form of wave and try to return to zero in three theories. While, for $b = 0$, the behavior of σ_{yy} begins to increase, then smooth decreases and takes the form of wave and try to return to zero in three theories. The stress component σ_{xy} with distance y indicated in Fig. 7. The behavior of σ_{xy} for

both theories is alike. It satisfied the boundary conditions and increasing in the range $0 \le y \le 1$ for $b = 0,\ 0.1$ and decreasing in the range $1 \le y \le 8$ and finally decays to zero.

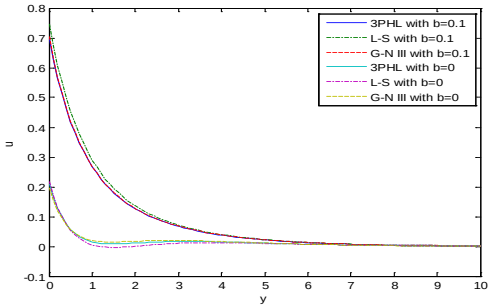

Figure 2. Horizontal displacement distribution u for $b = 0, 0.1$.

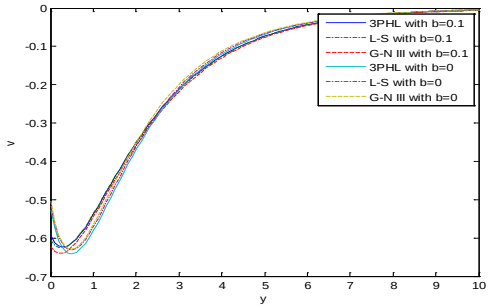

Figure 3. Vertical displacement distribution v for $b = 0, 0.1$.

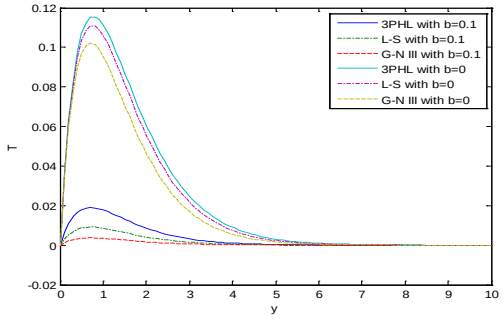

Figure 4. Temperature distribution T for $b = 0, 0.1$.

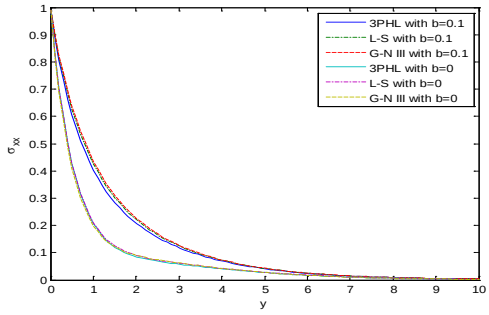

Figure 5. Distribution of stress component σ_{xx} for $b = 0, 0.1$.

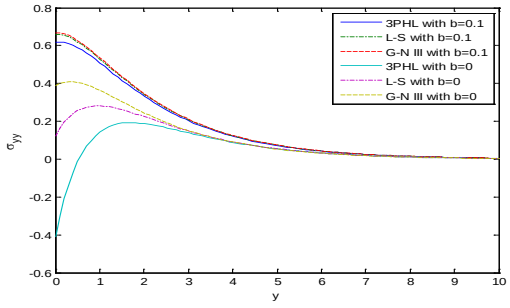

Figure 6. Distribution of stress component σ_{yy} for $b = 0, 0.1$.

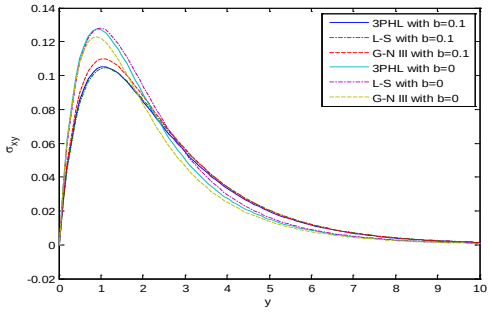

Figure 7. Distribution of stress component σ_{xy} for $b = 0, 0.1$.

Figs. 8-13 depict the variety of the displacement components u, v, the temperature T, the stress components σ_{xx}, σ_{yy} and σ_{xy} for different values of time ($t = 0.05 \cdot 10^{-13}$, $t = 0.09$) in the presence of laser pulse and two-temperatures.

Figs. 8 and 9 show the distributions of the displacement components u and v in the context of (3PHL), (L-S) and (G-N III) theories for $t = 0.05 \cdot 10^{-13}$ and $t = 0.09$. It is noticed that the distribution of u decreases for $(t = 0.05 \cdot 10^{-13},\ t = 0.09)$ while the distribution of v decreases for $(t = 0.05 \cdot 10^{-13}, t = 0.09)$ in the range $0 \le y \le 0.2$ and increases in the range $0.2 \le y \le 6$ in three theories. Fig. 10 demonstrates that the distribution of the temperature T always begins from zero and satisfies the boundary conditions. In the context of the (3PHL), (L-S) and (G-N III) theories, the values

of T increase in the beginning to a maximum value in the range $0 \le y \le 1,$ then decrease in the range $1 \le y \le 5$ and also move in wave propagation for $t = 0.05 \cdot 10^{-13}$ and $t = 0.09$. It is also noticed that the values of T for both (L-S) and (G-N III) theories are less in comparison to (3PHL) model. Fig. 11 depicts the distribution of the stress component σ_{xx} in the context of (3PHL), (L-S) and (G-N III) theories, for $t = 0.05 \cdot 10^{-13}$ and $t = 0.09$. It is observed that the distribution of σ_{xx} in the context of (3PHL), (L-S) and (G-N III) theories is decreasing for $t = 0.05 \cdot 10^{-13}$ and $t = 0.09,$ until it decay to zero. Fig. 12 depicts the distribution of the stress component σ_{yy} in the context of (3PHL), (L-S) and (G-N III) theories, for $t = 0.05 \cdot 10^{-13}$ and $t = 0.09$. It is observed that the distribution of σ_{yy} in the context of (3PHL), (L-S) and (G-N III) theories are decreasing for $t = 0.05 \cdot 10^{-13}$ and $t = 0.09,$ until it decay to zero. The distribution of the stress components σ_{xy} always begins from zero and satisfies the boundary conditions as demonstrated in Fig. 13. In the context of (3PHL), (L-S) and (G-N III) theories, the values of σ_{xy} increase in the beginning to a maximum value in the range $0 \le y \le 1,$ then decrease in the range $1 \le y \le 6$ for $t = 0.05 \cdot 10^{-13}$ and $t = 0.09,$ until it decay to zero.

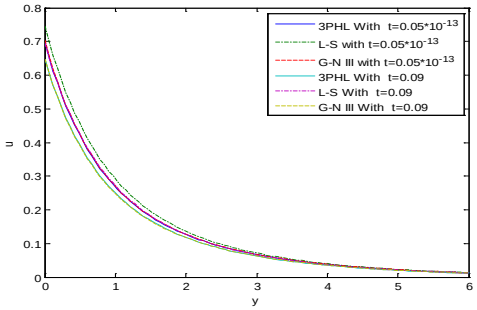

Figure 8. Horizontal displacement distribution u for $t = 0.05 \cdot 10^{-13},\ t = 0.09.$

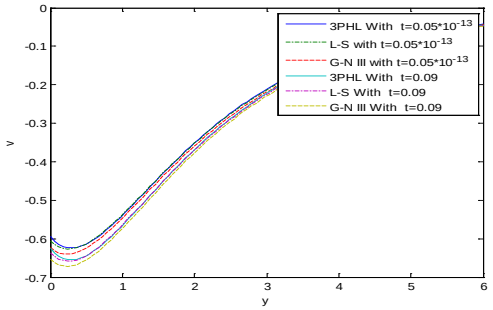

Figure 9. Horizontal displacement distribution v for $t = 0.05 \cdot 10^{-13},\ t = 0.09.$

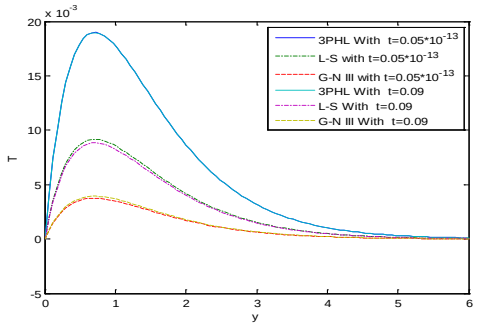

Figure 10. Temperature distribution T for $t = 0.05 \cdot 10^{-13}, t = 0.09.$

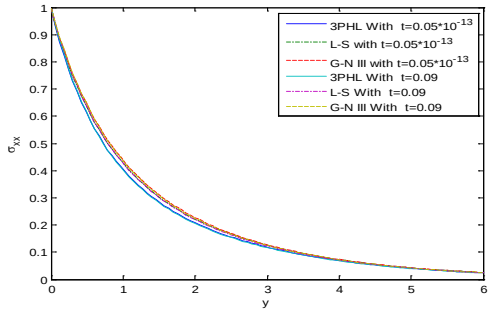

Figure 11. Distribution of stress component σ_{xx} for $t = 0.05 \cdot 10^{-13}, t = 0.09.$

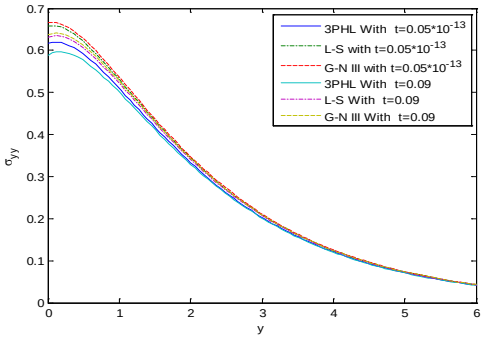

Figure 12. Distribution of stress component σ_{yy} for $t = 0.05 \cdot 10^{-13}, t = 0.09.$

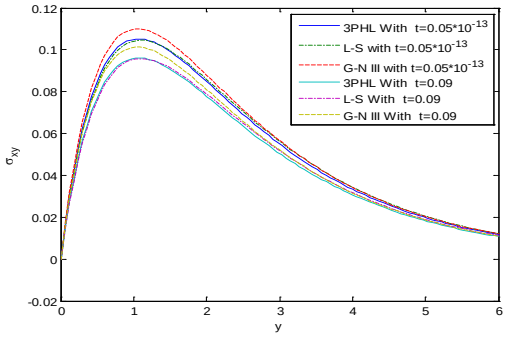

Figure 13. Distribution of stress component σ_{xy} for $t = 0.05 \cdot 10^{-13}, t = 0.09.$

6 Conclusions

By comparing the figures obtained under the three theories, important phenomena are observed:

(a) Analytical solutions based upon normal mode analysis of the thermoelastic problem in solids have been developed.
(b) The method that is used in the present article is applicable to a wide range of the problems in the hydrodynamics and thermoelasticity.
(c) There are significant differences in the field quantities under (L-S), (GN-III), (3PHL) theories.
(d) The presence of the laser pulse and two-temperature play a significant role on all the physical quantities.
(e) The comparison of the three theories of thermoelasticity, (L-S), (G-N III) and (3PHL) theories are carried out.
(f) The value of all the physical quantities converges to zero.

Analysis of the temperature, stress generated and displacement components in a body due to the application of the effect of a laser pulse and two-temperature are an interesting problem of thermoelasticity. The problem assumes great significance when we consider the real behavior of the material characteristics with appropriate geometry of the model.

References

Chen, P.J.; Gurtin, M.E.: On a theory of heat conduction involving two temperatures, *Z. Angew. Math. Phys*., 19, (1968), 614-627.

Green, A.E.; Lindsay, K.A.: Thermoelasticity, *J. Elast*., 2, (1972), 1-7.

Hetnarski, R.B.; Ignaczak, J.: Soliton-like waves in a low temperature non-linear thermoelastic solid, *Int. J. Eng. Sci*., 34, (1996), 1767-1787.

Hetnarski, R.B.; Ignaczak, J.: Generalized thermoelasticity, *J. Therm. Stress*., 22, (1999), 451-476.

Ieşan, D.: On the linear coupled thermoelasticity with two temperatures, *J. Appl. Mathath. and Phys*., 21, (1970), 583-591.

Ignaczak, J., Ostoja-Starzewski, M.: Thermoelasticity with Finite Wave Speeds. Oxford University Press, Oxford (2010)

Khamis, A.K.; Ismail, M.A.H.; Youssef, H.M.; El-Bary, A.A.: Thermal shock problem of two-temperature generalized thermoelasticity without energy dissipation with rotation, *Microsystem Technology*, 23, (2017), 4831-4839.

Lord, H.W.; Shulman Y.: A generalized dynamical theory of thermoelasticity, *J. the Mech. and Phys. of* Solids, 15, (1967), 299-309.

Marin, M.; Agarwal, R.P.; Othman, M.I.A.: Localization in time of solutions for thermoelastic micropolar materials with voids, Comput., Materials & Continua, 40, (2014), 35-48.

Magaña, A.; Quintanilla, R.: Uniqueness and growth of solutions in two-temperature generalized thermoelastic theories, *Math. and Mech. of Solids*, 14, (2009), 622-634.

Othman, M.I.A.; Atwa, S.Y.: Two-dimensional problems of a fibre-reinforced anisotropic thermoelastic medium comparison with the Green-Naghdi theory, *Comput. Math. and Model*, 24, (2013), 307-325.

Othman, M.I.A.; Abd-Elaziz, E.M.: The effect of thermal loading due to laser pulse in generalized thermoelastic medium with voids in dual phase lag model, *J. Therm. Stress*., 38, (2015), 1068-1082.

Othman, M.I.A.; Elmaklizi, Y.D.; Ahmed, E.A.A.: Influence of magnetic field on generalized piezo-thermoelastic rotating medium with two relaxation times, *Microsystem Technologies*, 23, (2017), 5599-5612.

Othman, M.I.A.; Eraki, E.E.M.: Generalized magneto-thermoelastic half-space with diffusion under initial stress using three-phase-lag model, *Mechanics Based Design of Struct. and Mach., An Int. J.*, 45, (2017), 145-159.

Othman, M.I.A.; Jahangir, A.; Nadia, A.: Microstretch thermoelastic solid with temperature-dependent elastic properties under the influence of magnetic and gravitational field, *J. Braz. Soc. of Mech. Sci. and Eng*., 40, (2018), 332-341.

Othman, M.I.A.; Eraki, E.E.M.: Effect of gravity on generalized thermoelastic diffusion due to laser pulse using dual-phase-lag model, *Multi.Model. Materials and Struct*., 14, (2018), 457-481.

Puri, P.; Jordan, P.M.: On the propagation of harmonic plane waves under the two-temperature theory, *Int. J. Eng. Sci*., 44, (2006), 1113-1126.

Quintanilla, R.: On existence, structural stability, convergence and spatial behavior in thermoelasticity with two temperatures, *Acta Mechanica*, 168, (2004), 61-73.

Quintanilla, R.; Racke, R.: A note on stability in three-phase-lag heat conduction, Int. J. Heat and Mass Transfer, 51, (2008), 24-29.
Roy Choudhuri, S.K.: On thermoelastic three phase lag model, *J. Therm. Stress*., 30, (2007), 231- 238.

Sangwan, A.; Singh, B.; Singh, J.: Reflection and transmission of plane waves at an interface between elastic and micropolar piezoelectric solid half-spaces, *Technische Mechanik*, 38(3), (2018), 267-285.

Sharma, K.; Marin, M.: Effect of distinct conductive and thermodynamic temperatures on the reflection of plane waves in micropolar elastic half-space, *UPB University Politehnica of Bucharest Scientific Bulletin, Series A, Appl. Math. and Phys*., 75, (2013), 121-132.

Sharma, J.N.; Singh, H.: Generalized thermoelastic waves in anisotropic media, *The Journal of the Acoustical Society of America*, 85, (1985), 1407-1413.

Sun, Y.; Fang, D.; Saka, M.; Soh, A.K.: Laser-induced vibrations of micro-beams under different boundary conditions, *Int. J. of Solids and Struct*., 45, (2008), 1993-2013.

Tzou, D.Y.: A unified field approach for heat conduction from macro-to micro-cales, *J. Heat Transfer*, 117, (1995), 8-16.

Youssef, H.M.: Theory of two-temperature generalized thermoelasticity, IMA *J. Appl. Math.*, 71, (2006), 383-390.

Addresses:
Mohamed I. A. Othman, Department of Mathematics, Faculty of Science, Zagazig University, P.O. Box 44519,Zagazig, Egypt. (Corresponding Author)
Nehal T. Mansour, Basic Sciences Department, Al-Safwa High Institute of Engineering,
Cairo, Egypt
email: m_i_a_othman@yahoo.com, nehal.tarek23@yahoo.com

DOI: 10.24352/UB.OVGU-2019-017 TECHNISCHE MECHANIK, 39, 2, (2019), 186 – 189
submitted: November 12, 2018

On Failure of Determinism in Classical Mechanics

A. Krawietz

Newtonian mechanics is generally considered to be deterministic: Once the initial conditions are known, all the future behaviour of a system can be predicted by solving the equations of motion. (That is the idea of Laplace's demon.) But a simple example will reveal that the solution of the initial value problem need not be unique. A prediction thus becomes impossible. An effect can happen without a cause, so that causality is annulled.

1 Introduction

Classical mechanics is ruled by differential equations. If the initial values of position and velocity of a system are given, the future values can, in principle, be calculated by integrating these equations. Laplace (1814) applied this idea to the whole universe and concluded that its future is fully determined by the presence. (The intelligent being who should know all the initial conditions and solve the equations was later on named Laplace's demon.) So Newtonian mechanics seems to be a fully deterministic theory. But this conviction is based on the tacit belief that the solution of the differential equations is unique.
We will present the following simple example that allows an infinite number of solutions and thus disproves the idea of determinism.

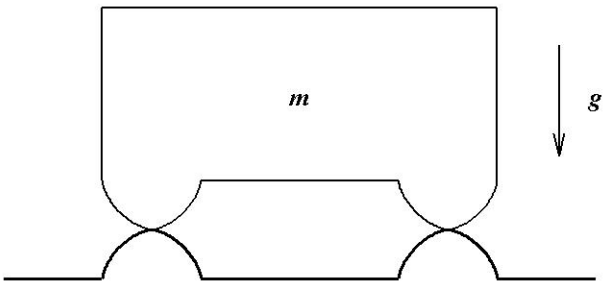

Figure 1: The state of rest of a plate under the influence of gravity

A rigid plate is supported by a rigid basis. The mutual contact occurs at the vertices of four geometrically identical cams. The situation depicted in Fig. 1 is obviously a state of equilibrium. So the plate can remain in this position for all times. Our question is whether it is also possible that the plate begins to move and leaves this position without noticeable cause.

2 The Geometry of our Example

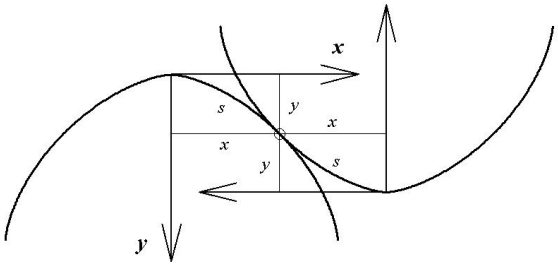

Figure 2: Contact of the cams during the motion

We describe the progress of the motion by the arc length s of the boundary of a cam from the vertex to the actual point of contact as shown in Fig. 2. The coordinates of the point of contact shall be given as

$$x = x(s)\,, \qquad y = y(s) \tag{1}$$

and the coordinates of the center of gravity of the plate are then

$$x_C = x_{C0} + 2x\,, \qquad y_C = y_{C0} + 2y \tag{2}$$

where x_{C0} and y_{C0} denote the position of the center of gravity in the state of rest. The square of the velocity of the center of gravity is

$$v_C^2 = \dot{x}_C^2 + \dot{y}_C^2 = 4(\dot{x}^2 + \dot{y}^2) = 4\left(\left(\frac{dx}{ds}\right)^2 + \left(\frac{dy}{ds}\right)^2\right)\left(\frac{ds}{dt}\right)^2 = 4\frac{dx^2+dy^2}{ds^2}\left(\frac{ds}{dt}\right)^2 = 4\dot{s}^2 \tag{3}$$

3 Frictionless Motion

The sum of the potential and kinetic energy remains constant during the motion.

$$(E+U)_0 = E + U = \frac{1}{2}mv_C^2 - mg(y_C - y_{C0}) = 2m\dot{s}^2 - 2mgy(s) \tag{4}$$

We are interested in motions that start from the state of rest with $s = 0,\ y = 0,\ \dot{s} = 0$, so that $(E+U)_0 = 0$ holds. The equation of motion then becomes

$$\dot{s} = +\sqrt{gy(s)} \equiv r(s) \tag{5}$$

We choose the positive square root to describe motions to the right.
An obvious solution is $s(t) \equiv 0,\ y(t) \equiv 0,\ \dot{s}(t) \equiv 0$, so that the plate remains in the state of rest for an arbitrarily long time. We want to know whether there are other solutions of the differential equation. Uniqueness requires the fulfilment of Lipschitz' condition. But that condition is surely violated if the derivative of the right-hand side $r(s)$ is not finite, *i.e.*

$$\left|\frac{dr(s)}{ds}(s=0)\right| = \infty \tag{6}$$

The last condition allows a geometric interpretation. Let α denote the angle of the tangent and κ the curvature of the boundary curve. Then

$$\sin\alpha = \frac{dy}{ds}\,, \qquad \kappa = \frac{d\alpha}{ds} = \frac{d\alpha}{d\sin\alpha}\frac{d\sin\alpha}{ds} = \frac{1}{\cos\alpha}\frac{d^2y}{ds^2} = \frac{y''(s)}{\sqrt{1-y'(s)^2}} \tag{7}$$

Now

$$y(s) = \frac{1}{g}r(s)^2\,, \qquad y'(s) = \frac{2}{g}r(s)r'(s)\,, \qquad y''(s) = \frac{2}{g}\Big(r'(s)^2 + r(s)r''(s)\Big) \tag{8}$$

At the vertex, we have $s = 0,\ \alpha = 0,\ \kappa(0) = y''(0) \propto r'(0)^2 = \infty$. So an infinite curvature at the vertex is sufficient to allow the spontaneous deviation of the plate from the state of rest. If this happens at some instant $t = t_D$, then the solution of our differential equation can be found by separation of the variables.

$$\int_{\hat{s}=0}^{s}\frac{d\hat{s}}{r(\hat{s})} = \int_{\hat{t}=t_D}^{t} d\hat{t} = t - t_D \tag{9}$$

4 A Special Geometry

We study the following class of boundary curves, depending on a positive constant a and a real parameter θ.

$$y(s) \equiv as^{2\theta}\,, \quad y'(s) \equiv 2\theta a s^{2\theta-1}\,, \quad y''(s) \equiv 2\theta(2\theta-1)as^{2(\theta-1)}\,, \quad r(s) \equiv \sqrt{ga}s^{\theta}\,, \quad r'(s) \equiv \theta\sqrt{ga}s^{\theta-1} \tag{10}$$

The condition $y'(0) = 0$ requires $\theta > 1/2$ and $r'(0)$ is infinite if $\theta < 1$. The curvature at the vertex $y''(0)$ is then infinite, too, as we already know. We are therefore only interested in values of θ satisfying $1/2 < \theta < 1$. Eq. (9) then gives

$$\frac{1}{\sqrt{ga}}\frac{s^{1-\theta}}{1-\theta} = t - t_D \qquad \Longrightarrow \qquad s(t) = \Big((1-\theta)\sqrt{ga}(t-t_D)\Big)^{\frac{1}{1-\theta}} \qquad\qquad t \geq t_D \tag{11}$$

Now let the initial conditions be $s(t_I) = 0$, $\dot{s}(t_I) = 0$ at some initial time $t_I < t_D$. A possible solution of this initial value problem is the remaining in the state of rest from t_I to the time t_D of deviation

$$s(t) \equiv 0 \qquad\qquad t_I \leq t \leq t_D \tag{12}$$

followed by a deviation off the state of rest according to eq. (11). Choosing the special value $\theta = 3/4$, we find

$$y(s) \equiv as^{\frac{3}{2}} \qquad \Longrightarrow \qquad s(t) \equiv \begin{cases} 0 & \text{if} \quad t_I \leq t \leq t_D \\ \left(\frac{ga}{16}\right)^2 (t-t_D)^4 & \text{if} \quad t \geq t_D \end{cases} \tag{13}$$

So an infinite set of solutions of the initial value problem exists, depending on the parameter t_D.

5 The Role of Friction

It would be erroneous to assume that our phenomenon of indeterminism depends on the crude idealization of a frictionless motion. Let $F(s)$ be the work of friction exerted during the motion at each of the two contacts. Then the balance of work (4) has to be modified as follows.

$$0 = E + U + 2F = 2m\dot{s}^2 - 2mgy(s) + 2F(s) \tag{14}$$

and the equation of motion (5) has to be replaced by

$$\dot{s} = +\sqrt{gy(s) - \frac{1}{m}F(s)} \equiv r(s) \tag{15}$$

A non-trivial solution can only exist if

$$F(s) < mgy(s) \tag{16}$$

The power of friction is the product of the frictional force f and the relative velocity $v_R = v_C = 2\dot{s}$ at the points of contact.

$$\dot{F} = F'(s)\dot{s} = 2f(s)\dot{s} \tag{17}$$

In the case of dry friction, $F'(0) = 2f(0) = 2f_0 > 0$ is finite but $y'(0)$ is zero. So the inequality (16) cannot be satisfied near $s = 0$ and a deviation from the state of rest is impossible. The same happens if sticking friction is present.
However, viscous damping can be allowed. To demonstrate this, we study the rather special case

$$F(s) = \lambda mgy(s) \qquad \text{with} \qquad 0 < \lambda < 1 \tag{18}$$

The equation of motion becomes

$$\dot{s} = +\sqrt{(1-\lambda)gy(s)} \tag{19}$$

The solutions of the frictionless case remain valid if g is replaced by $(1-\lambda)g$. The appertaining nonlinear viscous law is obtained as follows

$$f = \frac{1}{2}F'(s) = \lambda\theta mgas^{2\theta-1} = \lambda\theta mga\left(\frac{v_R}{2\sqrt{(1-\lambda)ga)}}\right)^{2-\frac{1}{\theta}} \equiv f(v_R) \tag{20}$$

6 Conclusions

Let us interpret our result (13). Newtonian mechanics reveals the following possibility: The plate remains in a state of rest for a certain time interval and then, at some instant t_D, suddenly starts a motion and leaves the state of rest.

- It is disturbing that the point t_D of deviation remains totally uncertain. Not even a statement of probability like a half-value time can be given.
- It cannot be known, too, whether the motion will ocur to the right-hand or the left-hand side.
- Our solution is an example of an indetermined motion. Note that the begin of the motion is not triggered by any external disturbance. No cause of this effect can be found. On the other hand, Laplace (1814), guided by his investigation on celestial mechanics, wrote : "Les événemens actuels ont avec les précédens, une liaison fondée sur le principe évident, qu'une chose ne peut pas commencer d'être, sans une cause qui la produise. Cet axiome connu sous le nom de *principe de la raison suffisante*, s'étend aux actions même les plus indifférentes. (The connexion of the actual events with the preceding ones is based on the evident principle that nothing can begin to exist without a reason by which it is produced. This axiom, known under the name of principle of sufficient reason, even applies to actions of utmost irrelevance.)" But our finding indicates that this principle of sufficient reason is perhaps not so evident and even invalid in special situations.
- It is surprising that the plate can start its motion although, at the beginning, it has no information whether the curvature at the vertex is infinite and the friction small enough to allow the motion at all.

7 Delimitation

- The phenomenon of indeterminacy may be considered as a heightened stage of instability. Whenever there is a positive curvature at the vertex then the state of rest of the plate is unstable. An arbitrarily small disturbance is sufficient to cause a permanent deviation from that state. In a case like $y = as^2$, such a disturbance is also necessary. Otherwise the plate remains at rest in a deterministic way. In our indeterminate case, however, the state of rest is of course unstable, but no disturbance at all is necessary to start the deviation.
- Indeterminate behaviour must not be confused with chaotic behaviour. The latter is deterministic and characterized by a sensitive dependence on initial conditions. So all the intermediate states of the orbit are unstable. In our indeterminate case, we do not discuss various initial conditions but only one, the state of rest. Only this state is unstable but not the following ones during the motion.
- Indeterminism is not a problem for engineers but one of natural philosophy. The plate of our example cannot be manufactured with sufficient accuracy to test its behaviour by an experiment.

Remark: The indeterminate behaviour of eq. (13) was already discussed by the author in a text book (Krawietz (1997), p. 262). It was inferred there from the motion of a point mass, which is a cruder idealization than our plate. The same example was afterwards presented by Norton (2003) in a critical philosophical treatment on the principle of causation.

References

Krawietz, A.: *MapleV für das Ingenieurstudium*, Springer, Berlin (1997)

Laplace, P.-S. de: *Essai philosophique sur les probabilités*, Paris (1814)

Norton, J.D.: Causation as folk science, *Philosophers' Imprint*, Vol.3, No.4 (2003)

Address: Prof. Dr.-Ing. A. Krawietz, Hildburghauser Str. 241b, 12209 Berlin, Germany
email: krawietz@t-online.de

DOI: 10.24352/UB.OVGU-2019-018 TECHNISCHE MECHANIK, 39, 2, (2019), 190 – 201
submitted: December 17, 2018

Ferromagnetic Convection in a Rotating Medium with Magnetic Field Dependent Viscosity. A Correction Applied

J. Prakash[1], K. Kumari[2], P. Kumar[3], R. Kumar[4], K.R. Sharma[5]

The effect of magnetic field dependent (MFD) viscosity on the thermal convection in a ferrofluid layer, heated from below, has been investigated in the simultaneous presence of a uniform vertical magnetic field and a uniform vertical rotation. A correction is applied to Vaidyanathan et al. (Ind. J. Pure Appl. Phy., 2001, 40, 159-165), which is very important in order to predict the correct behavior of MFD viscosity. A linear stability analysis has been carried out for stationary modes and oscillatory modes separately. The critical wave number and critical Rayleigh number for the onset of instability, for the case of free boundaries, are determined numerically for sufficiently large values of the magnetic parameter M_1. Numerical results are obtained and are illustrated graphically. It is shown that MFD viscosity has a destabilizing effect on the system for the case of stationary mode and stabilizing effect for the case of oscillatory mode, whereas magnetization has a destabilizing effect. Further, it is also shown that rotation has a stabilizing effect on the system.

1 Introduction

Synthetic magnetic fluids, also known as Ferrofluids, are the colloidal suspensions of solid single- domain ferromagnetic nano-particles, with typical dimensions of 10 nm, dispersed in an organic carrier (e.g. kerosene or ester) or water. In the recent past the studies on ferrofluids attracted several researchers due to their manifold applications in various fields such as acoustics, lubrication, vacuum technology, metals recovery, instrumentation, vibration damping etc. These researches have led to many commercial uses of ferrofluids which includes chemical reactor, medicine, novel zero-leakage rotary shaft seals used in computer disk drives, high speed silent printers, contrast enhancement of magnetic resonance imaging (MRI), pressure seals of compressors and blowers, cooling of loud speakers (Rosensweig, 1985; Odenbach, 2002a).

Ferrohydrodynamics, the study of the magnetic properties of colloidal suspensions has drawn considerable interest since the 1930 (Elmore, 1938), but the investigations on ferroconvection intensified noticeably, starting from the fundamental paper of Finlayson (1970). An authoritative introduction to ferrohydrodynamics is provided in a beautiful monograph by Rosensweig (1985). This book and the references therein laid a serious scientific foundation for further investigations in this field of enquiry. Currently, a significant body of literature exists devoted to ferroconvection. For a broad view of the subject one may referred to Lalas and Carmi (1971), Shliomis (1972), Aniss et al. (2001), Odenbach (2002b), Sunil et al. (2005), Suslov (2008), Lee and Shivakumara (2011), Prakash (2013a, b), Rahman and Suslov (2015, 2016) and Labusch et al. (2016).

The most specific characteristic property of a ferrofluid is the possibility to exert a significant influence to their flow and physical properties by means of moderate magnetic fields (Odenbach, 2002a). The effect on the viscous behavior of fluid due to the presence of an external magnetic field seems to be most prominent and is one of the most challenging topics of magnetic fluid research. Several research papers have been published by eminent researchers in this direction. Rosensweig et al. (1969) reported the investigation of a viscosity increase observed in ferrofluids containing nanosized magnetic particles in magnetic fields. The effect of a homogeneous magnetic field on the viscosity of the fluid with solid particles possessing intrinsic magnetic moments has been investigated by Shliomis (1974). Vaidyanathan et al. (2001) studied the influence of MFD viscosity on ferroconvection in a rotating medium heated from below using linear stability analysis. Vaidyanathan et al. (2002) further investigated the same problem of ferroconvection in a rotating sparsely distributed porous medium for the case of stationary and oscillatory modes. Ramanathan and Suresh (2004) studied the effect of magnetic field dependent viscosity and anisotropy of porous medium on ferroconvection. Sunil et al. (2005) investigated the effect of magnetic field dependent viscosity on a rotating ferromagnetic fluid heated and soluted from below saturating a porous medium. Prakash and Gupta (2013) derived upper bounds for the complex growth rate of oscillatory motions in ferromagnetic convection with MFD viscosity in a rotating fluid layer.

It is worth mentioning here that in the above cited papers on MFD viscosity, the researchers performed their analysis by considering MFD viscosity in the form $\mu = \mu_1(1 + \vec{\delta}.\vec{B})$, where μ_1 is fluid viscosity in the absence of magnetic field $\vec{B}$ and $\vec{\delta}$ is the variation coefficient of viscosity. They resolved μ into components μ_x, μ_y and μ_z which is not technically correct. Since μ, being a scalar quantity, cannot be resolved in such a manner. Undoubtedly, they have investigated a very important problem of ferrohydrodynamics, but their results cannot be relied upon due to this wrong assumption. Recently, Prakash and Bala (2016) and Prakash et al. (2017, 2018a, b) have rectified the above problem for some ferromagnetic convection configurations with MFD viscosity. In the present communication the attention has, particularly, been given to the above cited paper by Vaidyanathan et al. (2001) on ferromagnetic convection in a rotating medium with MFD viscosity. Keeping in view the above fact the basic equations have been reformulated and then mathematical and numerical analysis has been performed to remedy the weaknesses in the existing results and to give correct interpretation of the problem. It is also important to point out here that the role of viscosity for stationary convection is observed to destabilize the system which is in confirmation with the result obtained by Chandrasekhar (1981) for the case of ordinary fluid.

2 Mathematical Formulation

Consider a ferromagnetic fluid layer of infinite horizontal extension and finite vertical thickness dheated from below which is kept under the simultaneous action of a uniform vertical magnetic field $\vec{H}$ and uniform vertical rotation $\vec{\Omega}$ (see Fig.1). The magnetic fluid is assumed to be incompressible having a variable viscosity, given by $\mu = \mu_1(1 + \vec{\delta}.\vec{B})$, where μ_1 is the viscosity of the magnetic fluid when there is no magnetic field applied, μ is the magnetic field dependent viscosity and $\vec{B}$ is the magnetic induction. The variation coefficient of viscosity $\vec{\delta}$ has been taken to be isotropic, i.e. $\delta_1 = \delta_2 = \delta_3 = \delta$. The effect of shear dependence on viscosity is not considered since it has negligible effect for a mono dispersive system of large rotation and high field. As a first approximation for small field variation, linear variation of magneto viscosity has been used (Vaidyanathan et al., 2002).

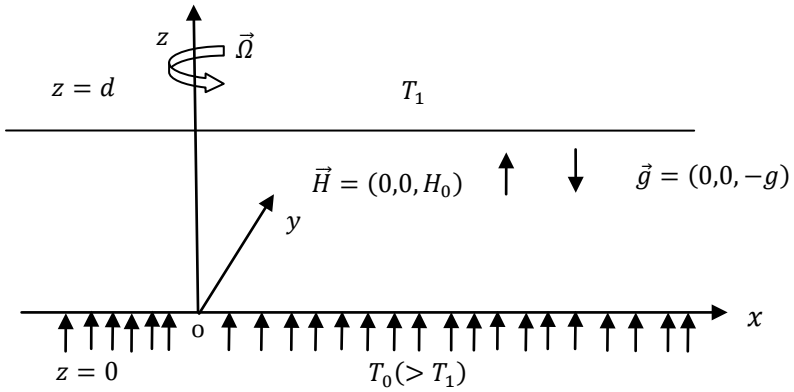

Fig.1 Geometrical configuration

The basic governing equations for the present problem are given by (Vaidyanathan et al., 2001):

$$\nabla.\vec{q} = 0, \tag{1}$$

$$\rho_0\left[\frac{\partial\vec{q}}{\partial t} + \vec{q}.\nabla\vec{q}\right] = -\nabla\bar{P} + \rho\vec{g} + \mu\nabla^2\vec{q} + \nabla.\left(\vec{H}\vec{B}\right) + 2\rho_0\left(\vec{q}\times\vec{\Omega}\right) + \frac{\rho_0}{2}\nabla\left(\left|\vec{\Omega}\times\vec{r}\right|^2\right), \tag{2}$$

$$\left[\rho_0 C_{V,H} - \mu_0\vec{H}.\left(\frac{\partial\vec{M}}{\partial T}\right)_{V,H}\right]\frac{DT}{Dt} + \mu_0 T\left(\frac{\partial\vec{M}}{\partial T}\right)_{V,H}.\frac{D\vec{H}}{Dt} = K_1\nabla^2 T + \phi, \tag{3}$$

$$\rho = \rho_0[1 + \alpha(T_0 - T)], \tag{4}$$

where $\vec{q} = (u, v, w)$ is the fluid velocity, $P = \bar{P} - \frac{\rho_0}{2}\nabla\left(\left|\vec{\Omega}\times\vec{r}\right|^2\right)$ is the pressure, $\vec{H}$ is the magnetic field, $\mu = \mu_1(1 + \vec{\delta}.\vec{B})$ is the variable viscosity, $\vec{g} = (0,\ 0, -g)$ is the acceleration due to gravity, $\vec{\Omega} = (0,\ 0,\ \Omega)$ is the angular velocity, $C_{V,H}$ is the heat capacity at constant volume and magnetic field, μ_0 is the magnetic permeability, T is the temperature, $\vec{M}$ is the magnetization, K_1 is the thermal conductivity, ϕ is the viscous

dissipation containing second order terms in velocity, α is the coefficient of volume expansion and ρ_0 is the density at some reference temperature T_0.

For a non-conducting fluid with no displacement current, the Maxwell's equations are given by

$$\nabla.\vec{B} = 0, \nabla \times \vec{H} = 0,\ \vec{B} = \mu_0\left(\vec{H} + \vec{M}\right). \tag{5a,b}$$

We assume that the magnetization is aligned with the magnetic field, but allow a dependence on the magnitude of the magnetic field as well as the temperature as

$$\vec{M} = \frac{\vec{H}}{H} M(H,T). \tag{6}$$

The linearized magnetic equation of state is

$$M = M_0 + \chi\,(H - H_0) - K_2(T - T_0), \tag{7}$$

where M_0 is the magnetization when magnetic field is H_0 and temperature T_0, $\chi = \left(\frac{\partial \vec{M}}{\partial \vec{H}}\right)_{H_0,T_0}$ is magnetic susceptibility and $K_2 = -\left(\frac{\partial \vec{M}}{\partial T}\right)_{H_0,T_0}$ is the pyromagnetic coefficient.

The basic state is assumed to be quiescent state and is given by

$$\vec{q} = \vec{q}_b = 0, \rho = \rho_b(z), P = P_b(z),\ T = T_b(z) = -\beta\, z + T_0,\ \beta = \frac{T_0 - T_1}{d}, \vec{H}_b = \left(H_0 - \frac{K_2 \beta z}{1+\chi}\right)\hat{k},$$

$$\vec{M}_b = \left(M_0 + \frac{K_2\,\beta z}{1+\chi}\right)\hat{k}, \vec{H}_b + \vec{M}_b = H_0 + M_0. \tag{8}$$

The Perturbed State Solutions are given by

$$\vec{q} = \vec{q}_b + \overrightarrow{q'}, \rho = \rho_b(z) + \rho', P = P_b(z) + P', T = T_b(z) + \theta', \vec{H} = \vec{H}_b(z) + \vec{H}',$$

$$\vec{M} = \vec{M}_b(z) + \vec{M}', \tag{9}$$

where $\overrightarrow{q'} = (u', v', w')$, ρ', $P', \theta', \vec{H}'$ and $\vec{M}'$ are perturbations in velocity, density, pressure, temperature, magnetic field intensity and magnetization respectively and are assumed to be small.

Substituting equation (9) into equations (1) -(7) and using equation (8), we get the following linearized perturbation equations

$$\frac{\partial u'}{\partial x} + \frac{\partial v'}{\partial y} + \frac{\partial w'}{\partial z} = 0, \tag{10}$$

$$\rho_0 \frac{\partial u'}{\partial t} = -\frac{\partial P'}{\partial x} + \mu_0(H_0 + M_0)\frac{\partial H_x'}{\partial z} + 2\rho_0 \Omega v' + \mu_1[1 + \delta\mu_0(H_0 + M_0)]\nabla^2 u', \tag{11}$$

$$\rho_0 \frac{\partial v'}{\partial t} = -\frac{\partial P'}{\partial y} + \mu_0(H_0 + M_0)\frac{\partial H_y'}{\partial z} - 2\rho_0 \Omega u' + \mu_1[1 + \delta\mu_0(H_0 + M_0)]\nabla^2 v', \tag{12}$$

$$\rho_0 \frac{\partial w'}{\partial t} = -\frac{\partial P'}{\partial z} + \mu_0(H_0 + M_0)\frac{\partial H_z'}{\partial z} - \mu_0 K_2 \beta H_z' + \frac{\mu_0 {K_2}^2 \beta \theta'}{(1+\chi)} + \rho_0 g \alpha \theta' + \mu_1[1 + \delta\mu_0(H_0 + M_0)]\nabla^2 w', \tag{13}$$

$$\rho_c \frac{\partial \theta'}{\partial t} - \mu_0 T_0\, K_2 \frac{\partial}{\partial t}\left(\frac{\partial \Phi'}{\partial z}\right) = \kappa_1 \nabla^2 \theta' + \left(\rho_c \beta - \frac{\mu_0 T_0\, {K_2}^2 \beta}{1+\chi}\right) w', \tag{14}$$

where $\rho_c = \rho_0\, C_{V,H} + \mu_0 K_2 H_0$, $H' = \nabla\Phi'$, Φ' is the perturbed magnetic potential

and $H_z' + M_z' = (1 + \chi)H_z' - K_2\theta'$, (15)

$$H_i' + M_i' = \left(1 + \frac{M_0}{H_0}\right)H_i'(i = 1, 2), \tag{16}$$

where we have assumed $K_2 \beta d \ll (1 + \chi)H_0$, as the analysis is restricted to physical situations, in which the magnetization induced by temperature variations is small compared to that induced by the external magneticfield.

Using equations (5b), (15) and (16), we get

$$\left(1+\frac{M_0}{H_0}\right)\nabla_1{}^2\Phi' + (1+\chi)\frac{\partial^2\Phi'}{\partial z^2} - K_2\frac{\partial\theta'}{\partial z} = 0, \tag{17}$$

where $\nabla_1{}^2 = \left(\frac{\partial^2}{\partial x^2}+\frac{\partial^2}{\partial y^2}\right)$.

Now we eliminate u' and v' between equations (11) and (12) by operating equation (11) by $\frac{\partial}{\partial x}$ and equation (12) by $\frac{\partial}{\partial y}$, adding the resulting equations and using equation (10). We obtain

$$\rho_0\frac{\partial}{\partial t}\left(\frac{\partial w'}{\partial z}\right) = \left(\frac{\partial^2 P'}{\partial x^2}+\frac{\partial^2 P'}{\partial y^2}\right) - 2\rho_0\Omega\zeta' + \mu_1[1+\delta\mu_0(H_0+M_0)]\nabla^2\left(\frac{\partial w'}{\partial z}\right) - \mu_0(H_0+M_0)\frac{\partial}{\partial z}\left(\frac{\partial H_x'}{\partial x}+\frac{\partial H_y'}{\partial y}\right), \tag{18}$$

where $\zeta' = \frac{\partial v'}{\partial x} - \frac{\partial u'}{\partial y}$ is the z component of vorticity.

Now eliminating P' between equations (13) and (18), we get

$$\rho_0\frac{\partial}{\partial t}\nabla^2 w' = -2\rho_0\Omega\frac{\partial\zeta'}{\partial z} + \mu_1[1+\delta\mu_0(H_0+M_0)]\frac{\partial^2}{\partial z^2}(\nabla^2 w') + \rho_0 g\alpha\nabla_1{}^2\theta' + \frac{\mu_0 K_2{}^2\beta\ \nabla_1{}^2\theta'}{1+\chi} + \mu_1\nabla_1{}^2(\nabla^2 w')$$

$$+\mu_0\mu_1\delta(H_0+M_0)\nabla_1{}^2(\nabla^2 w') - \mu_0 K_2\beta\frac{\partial}{\partial z}\nabla_1^2\Phi'. \tag{19}$$

Further, operating equation (11) by $\frac{\partial}{\partial y}$ and equation (12) by $\frac{\partial}{\partial x}$, subtracting the resulting equations and using equation (10), we get an equation describing vorticity as

$$\rho_0\frac{\partial\zeta'}{\partial t} = 2\rho_0\Omega\frac{\partial w'}{\partial z} + \mu_1[1+\delta\mu_0(H_0+M_0)]\nabla^2\zeta'. \tag{20}$$

Now we analyze the perturbations w', θ', ζ' and Φ' into two dimensional periodic waves and consider disturbances characterized by a particular wave number k. Thus we assume to all quantities describing the perturbation a dependence on x, y and t of the form

$$(w', \theta', \zeta', \Phi') = [w''(z), \theta''(z), \zeta''(z), \Phi''(z)]exp\left[i\left(k_x x + k_y y\right) + nt\right], \tag{21}$$

where k_x and k_y are the horizontal wave numbers and $k = \sqrt{k_x^2 + k_y^2}$ is the resultant wave number.

On using equation (21) in equations (19), (14), (17) and (20) and non-dimensionalizing the variables by setting

$$z_* = \frac{z}{d}, \quad w_* = \frac{dw''}{\nu}, \quad a = kd, \quad \zeta_* = \frac{d^2}{\nu}\zeta'', \quad D = d\frac{d}{dz}, \ \theta_* = \frac{K_1 aR^{1/2}}{\rho_c\beta\nu\, d}\theta'', \ \Phi_* = \frac{(1+\chi)K_1 aR^{1/2}}{K_2\rho_c\beta\nu\, d^2}\Phi'', \quad \nu = \frac{\mu}{\rho_0},$$
$$\sigma = \frac{\nu\rho_c}{K_1},$$

$$\delta_* = \mu_0\delta H_0(1+\chi), \quad R = \frac{g\alpha\beta d^4\rho_c}{K_1\nu}, \ M_1 = \frac{\mu_0 K_2{}^2\beta}{(1+\chi)\alpha\rho_0 g}, \ M_2 = \frac{\mu_0 T_0 K_2{}^2}{(1+\chi)\rho_c}, \quad M_3 = \frac{1+\frac{M_0}{H_0}}{(1+\chi)}, \ T_a = \frac{4\Omega^2 d^4}{\nu^2}, \ p = \frac{nd^2}{\nu} \tag{22}$$

we obtain the following non dimensional equations (dropping the asterisks for simplicity)

$$(D^2-a^2)\{(1+\delta M_3)(D^2-a^2) - p\}w = aR^{\frac{1}{2}}\{(1+M_1)\theta - M_1 D\Phi\} + T_a{}^{\frac{1}{2}}D\zeta, \tag{23}$$

$$(D^2 - a^2 - p\sigma)\theta + pM_2\sigma D\Phi = -(1-M_2)aR^{\frac{1}{2}}w, \tag{24}$$

$$\{(1+\delta M_3)(D^2-a^2) - p\}\zeta = -T_a{}^{\frac{1}{2}}Dw, \tag{25}$$

$$(D^2 - a^2 M_3)\Phi = D\theta. \tag{26}$$

Since, M_2 is of very small order (Finlayson, 1970), it is neglected in the subsequent analysis and thus equation

(24) takes the form

$$(D^2 - a^2 - p\sigma)\theta = -aR^{\frac{1}{2}}w. \tag{27}$$

The constant temperature boundaries are considered to be free. Thus the boundary conditions are given by

$$w = 0 = \theta = D^2 w = D\zeta = D\Phi \text{ at } z = 0 \text{ and } z = 1, \tag{28}$$

where z is the real independent variable such that $0 \leq z \leq 1$, represent the two boundaries. $D = \frac{d}{dz}$ is the differentiation along the vertical coordinate, a^2 is square of the wave number, $\sigma > 0$ is the Prandtl number, $R > 0$ is the Rayleigh number, $T_a > 0$ is the Taylor number, $M_1 > 0$ is the magnetic number which defines ratio of magnetic forces due to temperature fluctuation to buoyant forces, $M_3 > 0$ is the measure of the nonlinearity of magnetization, $M_2 > 0$ is a non-dimensional parameter which defines the ratio of thermal flux due to magnetization to magnetic flux, $p = p_r + ip_i$ is a complex constant in general such that p_r and p_i are real constants and as a consequence the dependent variables $w(z) = w_r(z) + iw_i(z)$, $\theta(z) = \theta_r(z) + i\theta_i(z)$, $\Phi(z) = \Phi_r(z) + i\Phi_i(z)$ and $\zeta(z) = \zeta_r(z) + i\zeta_i(z)$ are complex valued functions of the real variable z where $w_r(z), w_i(z), \theta_r(z), \theta_i(z), \Phi_r(z), \Phi_i(z), \zeta_r(z)$ and $\zeta_i(z)$ are real valued functions of the real variable z.

Further, it may be noted that the equation (23) and equations (25) -(28) describe an eigenvalue problem for p and govern ferromagnetic convection, with MFD viscosity, in the presence of uniform rotation.

3 Mathematical Analysis

Following the analysis of Finlayson (1970), the exact solutions satisfying the boundary conditions (28) are given by

$$w = A\,sin\pi z,\ \theta = B\,sin\pi z,\ \Phi = -\frac{C}{\pi}\,cos\pi z,\ \zeta = -\frac{D}{\pi}\,cos\pi z, D\Phi = C\,sin\pi z,\ D\zeta = D\,sin\pi z,$$

where A, B, C and D are constants. Substitution of above solutions in equations (23) and (25) -(27) yields a system of four linear homogeneous algebraic equations in the unknowns *A*, *B*, *C* and *D*. For the existence of non-trivial solutions of this system, the determinant of the coefficients of *A*, *B*, *C* and *D* must vanish. This determinant on simplification yields

$$Up^3 + Vp^2 + Wp + X = 0, \tag{29}$$

where

$$U = \sigma(\pi^2 + a^2)(\pi^2 + a^2 M_3), \tag{30}$$

$$V = (\pi^2 + a^2)^2(\pi^2 + a^2 M_3)[2\sigma(1 + \delta M_3) + 1], \tag{31}$$

$$W = (\pi^2 + a^2 M_3)[(\pi^2 + a^2)^3(1 + \delta M_3)\{(1 + \delta M_3)\sigma + 2\} + T_a\pi^2\sigma] - Ra^2[\pi^2 + a^2 M_3(1 + M_1)], \tag{32}$$

$$X = (\pi^2 + a^2)(\pi^2 + a^2 M_3)[(\pi^2 + a^2)^3(1 + \delta M_3)^2 + T_a\pi^2] - Ra^2(1 + \delta M_3)(\pi^2 + a^2)[\pi^2 + a^2 M_3(1 + M_1)]. \tag{33}$$

Substitution of $p = ip_i$ in equation (29) yields marginal state of convection. For $p_i = 0$, we have a case of stationary convection, while $p_i \neq 0$ defines the oscillatory convection.

From equation (29), the Rayleigh number for stationary convection can easily be derived as

$$R = \frac{(\pi^2 + a^2 M_3)\left[(\pi^2 + a^2)^3(1 + \delta M_3)^2 + T_a\pi^2\right]}{a^2(1 + \delta M_3)[\pi^2 + a^2 M_3(1 + M_1)]}. \tag{34}$$

In the expression (34), if we put $\delta = 0, T_a = 0$, we obtain the Rayleigh number for classical ferroconvection (Finlayson, 1970). If we put $\delta = 0 = M_3, T_a \neq 0$, we obtain Rayleigh number for classical rotatory hydrodynamic convection (Chandrasekhar, 1981) and if we put $\delta = 0 = M_3, T_a = 0$, we obtain Rayleigh number for convection in ordinary fluid heated from below (Chandrasekhar, 1981). If we put $T_a = 0$, $M_3 \neq 0$, we obtain Rayleigh number for ferroconvection with MFD viscosity (Prakash et al., 2017). If we put $\delta = 0, T_a \neq 0, M_3 \neq$

0, we obtain Rayleigh number for ferroconvection in a rotating ferrofluid layer (Venkatasubramanian and Kaloni, 1994).

When M_1 is very large, the magnetic Rayleigh number N $(= RM_1)$ for stationary mode can be expressed as

$$N = \frac{(\pi^2+a^2M_3)\left[(\pi^2+a^2)^3(1+\delta M_3)^2+T_a\pi^2\right]}{a^4(1+\delta M_3)M_3}. \quad (35)$$

To find the minimum value N_c of N with respect to wave number a, equation (35) is differentiated with respect to a^2 and equated to zero and the following polynomial is obtained

$$a^4(1+\delta M_3)(\pi^2+a^2)M_3[(\pi^2+a^2M_3)\{(\pi^2+a^2)^3(1+\delta M_3)^2+T_a\pi^2\}+(\pi^2+a^2)M_3\{(\pi^2+a^2)^3(1+\delta M_3)^2+T_a\pi^2\}+(\pi^2+a^2)(\pi^2+a^2M_3)3(\pi^2+a^2)^2(1+\delta M_3)^2]-(\pi^2+a^2)(\pi^2+a^2M_3)\{(\pi^2+a^2)^3(1+\delta M_3)^2+T_a\pi^2\}\{2a^2(1+\delta M_3)(\pi^2+a^2)M_3+a^4M_3(1+\delta M_3)\}=0. \quad (36)$$

The above equation is solved numerically by using the software Scientific Work Place for various values of M_3, δ and T_a, and the minimum value of a is obtained each time, hence N_c is obtained.

Table 1: Marginal stability of MFD viscosity of a ferrofluid in a rotating medium heated from below for stationary mode having $M_1 = 1000$, $T_a = 10^4$ and 10^5.

Taylor no. T_a	Coefficient of viscosity δ	Magnetization M_3	Critical wave no. a_c	$N_c = (RM_1)_c$
10^4	0.01	1	6.0655	6905.6
		3	5.7997	5895.6
		5	5.7012	5674.5
		7	5.6351	5571.7
	0.03	1	6.027	6909.2
		3	5.6872	5877.2
		5	5.5207	5637.1
		7	5.3926	5518.8
	0.05	1	5.9896	6913.4
		3	5.5828	5863.3
		5	5.3603	5611.2
		7	5.1854	5485.9
	0.07	1	5.9531	6918.0
		3	5.4856	5853.3
		5	5.2165	5594.6
		7	5.0057	5468.4
	0.09	1	5.9175	6923.2
		3	5.3947	5847.3
		5	5.0867	5585.8
		7	4.8478	5463.2
10^5	0.01	1	8.8651	24009
		3	8.6385	22100
		5	8.5422	21631
		7	8.4687	21376
	0.03	1	8.8075	23931
		3	8.4718	21837
		5	8.2762	21203
		7	8.1124	20800
	0.05	1	8.7514	23856
		3	8.3168	21598
		5	8.0393	20831
		7	7.8069	20321
	0.07	1	8.6967	23784
		3	8.1723	21378
		5	7.8262	20505

		7	7.5408	19918
	0.09	1	8.6434	23715
		3	8.037	21175
		5	7.6332	20216
		7	7.3059	19573

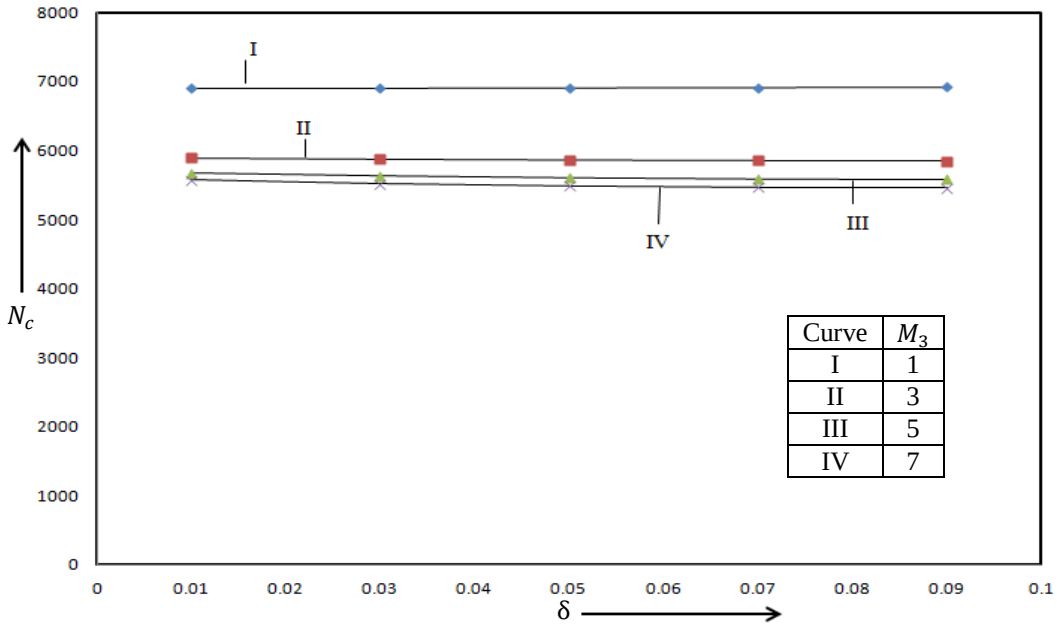

Fig.2 Effect of magnetic field on the variation of magnetic Rayleigh number (N_c) versus coefficient of field dependent viscosity (δ) for stationary mode for Taylor number $T_a = 10^4$.

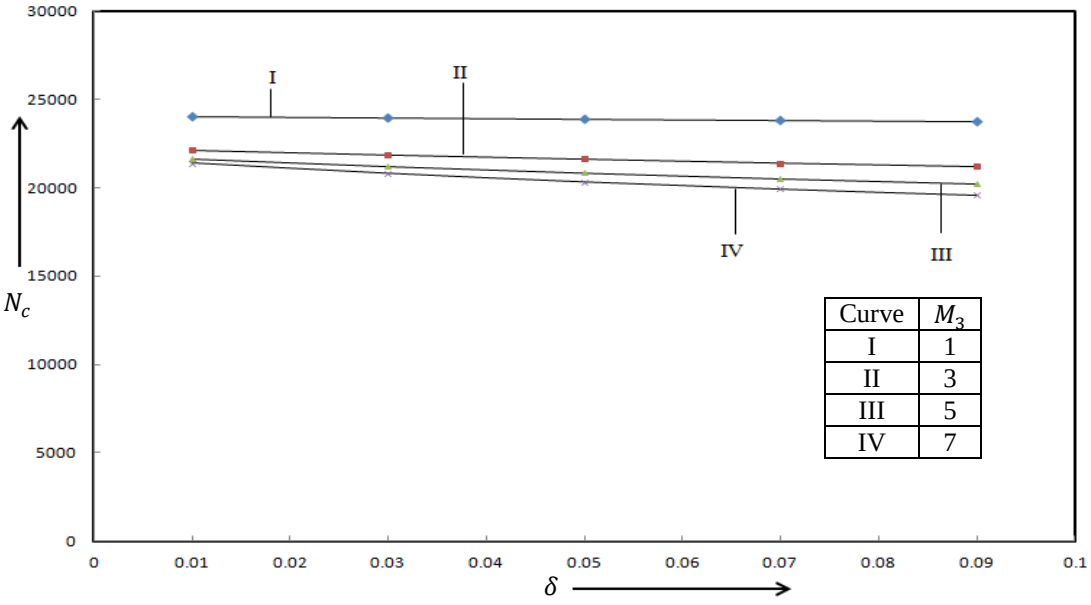

Fig.3 Effect of magnetic field on the variation of magnetic Rayleigh number (N_c) versus coefficient of field dependent viscosity (δ) for stationary mode for Taylor number $T_a = 10^5$.

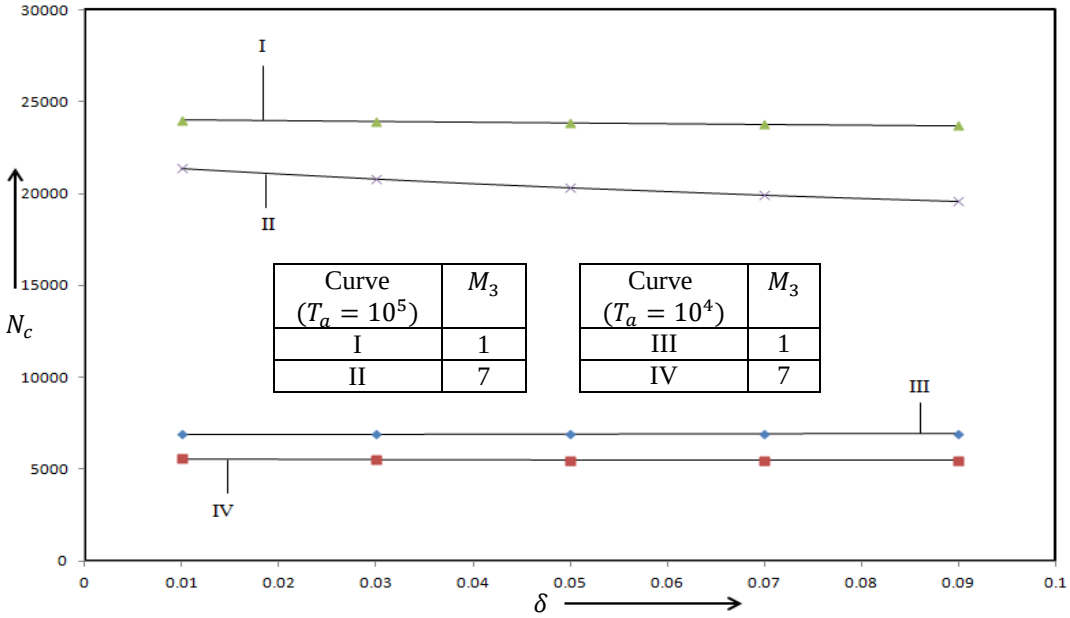

Fig.4 Effect of magnetic field on the variation of magnetic Rayleigh number (N_c) versus coefficient of field dependent viscosity (δ) for stationary mode for Taylor number $T_a = 10^4$ and 10^5.

From equation (29), the Rayleigh number for oscillatory mode can easily be obtained as

$$R^o = \frac{[2\sigma(1+\delta M_3)+1]\left[(\pi^2+a^2)^3(1+\delta M_3)\{(1+\delta M_3)\sigma+2\}+T_a\pi^2\sigma\right](\pi^2+a^2M_3) - \sigma(\pi^2+a^2M_3)\left[(\pi^2+a^2)^3(1+\delta M_3)^2+T_a\pi^2\right]}{a^2[\pi^2+a^2M_3(1+M_1)][\sigma(1+\delta M_3)+1]}. \quad (37)$$

When M_1 is very large, the magnetic Rayleigh number $N^o(=RM_1)^o$ for oscillatory mode can be obtained using

$$N^o = \frac{[2\sigma(1+\delta M_3)+1]\left[(\pi^2+a^2)^3(1+\delta M_3)\{(1+\delta M_3)\sigma+2\}+T_a\pi^2\sigma\right](\pi^2+a^2M_3) - \sigma(\pi^2+a^2M_3)\left[(\pi^2+a^2)^3(1+\delta M_3)^2+T_a\pi^2\right]}{a^4M_3[\sigma(1+\delta M_3)+1]}. \quad (38)$$

To find the minimum value N_c^o of N^o with respect to wave number a, equation (38) is differentiated with respect to a^2 and equated to zero and the following polynomial is obtained

$a^4M_3[\sigma(1+\delta M_3)+1][2\sigma(1+\delta M_3)+1]M_3(\pi^2+a^2)^3(1+\delta M_3)[\sigma(1+\delta M_3)+2]+T_a\pi^2\sigma M_3a^4M_3[\sigma(1+\delta M_3)+1][2\sigma(1+\delta M_3)+1]+a^4M_3[\sigma(1+\delta M_3)+1][2\sigma(1+\delta M_3)+1](\pi^2+a^2M_3)3(\pi^2+a^2)^2(1+\delta M_3)[\sigma(1+\delta M_3)+2]-a^4M_3[\sigma(1+\delta M_3)+1]\sigma(1+\delta M_3)^2(\pi^2+a^2M_3)3(\pi^2+a^2)^2-a^4M_3[\sigma(1+\delta M_3)+1]\sigma(1+\delta M_3)^2(\pi^2+a^2)^3M_3-a^4M_3[\sigma(1+\delta M_3)+1]T_a\pi^2\sigma M_3-[2\sigma(1+\delta M_3)+1](\pi^2+a^2)^3(1+\delta M_3)[\sigma(1+\delta M_3)+2]2a^2M_3[\sigma(1+\delta M_3)+1](\pi^2+a^2M_3)-[2\sigma(1+\delta M_3)+1]T_a\pi^2\sigma(\pi^2+a^2M_3)2a^2M_3[\sigma(1+\delta M_3)+1]+\sigma(\pi^2+a^2M_3)[(\pi^2+a^2)^3(1+\delta M_3)^2+T_a\pi^2]2a^2M_3[\sigma(1+\delta M_3)+1]=0.$

(39) The above equation is solved numerically by using the software Scientific Work Place for various values of M_3, δ and T_a, and the minimum value of a is obtained each time, hence N_c^o is obtained.

Table 2: Marginal stability of MFD viscosity of a ferrofluid in a rotating medium heated from below for oscillatory mode having $M_1 = 1000$, $T_a = 10^4$ and 10^5.

Taylor no. T_a	Coefficient of viscosity δ	Magnetization M_3	Critical wave no. a_c	$N_c^o = (RM_1)_c^o$
	0.01	1	4. 7997	13765
		3	4. 5176	11132
		5	4. 4251	10718
		7	4. 3727	10642
		1	4. 7861	14069
		3	4. 4763	11823

10^4	0.03	5	4. 3568	11793
		7	4. 2785	12101
	0.05	1	4. 7727	14375
		3	4. 4367	12521
		5	4. 2928	12882
		7	4. 1922	13588
	0.07	1	4. 7595	14682
		3	4. 3986	13226
		5	4. 2326	13988
		7	4. 1127	15103
	0.09	1	4. 7465	14682
		3	4. 3619	13228
		5	4. 1759	13995
		7	4. 0393	15117
10^5	0.01	1	6. 9344	40017
		3	6. 708	36018
		5	6. 6353	35660
		7	6. 5903	35840
	0.03	1	6. 913	40787
		3	6. 644	37979
		5	6. 5303	38799
		7	6. 4462	40148
	0.05	1	6. 8919	41557
		3	6. 5823	39935
		5	6. 4314	41919
		7	6. 3133	44417
	0.07	1	6. 8711	42327
		3	6. 5228	41885
		5	6. 3379	45022
		7	6. 1901	48656
	0.09	1	6. 8505	43097
		3	6. 4653	43830
		5	6. 2494	48112
		7	6. 0754	52872

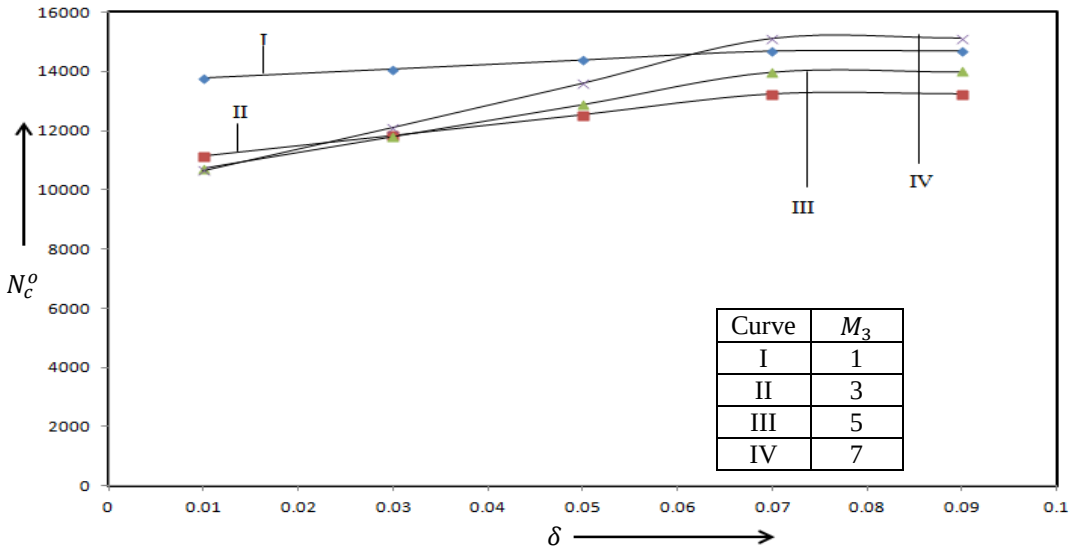

Fig.5 Effect of magnetic field on the variation of magnetic Rayleigh number (N_c^o) versus coefficient of field dependent viscosity (δ) for oscillatory mode for Taylor number $T_a = 10^4$ and $\sigma = 0.9$.

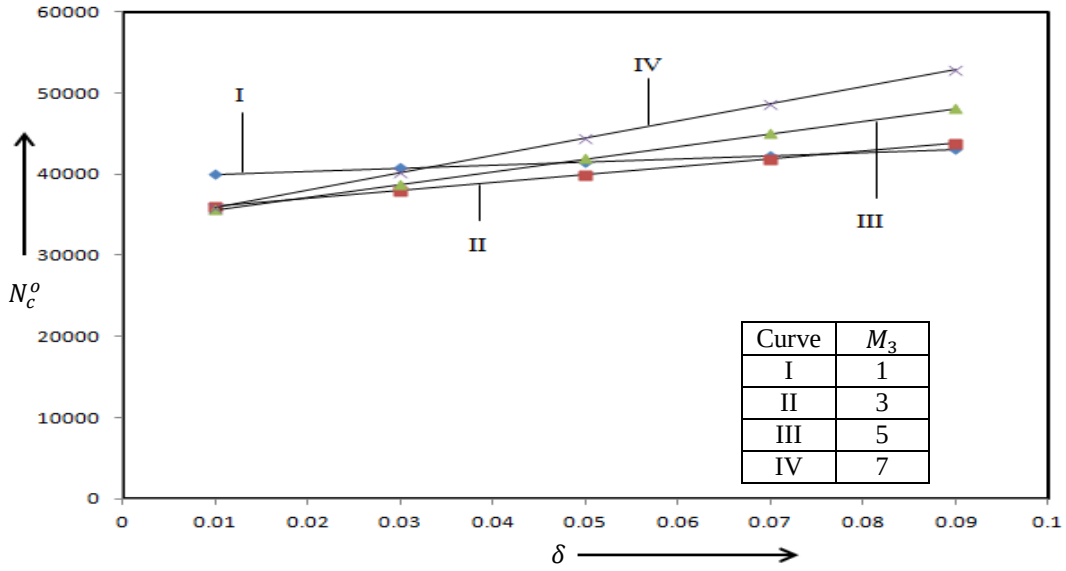

Fig.6 Effect of magnetic field on the variation of magnetic Rayleigh number (N_c^o) versus coefficient of field dependent viscosity (δ) for oscillatory mode for Taylor number $T_a = 10^5$ and $\sigma = 0.9$.

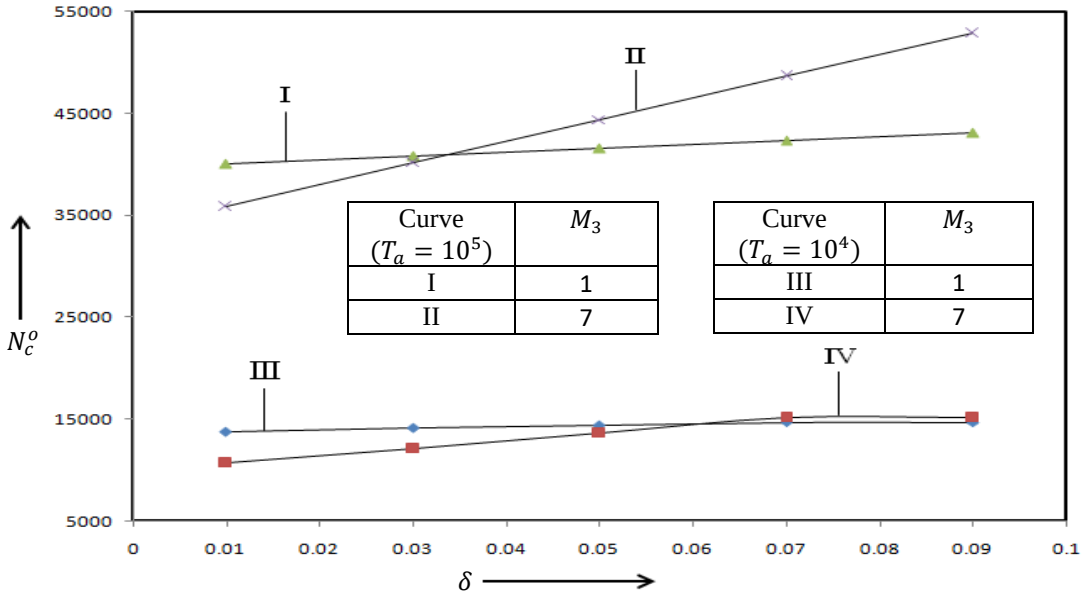

Fig.7 Effect of magnetic field on the variation of magnetic Rayleigh number (N_c^o) versus coefficient of field dependent viscosity (δ) for oscillatory mode for Taylor number $T_a = 10^4$ and $T_a = 10^5$ when $\sigma = 0.9$.

4 Discussion and Conclusion

In the present communication, the influence of magnetic field dependent viscosity on the thermal convection in a rotating ferrofluid layer heated from below in the presence of uniform vertical magnetic field has been investigated. The magnetization parameter M_1 is considered to be 1000 (Vaidyanathan et al., 1997). The value of M_2 being negligible (Finlayson, 1970), has been taken as zero. The values of the parameter M_3 are varied from 1 to 7. The values of the coefficient of magnetic field dependent viscosity δ, has been varied from 0.01 to 0.09.

Emphasize has been given to a paper published by Vaidyanathan et al. (2001). These researchers have carried out their analysis by considering MFD viscosity as $\mu = \mu_1(1 + \vec{\delta}.\vec{B})$. But they further resolved μ into components μ_x, μ_y and μ_z along the coordinate axes which is technically wrong. Since μ, being a scalar quantity, cannot be resolved into components. Thus a correction to their analysis is very much sought after in

order to give a correct interpretation of the problem. Keeping these facts in mind, the basic equations have been reformulated to the correct perspective and then mathematical and numerical analysis has been performed. The results so obtained have significant variations from the existing results which were otherwise obtained by using wrong assumption.

From table 1 and from figures 2-4, it is evident that the critical value of magnetic Rayleigh number, $N_c = (RM_1)_c$ decreases with the increase in the magnetization parameter M_3. Hence the magnetization has destabilizing effect on the system. The physical interpretation of this may be given as follows: As the value of M_3 increases the departure of linearity in the magnetic equation of state increases resulting into the increase in the velocity of the ferrofluid in the vertical direction favoring the manifestation of instability. This increase in magnetization releases extra energy, which adds up to thermal energy to destabilize the flow more quickly. Thus the magnetization parameter destabilizes the system. The similar result also obtained by Vaidyanathan et al. (2001), but the difference in the values of N_c is quite significant and increases with the increase in the value of δ. It is also evident from figures 2-4 that for stationary convection, the value of magnetic Rayleigh number decreases as the MFD viscosity parameter δ increases, predicting the destabilizing behavior of viscosity parameter δ. This unexpected result that 'the role of viscosity is inverted in the presence of rotation', has also been predicted by Chandrasekhar (1981) for the case of ordinary fluid.

It is also found from table 1 and figure 4, that the magnetic Rayleigh number increases with increase in the values of Taylor number T_a. Thus the rotation has stabilizing effect on the system. Again the difference in the existing values (Vaidyanathan et al., 2001) and the values obtained herein is significant.

It is interesting to note from figures 5 and 6 that for the case of oscillatory motions the value of magnetic Rayleigh number increases as the MFD viscosity parameter δ increases, thus resulting into the postponement of instability. Thus, MFD viscosity has a stabilizing effect on the system for the case of oscillatory convection, which is a result also obtained by Vaidyanathan et al. (2001).

Further, we may note from figures 5 and 6 that for the case of oscillatory convection also, M_3 prepone the onset of convection. Thus magnetization M_3 has destabilizing effect on the system for the case of oscillatory convection also. Finally, figure 7 predicts the stabilizing behavior of rotation on the system for the case of oscillatory convection.

Acknowledgments

The authors gratefully acknowledge the discussions with Professor R. G. Shandil to bring this manuscript in the present form. One of the authors (JP) also acknowledges the financial support by UGC, New Delhi in the form of MRP (Grant No. 43-420/ 2014 (SR)).

References

Aniss, S., Souhar, M. and Belhaq, M.: Effect of magnetic modulation on the stability of a magnetic liquid layer heated from below. *ASME J. Heat Transfer*, **123(3)**, (2001), 428- 433.

Chandrasekhar, S.: *Hydrodynamic and Hydromagnetic* Stability. Dover publications, INC., New York, (1981).

Elmore, W.C.: The magnetization of ferromagnetic colloids. *Phys. Rev.*, **54**, (1938), 1092-1095.

Finlayson, B.A.: Convective instability of ferromagnetic fluids. *J. Fluid Mech.*, **40**, (1970), 753-767.

Labusch, M., Keip, M.A., Shvartsman, V.V., Lupascu, D.C. and Schroder, J.: On the influence of ferroelectric

polarization states on the magneto-electric coupling in two phase composites. *Tech. Mech.,* **36(1-2)**, (2016), 73-87.

Lalas, D.P. and Carmi, S.: Thermoconvective stability of ferrofluids. *Phys. Fluids*, **14(2)**, (1971), 436-437.

Lee, J. and Shivakumara, I.S.: Onset of penetrative convection in a ferrofluid-saturated porous layer. *Spec. topics & Rev. Porous Media: An Int. Journal*, **2(3)**, (2011), 217-225.

Odenbach, S.: *Ferrofluids: Magnetically Controllable Fluids and their Applications*. Springer-Verlag, Berlin, Heidelberg, (2002b).

Odenbach, S.: *Magnetoviscous Effects in Ferrofluids*. Springer-Verlag, Berlin, Heidelberg, (2002a).

Prakash, J. and Bala, R.: On estimating the complex growth rates in ferromagnetic convection with magnetic field dependent viscosity in a rotating sparsely distributed porous medium. *J. Appl. Mech. Tech. Phys.*, **57(4)**, (2016), 623-636.

Prakash, J. and Gupta, S.: On arresting the complex growth rates in ferromagnetic convection with magnetic field dependent viscosity in a rotating ferrofluid layer. *J. Mag. Mag. Mater.*, **345**, (2013), 201-207.

Prakash, J., Kumar, P., Kumari, K. and Manan, S.: Ferromagnetic convection in a densely packed porous medium with magnetic field dependent viscosity- revisited. *Z. Naturforsch*, **73(3)**, (2018a), 181-189.

Prakash, J., Kumar, R. and Kumari, K.: Thermal convection in a ferromagnetic fluid layer with magnetic field dependent viscosity: A correction applied. *Studia Geotech. et Mech.*, **39(3)**, (2017), 39-46.

Prakash, J., Manan, S. and Kumar, P.: Ferromagnetic convection in a sparsely distributed porous medium with magnetic field dependent viscosity revisited. *J. Porous Media*, **21(8)**, (2018b), 749-762.

Prakash, J.: On arresting the complex growth rates in ferromagnetic convection in a ferrofluid saturated porous layer. *J. Porous Media*, **16(3)**, (2013b), 217-226.

Prakash, J.: On exchange of stabilities in ferromagnetic convection in a rotating porous medium. *Int. J. Fluid Mech. Res*., **40(5)**, (2013a), 391-404.

Rahman, H. and Suslov, S.A.: Magneto-gravitational convection in a vertical layer of ferrofluid in a uniform oblique magnetic Field. *J. Fluid Mech.*, **795**, (2016), 847-875.

Rahman, H. and Suslov, S.A.: Thermomagnetic convection in a layer of ferrofluids placed in a uniform oblique external magnetic field. *J. Fluid Mech.*, **764**, (2015), 316-348.

Ramanathan, A. and Suresh, G.: Effect of magnetic field dependent viscosity and anisotropy of porous medium on ferroconvection. *Int. J. Engng. Sc.*, **42(3-4)**, (2004), 411-425.

Rosensweig, R. E., Kaiser, R. and Miskolczy, G.: Viscosity of magnetic fluid in a magnetic field. *J. Colloid Inter. Sc.*, **29(4)**, (1969), 680-686.

Rosensweig, R.E.: *Ferrohydrodynamics*. Cambridge University Press, Cambridge, (1985).

Shliomis, M.I.: Effective viscosity of magnetic suspensions. *Soviet Physics JETP*, **34(6)**, (1972), 1291-1294.

Shliomis, M.I.: Magnetic fluids. *Soviet Phys. Uspekhi (Engl. Trans.)*, **17(2)**, (1974), 153-169.

Sunil, Divya and Sharma, R.C.: Effect of magnetic field dependent viscosity on a rotating ferromagnetic fluid heated and soluted from below, saturating a porous medium. *J. Porous Media*, **8(6)**, (2005), 569-588.

Sunil, Sharma, A., Kumar, P. and Gupta, U.: The effect of magnetic field dependent viscosity and rotation on ferrothermohaline convection saturating a porous medium in the presence of dust particles. *J. Geophys. Eng.*, **2**, (2005), 238-251.

Suslov, S.A.: Thermo-magnetic convection in a vertical layer of ferromagnetic fluid. *Phys. Fluids*, **20(8)**, (2008), 084101.

Vaidyanathan, G., Sekar, R. and Ramanathan, A.: Ferrothermohaline convection. *J. Mag. Mag. Mater.*, **176**, (1997), 321-330.

Vaidyanathan, G., Sekar, R. and Ramanathan, A.: The effect of magnetic field dependent viscosity on ferroconvection in rotating medium. *Indian J. Pure Appl. Phys.*, **40**, (2001), 159-165.

Vaidyanathan, G., Sekar, R., Vasanthakumari, R. and Ramanathan, A.: The effect of magnetic field dependent viscosity on ferroconvection in a rotating sparsely distributed porous medium. *J. Mag. Mag. Mater.*, **250**, (2002), 65-76.

Venkatasubramanian, S. and Kaloni, P.N.: Effects of rotation on the thermoconvective instability of a horizontal layer of ferrofluids. *Int. J. Engng. Sc.*, **32(2)**, (1994), 237-256.

Address: [1,2,3,4] Department of Mathematics and Statistics, Himachal Pradesh University, Shimla-171005, Himachal Pradesh, INDIA.
[1] Corresponding author E-mail: jpsmaths67@gmail.com; [2] Email: doctorpummy@gmail.com;
[3] Email: pankajthakur28.85@gmail.com; [4] Email: rajeevkumar2012math@gmail.com;
[5] NIC, B-Wing, Level-3 Delhi, Secretariat, Delhi-110002, INDIA; [5] Email: sharma_kraj@nic.in

TECHNISCHE MECHANIK
an open access journal

journal homepage: www.ovgu.de/techmech

Tech. Mech., Vol. 39, Is. 2, (2019), 202–219

Received: March 15,2019
Accepted: April 8, 2019
Available online: April 11, 2019

A Generalized Framework Towards Structural Mechanics of Three-layered Composite Structures

Marcus Aßmus[1⋆], Konstantin Naumenko[1], Andreas Öchsner[2], Victor A. Eremeyev[3], Holm Altenbach[1]

[1] Otto von Guericke University, Faculty of Mechanical Engineering, Universitätsplatz 2, 39108 Magdeburg, Germany
[2] Esslingen University of Applied Sciences, Faculty Mechanical Engineering, Kanalstraße 33, 73728 Esslingen, Germany
[3] Gdańsk University of Technology, Faculty of Civil and Environmental Engineering, Narutowicza 11/12, 80-233 Gdańsk, Poland

Abstract: Three-layered composite structures find a broad application. Increasingly, composites are being used whose layer thicknesses and material properties diverge strongly. In the perspective of structural mechanics, classical approaches to analysis fail at such extraordinary composites. Therefore, emphasis of the present approach is on arbitrary transverse shear rigidities and structural thicknesses of the individual layers. Therewith we employ a layer-wise approach for multiple (quasi-)homogeneous layers. Every layer is considered separately whereby this disquisition is based on the direct approach for deformable directed surfaces. We limit our considerations to geometrical and physical linearity. In this simple and familiar setting we furnish a layer-wise theory by introducing constraints at interfaces to couple the layers. Hereby we restrict our concern to surfaces where all material points per surface are coplanar and all surfaces are plane parallel. Closed-form solutions of the governing equations enforce a narrow frame since they are strongly restrictive in the context of available boundary conditions. Thus a computational solution approach is introduced using the finite element method. In order to determine the required spatially approximated equation of motion, the principle of virtual work is exploited. The discretization is realized via quadrilateral elements with quadratic shape functions. Hereby we introduce an approach where nine degrees of freedom per node are used. In combination with the numerical solution approach, this layer-wise theory has emerged as a powerful tool to analyze composite structures. In present treatise, we would like to clarify the broad scope of this approach.

Keywords: general composite structure, high contrast plates, generalized approach, layer-wise theory

1 Introduction

1.1 Motivation

Nowadays, composite structures are applied in a wide range of applications. Composites with unusual and unique properties are becoming more and more important. This statement refers to the fact that composites are increasingly being developed which consist of a broad spectrum of mechanical and geometrical properties. The definition of a composite structure in the context of thin-walled structural elements is primarily defined by its geometry, i.e. lengths L_α and layer thicknesses h^K while K is a layer index.

$$L_\alpha \gg H \qquad H = \sum_{K}^{NK} h^K \tag{1}$$

In general, the number of layers of the composite NK is arbitrary. However, we restrict our concern to composite structures with three layers ($NK = 3$). Up to now, classifications for composite structures are missing. Main representatives of this genus are depicted in Fig. 1. This subdivision is sufficient at least for engineering applications. The symmetry of the structural design depicted there is not a compelling limitation. Certainly there are other special cases. However, we can distinguish three kinds of three-layered composite structures (TLCS). Theses are laminates, sandwiches, and anti-sandwiches. They can be distinguished by typical geometric and material relationships. Sandwiches and anti-sandwiches exhibit shear-deformable core layers while the skin layers are shear-rigid. Conspicuously, sandwiches and anti-sandwiches are geometrically contrary. Laminates, on the other hand, have similar layer thicknesses and the material properties are all in the same order of magnitude.
Several theories for the treatment of mechanical problems at such composite structures exist. Thereby we reduce our perspective to the efficient and elegant treatment by means of theories for thin walled-structures, cf. Naghdi (1972). A comprehensive view at thin-walled structural elements incorporating historical remarks on relevant protagonists is given in Altenbach and Eremeyev (2017). In Carrera (2002, 2003), basic approaches to treat composite structures are discussed whereby it is distinguished between *equivalent single layer models* and *layer-wise models*. For the former, the *classical laminate theory* and *first-order shear deformation theory* are prominent instances. These modeling approaches are predominantly suitable for monocoque structures (single-layered, homogeneous, isotropic). Another acquaintance is the *sandwich theory*. However, these approaches fail when focusing on strongly divergent material properties and structural thicknesses. There are many theoretical approaches to this, but most of them are only suitable for special compositions and thus have only a limited scope of application. Therefore, a

⋆ E-mail address: marcus.assmus@ovgu.de
doi: 10.24352/UB.OVGU-2019-019

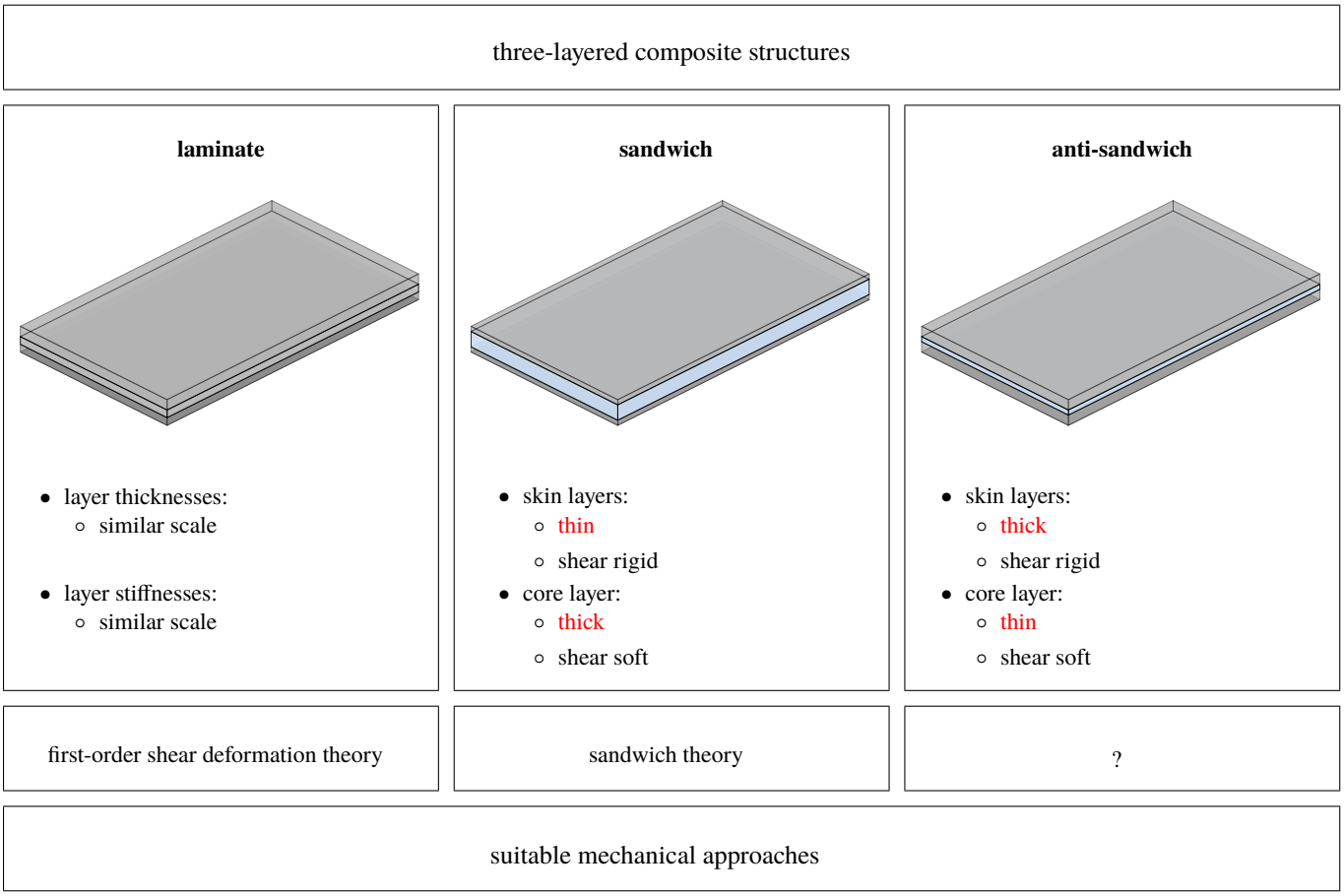

Fig. 1: Attempt of a general classification of three-layered composite structures used for applications in engineering sciences

generalized approach for a wide range of applications is of interest. Present treatise is dedicated to a generalized framework to handle structural mechanics problems at TLCS. For this, we introduce the so called *eXtended layer-wise theory* (XLWT) which also provides a very efficient solution approach for a wide range of mechanical problems in present genus.

1.2 Structure

In order to give our representation an easily readable and condensed shape, we make use of the direct tensor notation. Therefore, we explain present notational conventions and recapitulate the basics of tensor calculus before starting with the actual executions. After that, we will directly enter into the main features of our approach. In doing so, we follow the executions presented in Naumenko and Eremeyev (2014). This base is enlarged since we consider arbitrary transverse shear stiffnesses for all three layers. Thereby we follow a procedure called *direct approach* in spirit of Cosserat and Cosserat (1909), cf. Ganghoffer (2017). We operate on a deformable directed surface *ab initio*. This is a surface in the three-dimensional space in which a vector field is additionally assigned to each point (Zhilin, 1976). We introduce this surface as primitive concept, i.e. it is just an illustrative mean for the stretching, shearing, bending, and twisting of a single layer. However, in present context we introduce the restriction that all material points of this two-dimensional subset are coplanar, i.e. our surface is initially non-curved. In contrast to *derived approaches* where a hierarchic procedure for the derivation of two-dimensional balance equations and kinematic relations is presented, cf. Naghdi (1972), we are liberated from such purely pragmatic approaches, as they are usually applied in engineering sciences (Libai and Simmonds, 1983). This is why the attribute *geometrically exact* is often used in literature.
In progress, we embed the *direct approach* in a systematic framework to establish a layer-wise theory. Thereby, three surfaces are stacked plane parallel equidistantly whereby interfaces and outer faces are initiated for physical reasons. After introducing constraints, the governing equations of the composite structure are derived by the aid of global variables. These equations remain valid for arbitrary structural thicknesses and material parameters.
To construct approximate solutions we make us of the calculus of variations and exploit the principle of virtual work. Subsequently, a numerical method by the aid of the finite element method (FEM) is introduced to solve the algebraic form of the partial differential equations of the boundary value problem.
This is followed by a detailed analysis of the range of application whereby we reduce our investigations to symmetric composites for the sake of brevity. In particular, the roles of different transverse geometry and material compositions are discussed in some detail. As a central result, it is shown that the present approach spans a broad application range at least in context of engineering applications. Finally, the basic findings are summarized and relevant conclusions are drawn. In order to provide users with a complete tool for solving problems with three-layered composites, supplementary relevant matrices like constitutive quantities and differential operators are collected in the Appendix.

Notation. Throughout the whole text, a direct tensor notation is preferred. First- and second-order tensors are denoted by lowercase and uppercase bold letters, e.g., $\boldsymbol{a}$ and $\boldsymbol{A}$, respectively. Fourth-order tensors are designated by uppercase blackboard bold letters, e.g. $\mathbb{A}$. In continuation, some operations between these tensors need to be defined which will be done based on a Cartesian coordinate system. These operations are the dyadic product

$$\boldsymbol{a} \otimes \boldsymbol{b} = a_i b_j \boldsymbol{e}_i \otimes \boldsymbol{e}_j = \boldsymbol{C}\,, \tag{2}$$

the scalar product

$$\boldsymbol{a} \cdot \boldsymbol{b} = a_i b_j \boldsymbol{e}_i \cdot \boldsymbol{e}_j = a_i b_i = \alpha\,, \tag{3}$$

the composition of a second and a first order tensor

$$\boldsymbol{A} \cdot \boldsymbol{a} = A_{lm} a_i \boldsymbol{e}_l \otimes \boldsymbol{e}_m \cdot \boldsymbol{e}_i = A_{li} a_i \boldsymbol{e}_l = \boldsymbol{d}\,, \tag{4}$$

the double scalar product between a fourth and a second order tensor

$$\mathbb{A} : \boldsymbol{B} = A_{pqrs} B_{no} \boldsymbol{e}_p \otimes \boldsymbol{e}_q \otimes \boldsymbol{e}_r \otimes \boldsymbol{e}_s : \boldsymbol{e}_n \otimes \boldsymbol{e}_o = A_{pqrs} B_{sr} \boldsymbol{e}_p \otimes \boldsymbol{e}_q = \boldsymbol{D}\,, \tag{5}$$

the double scalar product between two fourth-order tensors

$$\mathbb{A} : \mathbb{B} = A_{pqrs} B_{tuvw} \boldsymbol{e}_p \otimes \boldsymbol{e}_q \otimes \boldsymbol{e}_r \otimes \boldsymbol{e}_s : \boldsymbol{e}_t \otimes \boldsymbol{e}_u \otimes \boldsymbol{e}_v \otimes \boldsymbol{e}_w = A_{pqrs} B_{srvw} \boldsymbol{e}_p \otimes \boldsymbol{e}_q \otimes \boldsymbol{e}_v \otimes \boldsymbol{e}_w = \mathbb{F}\,, \tag{6}$$

the cross product between tow first-order tensors

$$\boldsymbol{a} \times \boldsymbol{b} = a_i\, b_j\, \boldsymbol{e}_i \times \boldsymbol{e}_j = a_i b_j \epsilon_{ijk} \boldsymbol{e}_k = \boldsymbol{c}\,, \tag{7}$$

the cross product between a second and a first-order tensor

$$\boldsymbol{A} \times \boldsymbol{b} = A_{lm} b_j\, \boldsymbol{e}_l \otimes \boldsymbol{e}_m \times \boldsymbol{e}_j = A_{lm} b_j \epsilon_{mjk} \boldsymbol{e}_l \otimes \boldsymbol{e}_k = \boldsymbol{J}\,. \tag{8}$$

Herein we have introduced the Levi-Civita symbol ϵ_{ijk}.

$$\epsilon_{ijk} = -1/2\,(j - i)(k - j)(i - k) \tag{9}$$

The inverse of a tensor is defined by

$$\boldsymbol{A}^{-1} \cdot \boldsymbol{A} = \boldsymbol{A} \cdot \boldsymbol{A}^{-1} = \boldsymbol{1} \qquad \left[\boldsymbol{A}^{-1}\right]^{-1} = \boldsymbol{A} \tag{10}$$

while the transposed of a tensor is given by

$$\boldsymbol{a} \cdot \boldsymbol{A}^{\top} \cdot \boldsymbol{b} = \boldsymbol{b} \cdot \boldsymbol{A} \cdot \boldsymbol{a}\,. \tag{11}$$

Herein, $\boldsymbol{1} = \boldsymbol{e}_i \otimes \boldsymbol{e}_i$ is the identity on first order tensors. A tensor is said to be symmetric if $\boldsymbol{A}^{\top} = \boldsymbol{A}$ holds. The nabla operator is defined as $\boldsymbol{\nabla} = \boldsymbol{e}_i \partial/\partial x_i$ for threeâĂŘdimensional considerations. $\boldsymbol{\nabla} \cdot \square$ and $\boldsymbol{\nabla} \square$ is the gradient of a tensor, where $\square$ holds true for every differentiable tensor field. The transposed gradient is defined as $\boldsymbol{\nabla}^{\top} \square = [\boldsymbol{\nabla} \square]^{\top}$, and $\boldsymbol{\nabla}^{\mathrm{sym}} \square = 1/2 \left[\boldsymbol{\nabla} \square + \boldsymbol{\nabla}^{\top} \square\right]^{\top}$ is the symmetric part of the corresponding gradient, where $\square$ holds for all firstâĂŘorder tensors. However, in protruding introduction we have used latin indices, e.g. $i \in \{1, 2, 3\}$. The application of greek indices such as $\alpha \in \{1, 2\}$ applies analogously. A subscript zero refers to the reference placement of the material body manifold and a superscript star is used to designate prescribed quantities at boundaries. Material body manifolds are denoted by letters in gothic print (e.g. $\mathfrak{S}$ or $\mathfrak{R}$). For numerical vectors and matrices we make use of upright, sans-serif, lowercase and uppercase bold letters, e.g., $\mathbf{a}$ and $\mathbf{A}$, respectively.

2 Background

2.1 Theoretical Approach

As mentioned at the beginning, we follow the *direct approach*, i.e. we start operating on two-dimensional body manifolds *ab initio*. We introduce mid-surfaces $\mathfrak{S}^K$ for all three layers of the composite structure considered, namely the top layer (index t), the core layer (index c), and the bottom layer (index b). Nonetheless, our model is based on three-dimensional body manifolds so that every physical layer occupies the region $\mathfrak{S}^K \times [-h^K/2, h^K/2]$ whereby we assume uniform layer thicknesses. Herein we use $K = \{t, c, b\}$ as layer index. The surface $\mathfrak{S}^K$ is endowed with an orthonormal coordinate system $\{\boldsymbol{e}_\alpha, \boldsymbol{n}\}$. Every surface is spanned by a two-dimensional position vector $\boldsymbol{r}^K = X^K_\alpha \boldsymbol{e}_\alpha$, i.e. all material points are coplanar. The parameters X^K_α $\forall \alpha = \{1, 2\}$ are the coordinates of the corresponding surface.
Additionally, interfaces $\mathfrak{I}^K$ between the layers are used while the outer surfaces $\mathfrak{O}$ (front) and $\mathfrak{B}$ (back) are cultivated as load application areas. All surfaces, and thus also all interfaces as well as both outer surfaces are plane-parallel. The distance of the surface $\mathfrak{S}^K$ to the interfaces $\mathfrak{I}^K$ or respectively to the outer surface $\mathfrak{O}$ and $\mathfrak{B}$ is $\mp h^K/2$. The origin of the global coordinate system for present composite structure is set at $\mathfrak{S}^c$ concerning the transverse direction so that $-h^t - h^c/2 \leq X_3 \leq h^c/2 + h^b$ holds, cf. Fig. 2.

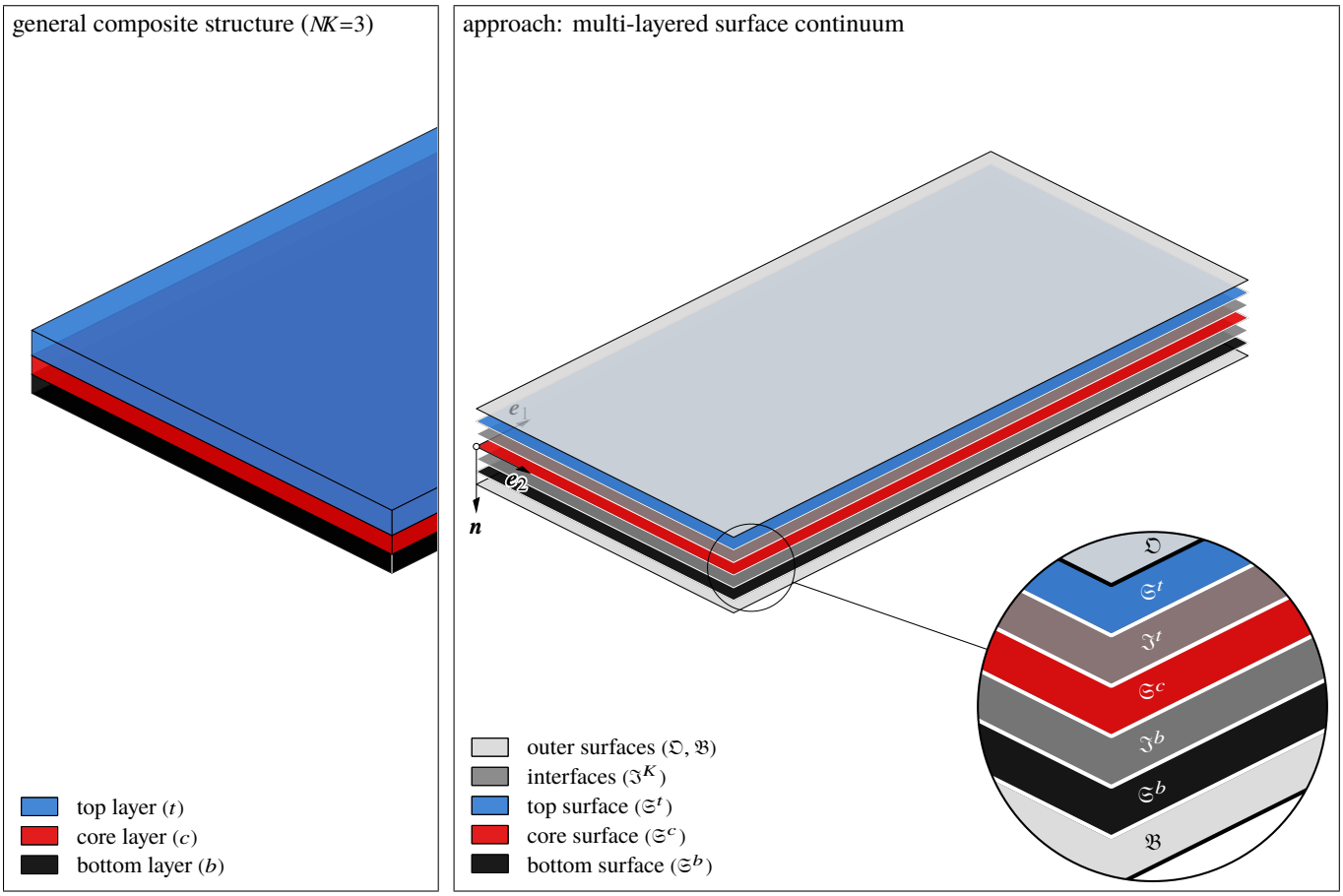

Fig. 2: General composite structure and theoretical considerations restricted to individual surfaces and interfaces

2.1.1 Kinematics

We are dealing with a five-parameter theory, i.e. every surface features three translational and two rotational degrees of freedom. These are summarized in the vectors of translations $\boldsymbol{a}$ and of rotations $\boldsymbol{\varphi}$.

$$\boldsymbol{a}^K = \boldsymbol{v}^K + w^K \boldsymbol{n} \qquad \text{with } \boldsymbol{v}^K = v_\alpha^K \boldsymbol{e}_\alpha \tag{12a}$$

$$\boldsymbol{\varphi}^K = \varphi_\alpha^K \boldsymbol{e}_\alpha \tag{12b}$$

In contrast to a Cosserat surface (with $\boldsymbol{\varphi} = \varphi_\alpha \boldsymbol{e}_\alpha + \varphi_3 \boldsymbol{n}\ \forall i \in \{1,2,3\}$) we neglect drilling rotations φ_3. This is justified since the resistance against wrinkling is much higher compared to that of bending, which is however a pragmatic approach, as is typical in engineering sciences. We furthermore introduce a more physical rotation vector $\boldsymbol{\psi} = -\varphi_2 \boldsymbol{e}_1 + \varphi_1 \boldsymbol{e}_2$ in the spirit of Mindlin (1951), related to the one introduced in Eq. (12b) by $\boldsymbol{\varphi} = \boldsymbol{\psi} \times \boldsymbol{n}$. Based on the degrees of freedoms utilised here, the following special set of deformation measures emerges.

$$\boldsymbol{G}^K = \boldsymbol{\nabla}^{\mathrm{sym}} \boldsymbol{v}^K \tag{13a}$$

$$\boldsymbol{K}^K = \boldsymbol{\nabla}^{\mathrm{sym}} \boldsymbol{\varphi}^K \tag{13b}$$

$$\boldsymbol{g}^K = \boldsymbol{\nabla} w^K + \boldsymbol{\varphi}^K \tag{13c}$$

Here, $\boldsymbol{G}^K = G_{\alpha\beta}^K \boldsymbol{e}_\alpha \otimes \boldsymbol{e}_\beta$ is the in-plane strain tensor, $\boldsymbol{K}^K = K_{\alpha\beta}^K \boldsymbol{e}_\alpha \otimes \boldsymbol{e}_\beta$ is the curvature change tensor, and $\boldsymbol{g}^K = g_\alpha^K \boldsymbol{e}_\alpha$ is the transverse shear strain vector.

2.1.2 Kinetics

Boundary quantities are defined by forces and moments acting at the surface which is in analogy of Cauchys theorem (Cauchy, 2009). Thereby we introduce tangential forces $\boldsymbol{s}_{\mathfrak{S}}^K$ and orthogonal forces $p_{\mathfrak{S}}^K$, as well as out-of-plane moments $\boldsymbol{m}_{\mathfrak{S}}^K$ acting at every single surface.

$$\boldsymbol{n}_{\mathfrak{V}}^K = \lim_{\Delta L \to 0} \frac{\Delta \boldsymbol{s}_{\mathfrak{S}}^K}{\Delta L} \qquad \boldsymbol{m}_{\mathfrak{V}}^K = \lim_{\Delta L \to 0} \frac{\Delta (\boldsymbol{m}_{\mathfrak{S}}^K \times \boldsymbol{n})}{\Delta L} \qquad q_{\mathfrak{V}}^K = \lim_{\Delta L \to 0} \frac{\Delta p_{\mathfrak{S}}^K}{\Delta L} \tag{14}$$

Herein L is a length measure. The vectors and the scalar of the left hand-sides indicate the boundary resultants of the in-plane state $\boldsymbol{n}_{\mathfrak{V}}^K$, the out-of-plane state $\boldsymbol{m}_{\mathfrak{V}}^K$ and the transverse shear state $q_{\mathfrak{V}}^K$. The orientation of the cut is defined by the corresponding

normal. Thereby we make use of the boundary normals $\boldsymbol{n}$ and $\boldsymbol{\nu}$, whereby $\boldsymbol{n}\cdot\boldsymbol{\nu} = 0$ holds. Following Cauchy, a tensor field exists to the boundary resultants introduced in Eq. (14). The following applies to boundaries with normals $\boldsymbol{n}$.

$$\boldsymbol{n}\cdot\boldsymbol{N}^K = \boldsymbol{o} \qquad \boldsymbol{n}\cdot\boldsymbol{L}^K = \boldsymbol{o} \qquad \boldsymbol{n}\cdot\boldsymbol{q}^K = 0 \tag{15}$$

However, with the boundary normal $\boldsymbol{\nu}$, which points along the plane directions, the following boundary loads result.

$$\boldsymbol{\nu}\cdot\boldsymbol{N}^K = \boldsymbol{n}_{\boldsymbol{\nu}}^K \qquad \boldsymbol{\nu}\cdot\boldsymbol{L}^K = \boldsymbol{m}_{\boldsymbol{\nu}}^K \qquad \boldsymbol{\nu}\cdot\boldsymbol{q}^K = q_{\boldsymbol{\nu}}^K \tag{16}$$

Analogous to Cauchys Lemma, the resultants at opposite edges are equal in magnitude, but antithetically.

$$\boldsymbol{n}_{\boldsymbol{\nu}}^K(-\boldsymbol{\nu}) = -\boldsymbol{n}_{\boldsymbol{\nu}}^K(\boldsymbol{\nu}) \qquad \boldsymbol{m}_{\boldsymbol{\nu}}^K(-\boldsymbol{\nu}) = -\boldsymbol{m}_{\boldsymbol{\nu}}^K(\boldsymbol{\nu}) \qquad q_{\boldsymbol{\nu}}^K(-\boldsymbol{\nu}) = -q_{\boldsymbol{\nu}}^K(\boldsymbol{\nu}) \tag{17}$$

Tensors for the stress resultants arise from Eqs. (15) and (16). Here $\boldsymbol{N}^K = N_{\alpha\beta}^K \boldsymbol{e}_\alpha \otimes \boldsymbol{e}_\beta$ is the in-plane force tensor, $\boldsymbol{L}^K = M_{\alpha\beta}^K \boldsymbol{e}_\alpha \otimes \boldsymbol{e}_\beta$ is the polar tensor of moments, and $\boldsymbol{q}^K = Q_\alpha^K \boldsymbol{e}_\alpha$ is the transverse shear force vector.

2.1.3 Constitutive Relations

We reduce our concern to homogeneous and isotropic materials and consider a simple elastic material in the spirit of Noll (1958), where the kinetics in maximum depend on the first gradient of the deformation measures. Since we consider decoupled deformations states, the dependencies can be given by the mappings $\mathcal{F}_i^K$ being constitutive functions.

$$\text{membrane state:} \quad \boldsymbol{N}^K = \mathcal{F}_1^K\left(\boldsymbol{G}^K\right) \tag{18a}$$

$$\text{bending state:} \quad \boldsymbol{L}^K = \mathcal{F}_2^K\left(\boldsymbol{K}^K\right) \tag{18b}$$

$$\text{transverse shear state:} \quad \boldsymbol{q}^K = \mathcal{F}_3^K\left(\boldsymbol{g}^K\right) \tag{18c}$$

When linearizing the functions $\mathcal{F}_i^K$, which is justified in a completely linear theory, we can determine the following constitutive tensors (Aßmus et al., 2017b).

$$\mathcal{F}_1^K: \quad \mathbb{A}^K = 2B^K h^K \quad \mathbb{P}_1 + 2G^K h^K \quad \mathbb{P}_2 \tag{19a}$$

$$\mathcal{F}_2^K: \quad \mathbb{D}^K = 2B^K \frac{\left(h^K\right)^3}{12}\mathbb{P}_1 + 2G^K \frac{\left(h^K\right)^3}{12}\mathbb{P}_2 \tag{19b}$$

$$\mathcal{F}_3^K: \quad \boldsymbol{Z}^K = 2G^K \frac{\kappa^K h^K}{2}\boldsymbol{P} \tag{19c}$$

We thereby make use of the projector representation which allows a clear split into dilatoric and deviatoric portions (Rychlewski, 1984). The fourth-order tensors $\mathbb{P}_\alpha$ and the second-order tensor $\boldsymbol{P}$ used therein are defined as follows.

$$\mathbb{P}_1 = {}^1\!/_2\, \boldsymbol{P} \otimes \boldsymbol{P} \tag{20}$$

$$\mathbb{P}_2 = \mathbb{P}^{\mathrm{sym}} - \mathbb{P}_1 \tag{21}$$

$$\boldsymbol{P} = \boldsymbol{e}_\alpha \otimes \boldsymbol{e}_\alpha \tag{22}$$

Herein, $\boldsymbol{P}$ is the first metric tensor and $\mathbb{P}^{\mathrm{sym}} = {}^1\!/_2\,(\boldsymbol{e}_\alpha \otimes \boldsymbol{e}_\beta \otimes \boldsymbol{e}_\alpha \otimes \boldsymbol{e}_\beta + \boldsymbol{e}_\alpha \otimes \boldsymbol{e}_\beta \otimes \boldsymbol{e}_\beta \otimes \boldsymbol{e}_\alpha)$ is the symmetric part of the fourth-order identity of a plane surface. In Eqs. (19a)–(19c) we've introduced two material parameters B^K and G^K. This is the compression modulus of the surface $B^K = {}^{Y^K}\!/_{(2-2\nu^K)}$ and the shear modulus $G^K = {}^{Y^k}\!/_{(2+\nu^K)}$, while Y^k is Young's modulus and ν^K is Poisson's ratio. We furthermore make use of the structural thickness of the individual layer (h^K) and an individual transverse shear correction factor ($0 < \kappa^K \leq 1$, Vlachoutsis (1992)). In order to relate this representation to the ones used in classical theories for thin-walled members, the stiffnesses associated with the individual deformation portions are introduced. These are the membrane stiffness D_{M}^K, the bending stiffness D_{B}^K, and the transverse shear stiffness D_{S}^K, determined by the arithmetic means of the stiffness measures introduced in (19a)–(19c).

$$D_{\mathrm{M}}^K = \frac{1}{2}\left[2B^K h^K \quad +2G^K h^K\right] \tag{23a}$$

$$D_{\mathrm{B}}^K = \frac{1}{2}\left[2B^K \frac{\left(h^K\right)^3}{12} \quad +2G^K \frac{\left(h^K\right)^3}{12}\right] \tag{23b}$$

$$D_{\mathrm{S}}^K = \kappa^K G^K h^K \tag{23c}$$

By the aid of these engineering stiffnesses, one can reformulate Eqs. (19a)–(19c) to a LamÃľ-like representation (Lamé, 1866), cf. Aßmus (2019). However, through above procedure we can write the constitutive relations as linear mappings in analogy to Hooke's law (Hooke, 1678).

$$\boldsymbol{N}^K = \mathbb{A}^K : \boldsymbol{G}^K \tag{24a}$$

$$\boldsymbol{L}^K = \mathbb{D}^K : \boldsymbol{K}^K \tag{24b}$$

$$\boldsymbol{q}^K = \boldsymbol{Z}^K \cdot \boldsymbol{g}^K \tag{24c}$$

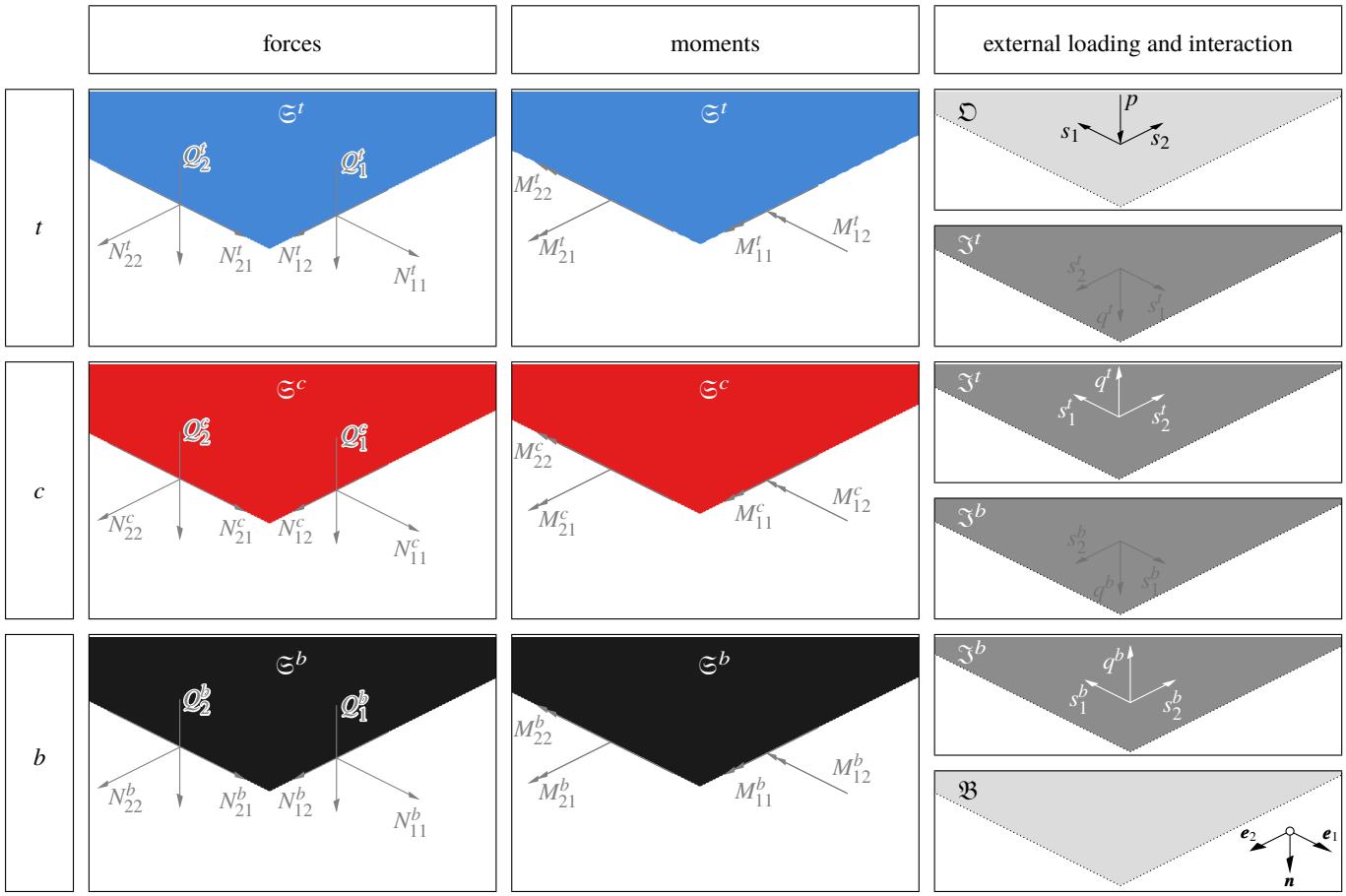

Fig. 3: Geometry, material, boundary conditions and discretization to determine the range of application of present approach

2.1.4 Boundary Conditions

For the description of the boundary conditions we distinguish between Dirichlet $\partial\mathfrak{S}_\mathrm{D}$ and Neumann boundaries $\partial\mathfrak{S}_\mathrm{N}$, which are defined at the boundary $\partial\mathfrak{S}$ of every two-dimensional body manifold.

$$\partial\mathfrak{S}^K = \partial\mathfrak{S}^K_\mathrm{D} \cup \partial\mathfrak{S}^K_\mathrm{N} \qquad\qquad \partial\mathfrak{S}^K_\mathrm{D} \cap \partial\mathfrak{S}^K_\mathrm{N} = \emptyset \tag{25}$$

First, we define constraints in the form of prescribed translations and rotations.

$$\begin{aligned} \boldsymbol{v}^K(\boldsymbol{r}_0) &= \left(\boldsymbol{v}^K\right)^\star(\boldsymbol{r}_0) \\ \boldsymbol{\varphi}^K(\boldsymbol{r}_0) &= \left(\boldsymbol{\varphi}^K\right)^\star(\boldsymbol{r}_0) \qquad\qquad \forall\, \boldsymbol{r}_0^K \in \partial\mathfrak{S}_\mathrm{D} \\ w^K(\boldsymbol{r}_0) &= \left(w^K\right)^\star(\boldsymbol{r}_0^K) \end{aligned} \tag{26}$$

Further, it is possible to link forces and moments that can act as loads at the boundary of the surface continuum with the stress resultants.

$$\boldsymbol{\nu}\cdot\boldsymbol{N}^K = \left(\boldsymbol{n}^K_{\boldsymbol{\nu}}\right)^\star \qquad \boldsymbol{\nu}\cdot\boldsymbol{L}^K = \left(\boldsymbol{m}^K_{\boldsymbol{\nu}}\right)^\star \qquad \boldsymbol{\nu}\cdot\boldsymbol{q}^K = \left(q^K_{\boldsymbol{\nu}}\right)^\star \qquad \forall\, \boldsymbol{r}_0^K \in \partial\mathfrak{S}_\mathrm{N} \tag{27}$$

2.1.5 Coupling Constraints

In order to couple the three layers whose basic equations have been considered separately up to this point, kinematic constraints are introduced. These are as follows.

- straight line hypothesis (Mindlin, 1951) holds true for every $\mathfrak{S}^K\ \forall\ K \in \{t, c, b\}$ separately
- identical deflections of all layers
- no slipping at interfaces (virgin state)

We use these restrictions to formulate subsequent constraints.

$$\boldsymbol{v}^t + \frac{h^t}{2}\boldsymbol{\psi}^t = \boldsymbol{v}^c - \frac{h^c}{2}\boldsymbol{\psi}^c \qquad \text{on } \Im^t \tag{28a}$$

$$\boldsymbol{v}^b - \frac{h^b}{2}\boldsymbol{\psi}^b = \boldsymbol{v}^c + \frac{h^c}{2}\boldsymbol{\psi}^c \qquad \text{on } \Im^b \tag{28b}$$

$$w = w^t = w^c = w^b \qquad \forall\, \Im^K \tag{28c}$$

By the aid of these simplifications we can reduce the number of independent degrees of freedom to nine, i.e. u_1^t, u_2^t, u_1^b, u_2^b, w, φ_1^t, φ_2^t, φ_1^b, and φ_2^b.

2.1.6 Global Variables

Due to the constraints introduced, the degrees of freedom depend on measures of the top and bottom layer only. That is why we introduce global variables with superscript indexes $^\circ$ and $^\Delta$. These quantities are introduced with respect to the global coordinate system with origin at $-h^t - {}^{h^c}/_2 \leq X_3 \leq {}^{h^c}/_2 + h^b$. We inaugurate these global quantities for the degrees of freedom

$$\boldsymbol{v}^\circ = {}^1/_2\left[\boldsymbol{v}^t + \boldsymbol{v}^b\right] \qquad \boldsymbol{v}^\Delta = {}^1/_2\left[\boldsymbol{v}^t - \boldsymbol{v}^b\right] \tag{29a}$$

$$\boldsymbol{\varphi}^\circ = {}^1/_2\left[\boldsymbol{\varphi}^t + \boldsymbol{\varphi}^b\right] \qquad \boldsymbol{\varphi}^\Delta = {}^1/_2\left[\boldsymbol{\varphi}^t - \boldsymbol{\varphi}^b\right], \tag{29b}$$

the deformation measures

$$\boldsymbol{G}^\circ = {}^1/_2\left[\boldsymbol{G}^t + \boldsymbol{G}^b\right] \qquad \boldsymbol{G}^\Delta = {}^1/_2\left[\boldsymbol{G}^t - \boldsymbol{G}^b\right] \tag{30a}$$

$$\boldsymbol{K}^\circ = {}^1/_2\left[\boldsymbol{K}^t + \boldsymbol{K}^b\right] \qquad \boldsymbol{K}^\Delta = {}^1/_2\left[\boldsymbol{K}^t - \boldsymbol{K}^b\right] \tag{30b}$$

$$\boldsymbol{g}^\circ = {}^1/_2\left[\boldsymbol{g}^t + \boldsymbol{g}^b\right] \qquad \boldsymbol{g}^\Delta = {}^1/_2\left[\boldsymbol{g}^t - \boldsymbol{g}^b\right], \tag{30c}$$

the constitutive tensors

$$\mathbb{A}^\circ = \mathbb{A}^t + \mathbb{A}^b \qquad \mathbb{A}^\Delta = \mathbb{A}^t - \mathbb{A}^b \tag{31a}$$

$$\mathbb{D}^\circ = \mathbb{D}^t + \mathbb{D}^b \qquad \mathbb{D}^\Delta = \mathbb{D}^t - \mathbb{D}^b \tag{31b}$$

$$\boldsymbol{Z}^\circ = \boldsymbol{Z}^t + \boldsymbol{Z}^b \qquad \boldsymbol{Z}^\Delta = \boldsymbol{Z}^t - \boldsymbol{Z}^b, \tag{31c}$$

and the stress resultants

$$\boldsymbol{N}^\circ = \sum_K \boldsymbol{N}^K \qquad \boldsymbol{N}^\Delta = \boldsymbol{N}^t - \boldsymbol{N}^b \tag{32a}$$

$$\boldsymbol{L}^\circ = \sum_K \boldsymbol{L}^K + \frac{1}{2}[h^c + h^b]\boldsymbol{N}^b + \frac{1}{2}[h^c + h^t]\boldsymbol{N}^t \qquad \boldsymbol{L}^\Delta = \boldsymbol{L}^t - \boldsymbol{L}^b \tag{32b}$$

$$\boldsymbol{q}^\circ = \sum_K \boldsymbol{q}^K \qquad \boldsymbol{q}^\Delta = \boldsymbol{q}^t - \boldsymbol{q}^b. \tag{32c}$$

For the sake of simplicity we introduce subsequent abbreviations for geometric measures.

$$h^\circ = {}^1/_2\left[h^t + h^b\right] \qquad h^\Delta = {}^1/_2\left[h^t - h^b\right] \tag{33a}$$

This helps us to keep the equations in the subsequent procedures as compact as possible. We have to point out that this introduction is arbitrary. As described in Aßmus (2019), all of these global quantities are clearly traceable to layer-wise quantities $K \in \{t, c, b\}$.

2.1.7 Variational Form

As usual, closed-form solutions are feasible for special compositions, boundary conditions, and loading scenarios only. Approaches to such solutions can be found in Naumenko and Eremeyev (2014) (plate strip with shear-rigid skins) or Eisenträger et al. (2015) (plate with shear-rigid skins), for example. A general closed-form solution of the present problem does not exist, which would have to be proven. In contrast to such laborious solution approaches, computational solutions gained huge popularity nowadays. The most popular one seems one seems to be the finite element method Finite Element Method (FEM). The FEM is based on the weak formulation since this relation usually represents a variational principle which is satisfied by the solution. This is achieved here by exploiting the principle of virtual work (PVW). PVW is characterized by the global virtual work balance.

$$\delta W_{\text{int}} = \delta W_{\text{ext}} \tag{34}$$

Considering aforementioned governing equations while involving the global variables introduced, weighting the balance equations with test functions equivalent to the vectors of the degrees of freedom and subsequent partial integration over the area of

investigation $\Re$, we can derive the following expressions for the virtual internal work

$$\begin{aligned}\delta W_{\text{int}} = \int_{\Re} \Big\{ & \delta \boldsymbol{G}^{\circ} : \mathbb{A}^{\circ} : \boldsymbol{G}^{\circ} + \delta \boldsymbol{G}^{\Delta} : \mathbb{A}^{\circ} : \boldsymbol{G}^{\Delta} + \delta \boldsymbol{G}^{\circ} : \mathbb{A}^{\Delta} : \boldsymbol{G}^{\Delta} \\ & + \delta \boldsymbol{G}^{\Delta} : \mathbb{A}^{\Delta} : \boldsymbol{G}^{\circ} + \left[\delta \boldsymbol{G}^{\circ} + \frac{1}{2} h^{\Delta} \delta \boldsymbol{K}^{\circ} + \frac{1}{2} h^{\circ} \delta \boldsymbol{K}^{\Delta} \right] : \mathbb{A}^{c} : \left[\boldsymbol{G}^{\circ} + \frac{1}{2} h^{\Delta} \boldsymbol{K}^{\circ} + \frac{1}{2} h^{\circ} \boldsymbol{K}^{\Delta} \right] \\ & + \delta \boldsymbol{g}^{\circ} \cdot \boldsymbol{Z}^{\circ} \cdot \boldsymbol{g}^{\circ} + \delta \boldsymbol{g}^{\Delta} \cdot \boldsymbol{Z}^{\circ} \cdot \boldsymbol{g}^{\Delta} + \delta \boldsymbol{g}^{\circ} \cdot \boldsymbol{Z}^{\Delta} \cdot \boldsymbol{g}^{\Delta} + \delta \boldsymbol{g}^{\Delta} \cdot \boldsymbol{Z}^{\circ} \cdot \boldsymbol{g}^{\circ} \\ & + \left[\delta \boldsymbol{g}^{\circ} - \frac{1}{h^{c}} \left(2 \delta \boldsymbol{v}^{\Delta} + (h^{c} + h^{\circ}) \, \delta \boldsymbol{\varphi}^{\circ} + h^{\Delta} \delta \boldsymbol{\varphi}^{\Delta} \right) \right] \cdot \boldsymbol{Z}^{c} \cdot \left[\boldsymbol{g}^{\circ} - \frac{1}{h^{c}} \left(2 \boldsymbol{v}^{\Delta} + (h^{c} + h^{\circ}) \, \boldsymbol{\varphi}^{\circ} + h^{\Delta} \boldsymbol{\varphi}^{\Delta} \right) \right] \\ & + \delta \boldsymbol{K}^{\circ} : \mathbb{D}^{\circ} : \boldsymbol{K}^{\circ} + \delta \boldsymbol{K}^{\Delta} : \mathbb{D}^{\circ} : \boldsymbol{K}^{\Delta} + \delta \boldsymbol{K}^{\circ} : \mathbb{D}^{\Delta} : \boldsymbol{K}^{\Delta} + \delta \boldsymbol{K}^{\Delta} : \mathbb{D}^{\Delta} : \boldsymbol{K}^{\circ} \\ & + \frac{1}{(h^{c})^{2}} \left[2 \delta \boldsymbol{G}^{\Delta} + h^{\circ} \delta \boldsymbol{K}^{\circ} + h^{\Delta} \delta \boldsymbol{K}^{\Delta} \right] : \mathbb{D}^{c} : \left[2 \boldsymbol{G}^{\Delta} + h^{\circ} \boldsymbol{K}^{\circ} + h^{\Delta} \boldsymbol{K}^{\Delta} \right] \Big\} \mathrm{d}\Re \,, \end{aligned} \tag{35a}$$

and the virtual external work

$$\begin{aligned}\delta W_{\text{ext}} = \int_{\partial \Re_{\text{p}}} \Big\{ & \left[\delta \boldsymbol{v}^{\circ} + \frac{1}{2} h^{\Delta} \delta \boldsymbol{\varphi}^{\circ} \right] \cdot \boldsymbol{n}_{\nu}^{\circ} + \left[\delta \boldsymbol{v}^{\Delta} + \frac{1}{2} (h^{c} + h^{\circ}) \, \delta \boldsymbol{\varphi}^{\circ} \right] \cdot \boldsymbol{n}_{\nu}^{\Delta} \\ & + \frac{1}{2} h^{\circ} \delta \boldsymbol{\varphi}^{\Delta} \cdot \boldsymbol{n}_{\nu}^{c} + \delta w q_{\nu}^{\circ} + \delta \boldsymbol{\varphi}^{\circ} \cdot \boldsymbol{m}_{\nu}^{\circ} + \delta \boldsymbol{\varphi}^{\Delta} \cdot \boldsymbol{m}_{\nu}^{\Delta} \\ & - \frac{1}{h^{c}} \left[2 \delta \boldsymbol{v}^{\Delta} + (h^{c} + h^{\circ}) \, \delta \boldsymbol{\varphi}^{\circ} + h^{\Delta} \delta \boldsymbol{\varphi}^{\Delta} \right] \cdot \boldsymbol{m}_{\nu}^{c} \Big\} \mathrm{d}\, \partial \Re_{\text{p}} \\ & + \int_{\Re_{\text{p}}} \left[\frac{h^{t}}{2} \left(\delta \boldsymbol{\varphi}^{\circ} + \delta \boldsymbol{\varphi}^{\Delta} \right) \cdot \boldsymbol{s} - \left(\delta \boldsymbol{v}^{\circ} + \delta \boldsymbol{v}^{\Delta} \right) \cdot \boldsymbol{s} + \delta w p \right] \mathrm{d}\, \Re_{\text{p}} \end{aligned} \tag{35b}$$

Hereby, $\Re_{\text{p}}$ and $\partial \Re_{\text{p}}$ denote the area and boundary of the reference surface $\Re$, where boundary conditions with respect to the stress resultants are prescribed.

$$\left. \begin{aligned} \boldsymbol{N}_{\text{p}}^{K} &= \boldsymbol{N}^{K} \big|_{\partial \Re_{\text{p}}} \\ \boldsymbol{L}_{\text{p}}^{K} &= \boldsymbol{L}^{K} \big|_{\partial \Re_{\text{p}}} \\ \boldsymbol{q}_{\text{p}}^{K} &= \boldsymbol{q}^{K} \big|_{\partial \Re_{\text{p}}} \end{aligned} \right\} \forall \, K \in \{\circ, \Delta, c\} \tag{36}$$

Furthermore, stress resultants on the boundary of the surface continuum have been introduced.

$$\left. \begin{aligned} \boldsymbol{n}_{\nu}^{K} &= \boldsymbol{\nu} \cdot \boldsymbol{N}_{\text{p}}^{K} \\ \boldsymbol{m}_{\nu}^{K} &= \boldsymbol{\nu} \cdot \boldsymbol{L}_{\text{p}}^{K} \\ q_{\nu}^{K} &= \boldsymbol{\nu} \cdot \boldsymbol{q}_{\text{p}}^{K} \end{aligned} \right\} \forall \, K \in \{\circ, \Delta, c\} \tag{37}$$

However, we can identify nine independent global degrees of freedom, i.e. v_1°, v_2°, v_1^{Δ}, v_2^{Δ}, w, φ_1°, φ_2°, φ_1^{Δ}, and φ_2^{Δ}.

2.2 Computational Implementation

The FEM is based on a strict separation of structural Ω and element level Ω^e.

$$\Omega = \bigcup_{e=1}^{NE} \Omega^e \qquad \Omega^i \cap \Omega^j = \emptyset \quad \text{for} \quad i \neq j \quad \text{while } i, j = \{1 \dots NE\} \tag{38}$$

In what follows we utilize quadrilateral elements of Ω^e. However, the virtual works of the overall domain are formed by the summation of the individual contributions of the sub-domains, i.e. of the finite elements.

$$\delta W_{\text{int}} = \sum_{e=1}^{NE} \delta W_{\text{int}}^{e} \qquad \delta W_{\text{ext}} = \sum_{e=1}^{NE} \delta W_{\text{ext}}^{e} \tag{39}$$

Herein, NE is the number of elements in the overall domain. In the sequel, for reasons of practicability, we make use of the vector-matrix notation, cf. Voigt (1889). In principle, the present approach is in accordance with the procedure presented in Eisenträger et al. (2015) while we here give a detailed disclosure of the computational implementation. However, the origin for the numerical implementation certainly lies in the work of Simo and Fox (1989) and Simo et al. (1989).

2.2.1 Approximation of Field Quantities

In present context it is sufficient to use the two-dimensional position vector for the geometrical description of a material point at the reference surface $\Re$.

$$\mathbf{x} = \begin{bmatrix} X_1 & X_2 \end{bmatrix}^\top \tag{40}$$

This is possible since we have reduced our concern to a global coordinate system $\{e_\alpha, \boldsymbol{n}\}$ with the definition of a reference surface $\Re$ which coincides with the mid surface of the core layer. Thus all layers can be represented by only one element in thickness direction. In order to discretize equations, the vector of DOF's at every node i is specified as follows.

$$\mathbf{a}^i = \begin{bmatrix} v_1^{\circ i} & v_2^{\circ i} & v_1^{\Delta i} & v_2^{\Delta i} & w^i & \varphi_1^{\circ i} & \varphi_2^{\circ i} & \varphi_1^{\Delta i} & \varphi_2^{\Delta i} \end{bmatrix}^\top \qquad \forall\, i = \{1, \ldots, NN\} \tag{41}$$

while $NN = 8$ is the number of nodes per element for the present implementation. It becomes apparent that this definition results from the introduction of global degrees of freedom as presented in Eqs. (29a) and (29b). All node vectors of the degrees of freedom are combined in the element vector.

$$\mathbf{a}^e = \begin{bmatrix} \mathbf{a}^1 & \mathbf{a}^2 & \mathbf{a}^3 & \ldots & \mathbf{a}^{NN} \end{bmatrix}^\top \tag{42}$$

In order to obtain the fields of DOF's over the element with respect to the natural coordinates $\boldsymbol{\xi}$, the DOF's are interpolated into the shape functions, applying the isoparametric element concept.

$$\mathbf{a}(\boldsymbol{\xi}) = \begin{bmatrix} v_1^\circ(\boldsymbol{\xi}) & v_2^\circ(\boldsymbol{\xi}) & v_1^\Delta(\boldsymbol{\xi}) & v_2^\Delta(\boldsymbol{\xi}) & w(\boldsymbol{\xi}) & \varphi_1^\circ(\boldsymbol{\xi}) & \varphi_2^\circ(\boldsymbol{\xi}) & \varphi_1^\Delta(\boldsymbol{\xi}) & \varphi_2^\Delta(\boldsymbol{\xi}) \end{bmatrix}^\top \approx \mathbf{N}(\boldsymbol{\xi})\, \mathbf{a}^e \tag{43}$$

Herein $\mathbf{N}(\boldsymbol{\xi})$ is the matrix of shape functions.

$$\mathbf{N}(\boldsymbol{\xi}) = \begin{bmatrix} \mathbf{N}^1(\boldsymbol{\xi}) & \mathbf{N}^2(\boldsymbol{\xi}) & \ldots & \mathbf{N}^{NN}(\boldsymbol{\xi}) \end{bmatrix} \tag{44}$$

2.2.2 Shape Functions and Coordinate Transformations

As demonstrated, shape functions have to be introduced to approximate solutions. In the sequel we make use of SERENDIPITY-type shape functions, i.e. introduce functions of the polynomial degree $PG = 2$ (Szabó and Babuška, 1991).

$$N^i(\boldsymbol{\xi}) = {}^1\!/_4 \left[1 + \xi_1^i \xi_1\right] \left[1 + \xi_2^i \xi_2\right] \left[\xi_1^i \xi_1 + \xi_2^i \xi_2 - 1\right] \qquad i \in \{1, \ldots, 4\} \tag{45a}$$

$$N^i(\boldsymbol{\xi}) = {}^1\!/_2 \left[1 + \xi_1^i \xi_1\right] \left[1 - \xi_2^2\right] \qquad i \in \{6, 8\} \tag{45b}$$

$$N^i(\boldsymbol{\xi}) = {}^1\!/_2 \left[1 + \xi_2^i \xi_2\right] \left[1 - \xi_1^2\right] \qquad i \in \{5, 7\} \tag{45c}$$

With the aid of these shape functions, we can assemble the matrix of shape functions at every node i.

$$\mathbf{N}^i(\boldsymbol{\xi}) = N^i(\boldsymbol{\xi})\, \mathbf{I}\,, \tag{46}$$

Thereby, $\mathbf{I}$ is a unit matrix, whose number of columns and rows is equal to the number of DOF's per node. This interpolation is performed in the natural coordinates of the finite element $-1 \le \xi_\alpha \le 1\ \forall\, \alpha \in \{1, 2\}$. Since the functions are represented by isoparametric coordinates, a transformation relation between the two coordinate systems (physical and natural) is sought. This is realized via the so called Jacobi matrix $\mathbf{J}(\boldsymbol{\xi})$. In two dimensions, the transformations can be represented as follows (Oñate, 2013).

$$\frac{\partial}{\partial \boldsymbol{\xi}} = \mathbf{J}(\boldsymbol{\xi}) \frac{\partial}{\partial \mathbf{x}} \qquad\qquad \frac{\partial}{\partial \mathbf{x}} = \mathbf{J}(\boldsymbol{\xi})^{-1} \frac{\partial}{\partial \boldsymbol{\xi}} \tag{47}$$

The Jacobi matrices and the individual derivatives are as follows.

$$\mathbf{J}(\boldsymbol{\xi}) = \begin{bmatrix} \dfrac{\partial X_1}{\partial \xi_1} & \dfrac{\partial X_2}{\partial \xi_1} \\ \dfrac{\partial X_1}{\partial \xi_2} & \dfrac{\partial X_2}{\partial \xi_2} \end{bmatrix} \qquad\qquad \mathbf{J}(\boldsymbol{\xi})^{-1} = \frac{1}{|\mathbf{J}(\boldsymbol{\xi})|} \begin{bmatrix} \dfrac{\partial X_2}{\partial \xi_2} & -\dfrac{\partial X_2}{\partial \xi_1} \\ -\dfrac{\partial X_1}{\partial \xi_2} & \dfrac{\partial X_1}{\partial \xi_1} \end{bmatrix} \tag{48}$$

2.2.3 Kinematic Relations

We hereby introduce global deformation measures $\mathbf{e}$ for the membrane (index M), bending (index B), and the transverse shear state (index S).

$$\mathbf{e}_{\mathrm{MB}}(\boldsymbol{\xi}) = \begin{bmatrix} \mathbf{e}_{\mathrm{M}}^\circ & \mathbf{e}_{\mathrm{M}}^\Delta & \mathbf{e}_{\mathrm{B}}^\circ & \mathbf{e}_{\mathrm{B}}^\Delta \end{bmatrix}^\top \qquad\qquad \mathbf{e}_{\mathrm{S}}(\boldsymbol{\xi}) = \begin{bmatrix} \mathbf{e}_{\mathrm{S}}^\circ & \mathbf{e}_{\mathrm{S}}^\Delta \end{bmatrix}^\top \tag{49}$$

The sub measures introduced therein are defined as follows.

$$\mathbf{e}_{\mathrm{M}}^{\circ} = \begin{bmatrix} G_{11}^{\circ} & G_{22}^{\circ} & 2G_{12}^{\circ} \end{bmatrix}^{\mathrm{T}} = \begin{bmatrix} v_{1,1}^{\circ} & v_{2,2}^{\circ} & v_{1,2}^{\circ} + v_{2,1}^{\circ} \end{bmatrix}^{\mathrm{T}} \tag{50a}$$

$$\mathbf{e}_{\mathrm{M}}^{\Delta} = \begin{bmatrix} G_{11}^{\Delta} & G_{22}^{\Delta} & 2G_{12}^{\Delta} \end{bmatrix}^{\mathrm{T}} = \begin{bmatrix} v_{1,1}^{\Delta} & v_{2,2}^{\Delta} & v_{1,2}^{\Delta} + v_{2,1}^{\Delta} \end{bmatrix}^{\mathrm{T}} \tag{50b}$$

$$\mathbf{e}_{\mathrm{B}}^{\circ} = \begin{bmatrix} K_{11}^{\circ} & K_{22}^{\circ} & 2K_{12}^{\circ} \end{bmatrix}^{\mathrm{T}} = \begin{bmatrix} \varphi_{1,1}^{\circ} & \varphi_{2,2}^{\circ} & \varphi_{1,2}^{\circ} + \varphi_{2,1}^{\circ} \end{bmatrix}^{\mathrm{T}} \tag{50c}$$

$$\mathbf{e}_{\mathrm{B}}^{\Delta} = \begin{bmatrix} K_{11}^{\Delta} & K_{22}^{\Delta} & 2K_{12}^{\Delta} \end{bmatrix}^{\mathrm{T}} = \begin{bmatrix} \varphi_{1,1}^{\Delta} & \varphi_{2,2}^{\Delta} & \varphi_{1,2}^{\Delta} + \varphi_{2,1}^{\Delta} \end{bmatrix}^{\mathrm{T}} \tag{50d}$$

$$\mathbf{e}_{\mathrm{S}}^{\circ} = \begin{bmatrix} g_1^{\circ} & g_2^{\circ} \end{bmatrix}^{\mathrm{T}} = \begin{bmatrix} w_{,1} + \varphi_1^{\circ} & w_{,2} + \varphi_2^{\circ} \end{bmatrix}^{\mathrm{T}} \tag{50e}$$

$$\mathbf{e}_{\mathrm{S}}^{\Delta} = \begin{bmatrix} g_1^{\Delta} & g_2^{\Delta} \end{bmatrix}^{\mathrm{T}} = \begin{bmatrix} \varphi_1^{\Delta} & \varphi_2^{\Delta} \end{bmatrix}^{\mathrm{T}} \tag{50f}$$

All of aforementioned measures represent fields, i.e. they depend on the natural coordinates. However, for reasons of space this dependency was not explicitly specified here. These deformation fields are approximated analogously to the degrees of freedom.

$$\mathbf{e}_{\mathrm{MB}}(\boldsymbol{\xi}) \approx \mathbf{B}_{\mathrm{MB}}(\boldsymbol{\xi})\,\mathbf{a}^{e} \qquad \mathbf{e}_{\mathrm{S}}(\boldsymbol{\xi}) \approx \mathbf{B}_{\mathrm{S}}(\boldsymbol{\xi})\,\mathbf{a}^{e} \tag{51}$$

The $\mathbf{B}$ matrices are compiled from the differential operator $\mathbf{D}$ and the matrix of the shape functions $\mathbf{N}$.

$$\mathbf{B}_{\mathrm{MB}}(\boldsymbol{\xi}) = \mathbf{D}_{\mathrm{MB}}\mathbf{N}(\boldsymbol{\xi}) \qquad \mathbf{B}_{\mathrm{S}}(\boldsymbol{\xi}) = \mathbf{D}_{\mathrm{S}}\mathbf{N}(\boldsymbol{\xi}) \tag{52}$$

The construction of the matrices $\mathbf{B}$ and $\mathbf{D}$ is given in App. A.1.

2.2.4 Constitutive Equations

To implement the constitutive laws, the expressions of the virtual work must be converted into vector-matrix notation also. The basic procedure for transferring constitutive quantities is given in App. A.1. The constitutive equations of the composite level are as follows while we introduce $\mathbf{s}$ as global kinetic measure.

$$\mathbf{s}_{\mathrm{M}}^{\circ} = \left(\hat{\mathbf{C}}_{\mathrm{M}}^{\circ} + \hat{\mathbf{C}}_{\mathrm{M}}^{c}\right)\mathbf{e}_{\mathrm{M}}^{\circ} + \hat{\mathbf{C}}_{\mathrm{M}}^{\Delta}\mathbf{e}_{\mathrm{M}}^{\Delta} + \frac{1}{2}\hat{\mathbf{C}}_{\mathrm{M}}^{c}\left(h^{\Delta}\mathbf{e}_{\mathrm{B}}^{\circ} + h^{\circ}\mathbf{e}_{\mathrm{B}}^{\Delta}\right) \tag{53a}$$

$$\mathbf{s}_{\mathrm{M}}^{\Delta} = \hat{\mathbf{C}}_{\mathrm{M}}^{\circ}\mathbf{e}_{\mathrm{M}}^{\Delta} + \hat{\mathbf{C}}_{\mathrm{M}}^{\Delta}\mathbf{e}_{\mathrm{M}}^{\circ} \tag{53b}$$

$$\mathbf{s}_{\mathrm{M}}^{c} = \hat{\mathbf{C}}_{\mathrm{M}}^{c}\left[\mathbf{e}_{\mathrm{M}}^{\circ} + \frac{1}{2}\left(h^{\Delta}\mathbf{e}_{\mathrm{B}}^{\circ} + h^{\circ}\mathbf{e}_{\mathrm{B}}^{\Delta}\right)\right] \tag{53c}$$

$$\mathbf{s}_{\mathrm{S}}^{\circ} = \hat{\mathbf{C}}_{\mathrm{S}}^{\circ}\mathbf{e}_{\mathrm{S}}^{\circ} + \hat{\mathbf{C}}_{\mathrm{S}}^{\Delta}\mathbf{e}_{\mathrm{S}}^{\Delta} + \hat{\mathbf{C}}_{\mathrm{S}}^{c}\left(\mathbf{e}_{\mathrm{S}}^{\circ} + \mathbf{A}_1\mathbf{a}\right) \tag{53d}$$

$$\mathbf{s}_{\mathrm{S}}^{\Delta} = \hat{\mathbf{C}}_{\mathrm{S}}^{\circ}\mathbf{e}_{\mathrm{S}}^{\Delta} + \hat{\mathbf{C}}_{\mathrm{S}}^{\Delta}\mathbf{e}_{\mathrm{S}}^{\circ} \tag{53e}$$

$$\mathbf{s}_{\mathrm{S}}^{c} = \hat{\mathbf{C}}_{\mathrm{S}}^{c}\left(\mathbf{e}_{\mathrm{S}}^{\circ} + \mathbf{A}_1\mathbf{a}\right) \tag{53f}$$

$$\mathbf{s}_{\mathrm{B}}^{\circ} = \hat{\mathbf{C}}_{\mathrm{B}}^{\circ}\mathbf{e}_{\mathrm{B}}^{\circ} + \hat{\mathbf{C}}_{\mathrm{B}}^{\Delta}\mathbf{e}_{\mathrm{B}}^{\Delta} - \frac{1}{h^{c}}\hat{\mathbf{C}}_{\mathrm{B}}^{c}\left(2\mathbf{e}_{\mathrm{M}}^{\Delta} + h^{\circ}\mathbf{e}_{\mathrm{B}}^{\circ} + h^{\Delta}\mathbf{e}_{\mathrm{B}}^{\Delta}\right) - \frac{1}{2}\hat{\mathbf{C}}_{\mathrm{M}}^{\circ}\left[h^{\Delta}\mathbf{e}_{\mathrm{M}}^{\circ} + \left(h^{c} + h^{\circ}\right)\mathbf{e}_{\mathrm{M}}^{\Delta}\right] - \frac{1}{2}\hat{\mathbf{C}}_{\mathrm{M}}^{\Delta}\left[h^{\Delta}\mathbf{e}_{\mathrm{M}}^{\Delta} + \left(h^{c} + h^{\circ}\right)\mathbf{e}_{\mathrm{M}}^{\circ}\right] \tag{53g}$$

$$\mathbf{s}_{\mathrm{B}}^{\Delta} = \hat{\mathbf{C}}_{\mathrm{B}}^{\circ}\mathbf{e}_{\mathrm{B}}^{\Delta} + \hat{\mathbf{C}}_{\mathrm{B}}^{\Delta}\mathbf{e}_{\mathrm{B}}^{\circ} \tag{53h}$$

$$\mathbf{s}_{\mathrm{B}}^{c} = -\frac{1}{h^{c}}\hat{\mathbf{C}}_{\mathrm{B}}^{c}\left(2\mathbf{e}_{\mathrm{M}}^{\Delta} + h^{\circ}\mathbf{e}_{\mathrm{B}}^{\circ} + h^{\Delta}\mathbf{e}_{\mathrm{B}}^{\Delta}\right) \tag{53i}$$

The constitutive matrices $\hat{\mathbf{C}}_{\mathrm{M}}^{K}$, $\hat{\mathbf{C}}_{\mathrm{B}}^{K}$, $\hat{\mathbf{C}}_{\mathrm{S}}^{K}$ $\forall K \in \{\circ, \Delta, c\}$ and the auxiliary matrix $\mathbf{A}_1$ introduced here are enclosed in App. A.1.

2.2.5 Spatial Discretization of Virtual Work

The virtual internal work from Eq. (35a) can now be rewritten as follows.

$$\begin{aligned}\delta W_{\mathrm{int}}^{e} = \int_{\Omega^{e}} \delta\mathbf{a}^{e\,\mathrm{T}} \Big[&\mathbf{B}_{\mathrm{S}}^{\mathrm{T}}\left(\mathbf{C}_{\mathrm{S}}^{\circ} + \mathbf{C}_{\mathrm{S}}^{\Delta} + \mathbf{C}_{\mathrm{S}}^{\Delta\,\mathrm{T}} + \mathbf{A}_2^{\mathrm{T}}\hat{\mathbf{C}}_{\mathrm{S}}^{c}\mathbf{A}_2\right)\mathbf{B}_{\mathrm{S}} + \mathbf{B}_{\mathrm{S}}^{\mathrm{T}}\mathbf{A}_2^{\mathrm{T}}\hat{\mathbf{C}}_{\mathrm{S}}^{c}\mathbf{A}_1\mathbf{N} + \left(\mathbf{B}_{\mathrm{S}}^{\mathrm{T}}\mathbf{A}_2^{\mathrm{T}}\hat{\mathbf{C}}_{\mathrm{S}}^{c}\mathbf{A}_1\mathbf{N}\right)^{\mathrm{T}} + \mathbf{N}^{\mathrm{T}}\mathbf{A}_1^{\mathrm{T}}\hat{\mathbf{C}}_{\mathrm{S}}^{c}\mathbf{A}_1\mathbf{N} \\ &+ \mathbf{B}_{\mathrm{MB}}^{\mathrm{T}}\left(\mathbf{C}_{\mathrm{MB}}^{\circ} + \mathbf{C}_{\mathrm{MB}}^{\Delta} + \mathbf{C}_{\mathrm{MB}}^{\Delta\,\mathrm{T}} + \mathbf{A}_3^{\mathrm{T}}\hat{\mathbf{C}}_{\mathrm{M}}^{c}\mathbf{A}_3 + \mathbf{A}_4^{\mathrm{T}}\hat{\mathbf{C}}_{\mathrm{B}}^{c}\mathbf{A}_4\right)\mathbf{B}_{\mathrm{MB}}\Big]\mathbf{a}^{e}\,\mathrm{d}\Omega^{e}\end{aligned} \tag{54}$$

In addition to the material properties in $\mathbf{C}_{\square}^{K}$ und $\hat{\mathbf{C}}_{\square}^{K}$ $\forall \square \in \{\mathrm{M}, \mathrm{B}, \mathrm{MB}, \mathrm{S}\} \wedge K \in \{\circ, \Delta, c\}$, the expression now only contains the degrees of freedom $[\mathbf{a}^{e}]^{\mathrm{T}}$. $\mathbf{A}_i$ $\forall i \in \{2, 3, 4\}$ are auxiliary matrices so that all quantities correspond to the specified vector of degrees of freedom. The detailed structure of all matrices from (54) can be found in App. A.1. Now we can get the stiffness matrices for membrane-bending and transverse shear separately.

$$\mathbf{K}_{\mathrm{MB}}^{e} = \int_{\Omega^{e}} \left[\mathbf{B}_{\mathrm{MB}}^{\mathrm{T}}\left(\mathbf{C}_{\mathrm{MB}}^{\circ} + \mathbf{C}_{\mathrm{MB}}^{\Delta} + \mathbf{C}_{\mathrm{MB}}^{\Delta\,\mathrm{T}} + \mathbf{A}_3^{\mathrm{T}}\hat{\mathbf{C}}_{\mathrm{M}}^{c}\mathbf{A}_3 + \mathbf{A}_4^{\mathrm{T}}\hat{\mathbf{C}}_{\mathrm{B}}^{c}\mathbf{A}_4\right)\mathbf{B}_{\mathrm{MB}}\right]\mathrm{d}\Omega^{e} \tag{55a}$$

$$\mathbf{K}_{\mathrm{S}}^{e} = \int_{\Omega^{e}} \left[\mathbf{B}_{\mathrm{S}}^{\mathrm{T}}\left(\mathbf{C}_{\mathrm{S}}^{\circ} + \mathbf{C}_{\mathrm{S}}^{\Delta} + \mathbf{C}_{\mathrm{S}}^{\Delta\,\mathrm{T}} + \mathbf{A}_2^{\mathrm{T}}\hat{\mathbf{C}}_{\mathrm{S}}^{c}\mathbf{A}_2\right)\mathbf{B}_{\mathrm{S}} + \mathbf{B}_{\mathrm{S}}^{\mathrm{T}}\mathbf{A}_2^{\mathrm{T}}\hat{\mathbf{C}}_{\mathrm{S}}^{c}\mathbf{A}_1\mathbf{N} + \left(\mathbf{B}_{\mathrm{S}}^{\mathrm{T}}\mathbf{A}_2^{\mathrm{T}}\hat{\mathbf{C}}_{\mathrm{S}}^{c}\mathbf{A}_1\mathbf{N}\right)^{\mathrm{T}} + \mathbf{N}^{\mathrm{T}}\mathbf{A}_1^{\mathrm{T}}\hat{\mathbf{C}}_{\mathrm{S}}^{c}\mathbf{A}_1\mathbf{N}\right]\mathrm{d}\Omega^{e} \tag{55b}$$

The separation is introduced to counter artificial stiffening effects correlated to transverse shear locking. The overall stiffness matrix is now additively composed of both sub matrices.

$$\mathbf{K}^e = \mathbf{K}^e_{\mathrm{MB}} + \mathbf{K}^e_{\mathrm{S}} \tag{56}$$

Eq. (35b) is converted in an analogous way. This results in the following expression.

$$\delta W^e_{\mathrm{ext}} = \int\limits_{\partial\Omega^e_{\mathrm{p}}} \delta\mathbf{a}^{e\top}\mathbf{N}^{\top}\mathbf{A}_5\mathbf{t}\,\mathrm{d}\,\partial\Omega^e_{\mathrm{p}} + \int\limits_{\Omega^e} \delta\mathbf{a}^{e\top}\mathbf{N}^{\top}\mathbf{q}\,\mathrm{d}\Omega^e \tag{57}$$

The vectors $\mathbf{t}$ and $\mathbf{q}$ contain loads distributed over a curve or a surface.

$$\mathbf{t} = \left[\mathbf{n}^{\circ}_{\nu} \quad \mathbf{n}^{\Delta}_{\nu} \quad \mathbf{n}^{c}_{\nu} \quad q^{\circ}_{\nu} \quad \mathbf{m}^{\circ}_{\nu} \quad \mathbf{m}^{\Delta}_{\nu} \quad \mathbf{m}^{c}_{\nu}\right]^{\top} \tag{58}$$

$$\mathbf{q} = \left[-s_1 \quad -s_2 \quad -s_1 \quad -s_2 \quad p \quad \tfrac{h^t}{2}s_1 \quad \tfrac{h^t}{2}s_2 \quad \tfrac{h^t}{2}s_1 \quad \tfrac{h^t}{2}s_2\right]^{\top} \tag{59}$$

The vectors $\mathbf{n}^{\circ}_{\nu}$, $\mathbf{n}^{\Delta}_{\nu}$, $\mathbf{n}^{c}_{\nu}$, $\mathbf{m}^{\circ}_{\nu}$, $\mathbf{m}^{\Delta}_{\nu}$, and $\mathbf{m}^{c}_{\nu}$ refer to expressions in Eq. (37), which are given there in tensor notation. These can be converted into vector-matrix notation and referenced to the domain element Ω^e. However, the right-hand-side vector $\mathbf{r}^e$ comprises line loads $\mathbf{r}^e_1$ and surface loads $\mathbf{r}^e_2$ on the element.

$$\mathbf{r}^e = \mathbf{r}^e_1 + \mathbf{r}^e_2 \tag{60}$$

The sub vectors are determined as follows.

$$\mathbf{r}^e_1 = \int\limits_{\partial\Omega^e_{\mathrm{p}}} \mathbf{N}^{\top}\mathbf{A}_5\mathbf{t}\,\mathrm{d}\,\partial\Omega^e_{\mathrm{p}} \qquad \mathbf{r}^e_2 = \int\limits_{\Omega^e_{\mathrm{p}}} \mathbf{N}^{\top}\mathbf{q}\,\mathrm{d}\Omega^e_{\mathrm{p}} \tag{61}$$

2.2.6 Assembly and Structural Equation

Structure level quantities are generated by summing all elements $e \in [1, NE]$ in Ω. In symbolic notation we make use of the $\cup$ operator.

$$\mathbf{K} = \bigcup_{e=1}^{NE} \mathbf{K}^e \qquad \mathbf{a} = \bigcup_{e=1}^{NE} \mathbf{a}^e \qquad \mathbf{r} = \bigcup_{e=1}^{NE} \mathbf{r}^e \tag{62}$$

Though this assembling we can formulate the spatially approximated weak form.

$$\begin{aligned} \delta W_{\mathrm{int}} &= \delta W_{\mathrm{ext}} \\ \delta\mathbf{a}\cdot\mathbf{K}\,\mathbf{a} &= \delta\mathbf{a}\cdot\mathbf{r} \end{aligned} \tag{63}$$

From Eqs. (34) and (39) it can be deduced that the sum of the virtual works must be zero.

$$\delta W \approx \delta\mathbf{a}\cdot[\mathbf{K}\,\mathbf{a} - \mathbf{r}] = 0 \tag{64}$$

For arbitrary virtual degrees of freedom $\delta\mathbf{a}$ the discrete equation of motion is obtained.

$$\mathbf{K}\,\mathbf{a} = \mathbf{r} \tag{65}$$

The solution of this system of equations is realized by the left-hand multiplication with the inverse of the stiffness matrix $\mathbf{K}^{-1}$.

$$\mathbf{K}^{-1}\mathbf{K}\,\mathbf{a} = \mathbf{I}\,\mathbf{a} = \mathbf{a} = \mathbf{K}^{-1}\,\mathbf{r} \tag{66}$$

The stiffness matrix must not be singular, since the invertibility is then no longer guaranteed. In order to prevent this, so many Dirichlet boundary conditions must be introduced into the structural equation that no rigid body motions are possible. However, in present context we made use of the finite element program system ABAQUS. To solve problems in the manner set forth above, we have programmed a user-defined element (UEL) in a FORTRAN subroutine.

3 Application Range

3.1 Preliminary Remarks

In present contribution we want to emphasize the universality of the proposed approach by highlighting the range of applicability. To be more precise, we seek to determine the broadness in the filed of TLCS. Therefore, we will execute parameter studies at the simple case of constant, homogeneous, and orthogonal loading with a small test load while free supports are applied at all layer boundaries with normals $\boldsymbol{e}_\alpha$. The spatial discretization is realized via an structured mesh where all elements show an aspect ratio $AR = {}^{h^e_{\max}}\!/_{h^e_{\min}} = 1$ while all elements feature inner angles with 90°. Herein, h^e_α is the element edge length. The mesh grid is

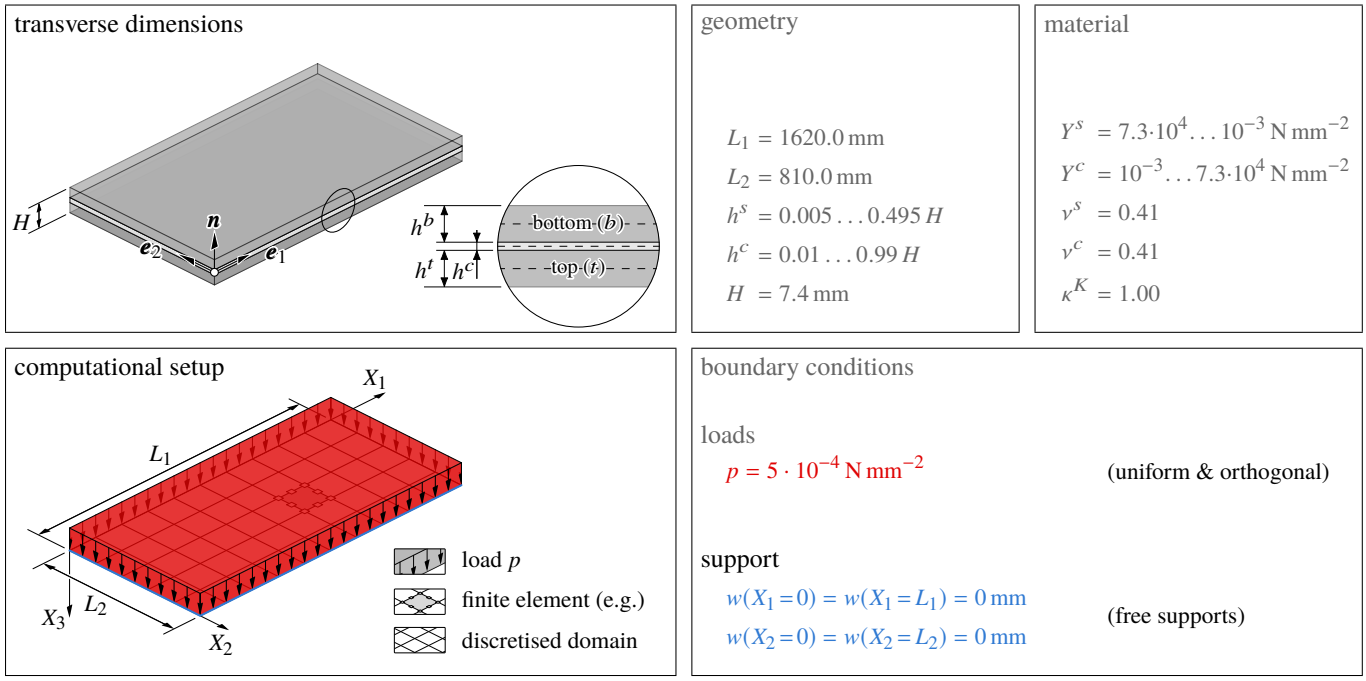

Fig. 4: Geometry, material, boundary conditions and discretization to determine the range of application of present approach

$256 \times 128 = 32768$ elements ($h^e_\alpha \approx 6.33\,\text{mm}$) to guarantee convergence for all subsequent scrutinies. For the sake of simplicity we reduce our concern to a symmetric composite structure. Therefore, the following relations holds true, while we introduce the superscript index s for the skin layers.

$$h^t = h^b = h^s \qquad Y^t = Y^b = Y^s \qquad \nu^t = \nu^b = \nu^s \tag{67}$$

Consequently, the following also applies.

$$B^t = B^b = B^s \qquad G^t = G^b = G^s \qquad D^t_\square = D^b_\square = D^s_\square \qquad \forall\,\square \in \{\mathrm{M}, \mathrm{B}, \mathrm{S}\} \tag{68}$$

We consider a test structure with plane dimensions $L_1 = 1620\,\text{mm}$ and $L_2 = 810\,\text{mm}$ as exemplary values. For present work we want to investigate the limit behavior for three-layered composite structures. Therefore, we introduce two geometrical limiting cases and a transversely evenly distributed geometrical case in context of aforementioned restrictions. These are as follows.

- $h^c = h^s$ (even distributed)
- $h^c = 0.99\,H$ (thick core bound)
- $h^c = 0.01\,H$ (thin core bound)

The corresponding skin layer thicknesses arise from the restriction for the overall thickness H.

$$h^s = \frac{H - h^c}{2} \qquad H \stackrel{!}{=} 7.4\,\text{mm} \tag{69}$$

For the evenly distributed (equal thicknesses) composite this results in a transverse geometry with $h^k = {}^{37}/_{15}\,\text{mm}\ \forall K \in \{c, s\}$. The thin core bound is characterized by $h^c = 0.074\,\text{mm}$ while the thick core is by $h^c = 7.326\,\text{mm}$. However, for all cases it becomes obvious that $L_\alpha \gg H$ holds true.
To determine the working range of XLWT we vary the shear modulus ratio GR, which is a significant measure of the diverging material properties of core and skin layers, determined as follows.

$$GR = \frac{G^c}{G^s} \tag{70}$$

For the sake of simplicity, we reduce our concern to transverse shear correction factors $\kappa^K \equiv 1\ \forall K \in \{t, c, b\}$. The variety of material parameters is given Fig. 4. This results in a shear modulus ratio GR_{min} below 10^{-7} for present investigations, i.e. a maximum difference of more than seven magnitudes of order between the shear moduli alone. In present investigations, this also applies to the Young's modulus ratio $YR = {}^{Y^c}/_{Y^s}$ since $\nu^c = \nu^s$ holds. In this context, the designation *high contrast plates* retains validity. However, we reduce our concern to the case of $GR \leq 1$. In connection with engineering applications, this represents a reasonable limit. Applications with soft skins while the core is stiff seem extremely uncommon. For the opposite limit therefore $GR_{\text{max}} = 1$ holds. Therewith, we can depict two bounds arising from monocoque structures known from theory. So it is possible to determine clearly, two, so-called monolithic limits. This is the shear-rigid monolith (Kirchhoff theory) and the shear-deformable monolith (Mindlin or Reissner theory). From these limits we carry out two investigations whereby we vary the shear modulus ratio through systematically. In a first attempt we decrease the shear modulus of the core layer G^c when starting

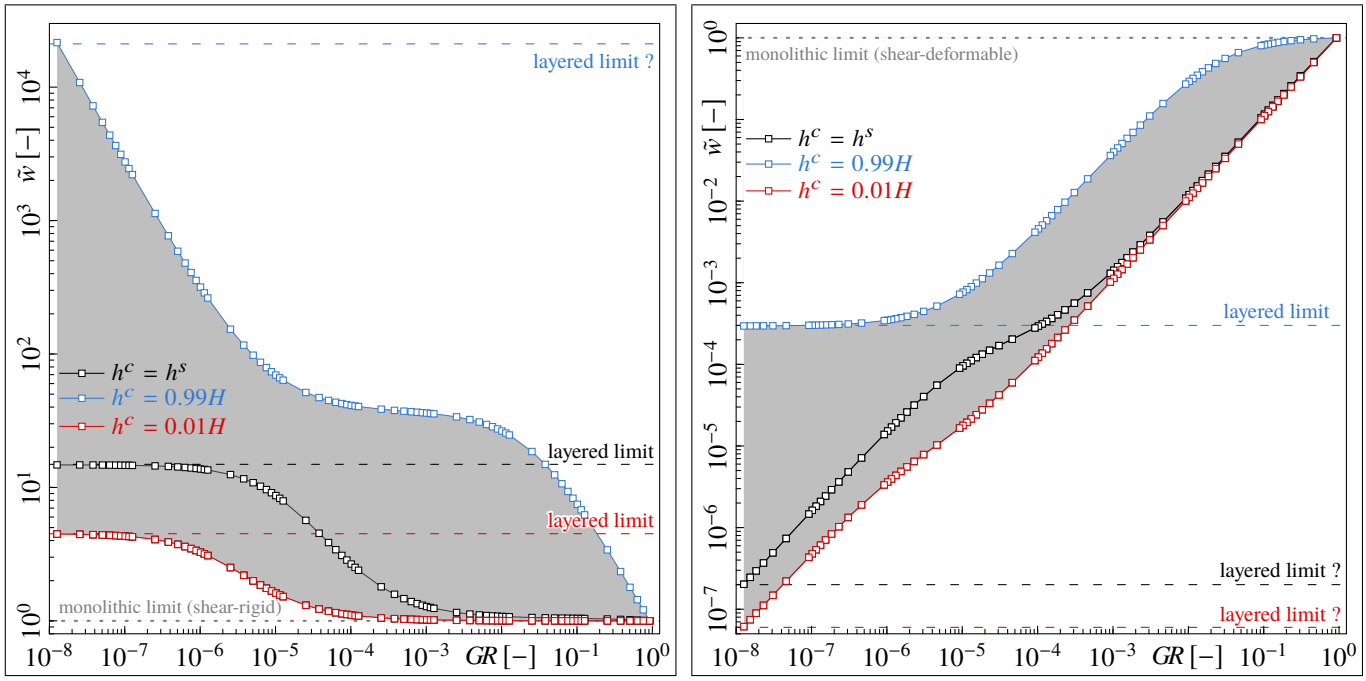

Fig. 5: Results of parameter studies starting from shear-rigid (left) and shear-deformable (right) monolithic limit of symmetric TLCS

from $Y^c = Y^s = 73,000\,{}^{\mathrm{N}}/_{\mathrm{mm}^2}$ ($\Rightarrow$ $GR = 1$, shear-rigid). The second attempt is implemented by the increase of the shear modulus of the skin layers G^s when starting from $Y^c = Y^s = 0.001\,{}^{\mathrm{N}}/_{\mathrm{mm}^2}$ ($\Rightarrow$ $GR = 1$, but shear-deformable). As evaluation criterion we use the deflection of the composite. However, for all variations of GR, we normalize our results of the maximum deflection $w_{\max}$ in the following way for the admissible regime of GR.

$$\tilde{w} = \frac{w_{\max}(GR)}{w_{\max}(GR_{\max})} \qquad w_{\max} = w\left({}^{X_\alpha}/_2\right) \qquad GR_{\min} \leq GR \leq GR_{\max} \tag{71}$$

3.2 Results and Discussion

The results of present investigations are depicted in Fig. 5. On the left-hand side are the results of the examination starting from the shear-rigid monolithic limit and on the right-hand-side are the ones of the examination starting from the shear-deformable monolithic limit.

As previously indicated, for material and geometrical constellations we have used extremal parameters, at least in context of engineering applications (technical feasibility limits and limits of the sensuality). The range of application is localized by the thin core bound (lower bound) and the thick core bound (upper bound) for both procedures. Unsurprisingly, the even distributed composite lies between these two results. The course of the this even distributed composite follows that of the thin core bound. Also appears logical that deflections are increasing when starting present investigations from shear-rigid monolithic limit with decreasing G^c. Vice versa, deflections are decreasing when starting from shear-deformable monolithic limit while increasing G^s. For both investigations the range of application increases with decreasing shear modulus ratio. The results of all geometrical extremal cases coincide in the case $GR = 1$.

As can be found in some publications already (Naumenko and Eremeyev, 2014; Aßmus et al., 2017a), the thin core bound reaches its limits asymptotically when starting from a shear-rigid limit. This also applies to the even distributed composite. In both cases we can identify so called layered limits. This is the case when skin layers glide on each other with almost none resistance. However, for the thick core bound, such a limit does not exist when stating from a shear-rigid monolith. In addition, no asymptotic behavior can be detected either.

Contrary, when starting from the shear-deformable monolithic limit, the thick core bound exhibits an asymptotic behavior, while the layered limit of this bound is clearly identifiable. On the other hand, the existence of layered limits for both, thin core bound and even distributed composite are questionable, at least in the admissible range of GR.

In principle, it must therefore be stated that the use of the *eXtended layer-wise theory* presented here is indispensable, especially for cases in which no layered limit is achieved. However, it is precisely these limit cases that open up the scope of the approach presented here. By the best knowledge of the authors, there is no other known theory for the treatment of mechanical problems at three-layered composite structures with such a wide range of applicability. As already mentioned at the beginning, modern applications require such generalized approaches in order to meet the requirements of strongly diverging material pairings and geometry compositions.

For the sake of completeness, the numerical burden should be mentioned. The computation times were around 30 to 60 seconds on a standard pc (Intel i7-3820 processor, 32 GB RAM, 64 Bit Windows 7 operating system), depending on the material and geometrical constellations. Such short computation times emphasize the efficiency of the approach presented here.

4 Concluding Remarks

4.1 Conclusion

In this work we have introduced a generalized framework for three-layered composite structures to consider strong divergent geometrical and material properties. This was done in the framework of a layer-wise procedure while starting by the aid of the direct approach. Therewith, present approach is geometrically exact. This expression arises from the exact kinematic representation of the two-dimensional surface. This means, that results gained are exact on the mid surface of the individual layer only. The restrictions introduced to couple layers are justifiable for engineering applications. There they will find a broad application, at least in the determination of composite stiffness relations.
In context of the computational solution procedure introduced, the approach to reduce all considerations to a single reference surface simplifies the calculation of present structures where at the same time a large number of composites with arbitrary properties can be computed. Furthermore, we only have low requirements on the shape functions and boundary conditions since present approach requires C^0 continuity only, i.e. only the DOFs themselves have to be continuous on the element boundaries (Hinton et al., 1990). That is a not negligible advantage over C^1 continuous elements as they are needed for the use of shear-rigid theories, i.e. when using the Kirchhoff theory (Kirchhoff, 1850).
We note that the purpose of this paper is to show the the broad scope of application and general validness of the layer-wise model. In that sense, the first-order shear deformation theory and the classical laminate theory that are commonly used arise as special cases when different simplifications are imposed. This is surely also the case to what is known as sandwich theory which has not been identified in the context of present investigations. Some general examples for special cases at layer-level have been given in Aßmus et al. (2019), which show that plate model obtained by the direct approach attains universality, at least in context of engineering applications. However, the broadness of applicability of present layerwise generalisation seems unique.

4.2 Outlook

In present context we reduced our concern to the static load case, linear elastic material behaviour, and small deformations. As in classical continuum theory, extensions lie in the consideration of

- inertia,
- dynamic loading, and
- damping.

Regarding enlargements with respect to kinematics introduced, it is possible to consider

- moderate deformations, i.e.
  - large deflections
  - small in-plane displacements
  - small rotations
- or large deformations, i.e.
  - large deflections
  - large displacements
  - large rotations

while the latter being preferred in context of a consistent generalization. At least in this case, we also have to refomulate the kinematical restrictions (28a) and (28b). The constitutive relations can be extended to nonlinear elastic or inelastic behaviour, e.g.

- viscoelasticity,
- (visco-)plasticity,
- fatigue, and
- damage.

In addition, the consideration of anisotropic material behavior is certainly also a focal point. This may also have to include coupling effects between the different deformation states considered at layer-level, which until now have only been superimposed. All theses extensions hold true for the individual layers. However, within the modular structure of the approach presented here it is simple to enlarge its frame to analyze three-layered composite structures for arbitrary deformations, material behavior and loading conditions, at least up to the borders that exist in classical theory of three-dimensional continua (e.g. uniqueness, etc.). Couplings with thermodynamics, electrodynamics and other non-mechanical influences such as hygroscopic ones are also conceivable.
A special feature of the present approach using a layer-wise contemplation is the consideration of delamination. Thereby it is possible to relax the kinematical constraints (28a) and (28b) whereby advanced traction-separation laws for the interaction between the layers can be introduced.
However, present theory is based on whats known as plate or more generally shell theories. It is generally accepted, that such theories are not capable to prognosticate full and exact information concerning a three-dimensional body manifold which forms the basis of every treatment.

Acknowledgment

The results presented here are outcome of perennial research which was largely funded by the German Research Foundation (grant number 83477795). This support is highly acknowledged. Furthermore, we would like to thank our colleague Stefan Bergmann for reviewing an early draft of present manuscript.

Appendix

A.1 Constitutive Relations in Vector-Matrix Formulation

Consequently, the matrices required in the FEM are to be given in terms of global variables (indices $\circ$, Δ, c) for the three layered composite in vector-matrix form. The constitutive tensors of the global quantities can be introduced in matrix notation as follows, introducing $\mathbf{C}$ as a global stiffness quantity for the sake of simplicity.

$$\hat{\mathbf{C}}_{\mathrm{M}}^{K} = \begin{bmatrix} a_{\mathrm{M}}^{K} + 2b_{\mathrm{M}}^{K} & b_{\mathrm{M}}^{K} & 0 \\ a_{\mathrm{M}}^{K} & a_{\mathrm{M}}^{K} + 2b_{\mathrm{M}}^{K} & 0 \\ 0 & 0 & b_{\mathrm{M}}^{K} \end{bmatrix} \qquad \forall\, K \in \{\circ, \Delta, c\} \tag{A.1a}$$

$$\hat{\mathbf{C}}_{\mathrm{B}}^{K} = \begin{bmatrix} a_{\mathrm{B}}^{K} + 2b_{\mathrm{B}}^{K} & b_{\mathrm{B}}^{K} & 0 \\ a_{\mathrm{B}}^{K} & a_{\mathrm{B}}^{K} + 2b_{\mathrm{B}}^{K} & 0 \\ 0 & 0 & b_{\mathrm{B}}^{K} \end{bmatrix} \qquad \forall\, K \in \{\circ, \Delta, c\} \tag{A.1b}$$

$$\hat{\mathbf{C}}_{\mathrm{S}}^{K} = a_{\mathrm{S}}^{K} \begin{bmatrix} 1 & 0 \\ 0 & 1 \end{bmatrix} \qquad \forall\, K \in \{\circ, \Delta, c\} \tag{A.1c}$$

Here, the following abbreviations have been introduced based on the engineering interpretations for membrane stiffness D_{M}, bending stiffness D_{B}, and transverse shear stiffness D_{S}.

$$a_{L}^{K} = \begin{cases} D_{L}^{t}\nu^{t} + D_{L}^{b}\nu^{b} & \text{if } K = \circ \\ D_{L}^{t}\nu^{t} - D_{L}^{b}\nu^{b} & \text{if } K = \Delta \\ D_{L}^{c}\nu^{c} & \text{if } K = c \end{cases} \qquad \forall\, L \in \{\mathrm{M}, \mathrm{B}\} \tag{A.2a}$$

$$b_{L}^{K} = \begin{cases} \frac{1-\nu^{t}}{2} D_{L}^{t} + \frac{1-\nu^{t}}{2} D_{L}^{b} & \text{if } K = \circ \\ \frac{1-\nu^{t}}{2} D_{L}^{t} - \frac{1-\nu^{t}}{2} D_{L}^{b} & \text{if } K = \Delta \\ \frac{1-\nu^{t}}{2} D_{L}^{c} & \text{if } K = c \end{cases} \qquad \forall\, L \in \{\mathrm{M}, \mathrm{B}\} \tag{A.2b}$$

$$a_{\mathrm{S}}^{K} = \begin{cases} D_{\mathrm{S}}^{t} + D_{\mathrm{S}}^{b} & \text{if } K = \circ \\ D_{\mathrm{S}}^{t} - D_{\mathrm{S}}^{b} & \text{if } K = \Delta \\ D_{\mathrm{S}}^{c} & \text{if } K = c \end{cases} \tag{A.2c}$$

With the above representation, the generalized stiffness matrices can be specified.

$$\mathbf{C}_{\mathrm{MB}}^{\circ} = \begin{bmatrix} \hat{\mathbf{C}}_{\mathrm{M}}^{\circ} & \mathbf{0} & \mathbf{0} & \mathbf{0} \\ \mathbf{0} & \hat{\mathbf{C}}_{\mathrm{M}}^{\circ} & \mathbf{0} & \mathbf{0} \\ \mathbf{0} & \mathbf{0} & \hat{\mathbf{C}}_{\mathrm{B}}^{\circ} & \mathbf{0} \\ \mathbf{0} & \mathbf{0} & \mathbf{0} & \hat{\mathbf{C}}_{\mathrm{B}}^{\circ} \end{bmatrix} \tag{A.3a}$$

$$\mathbf{C}_{\mathrm{MB}}^{\Delta} = \begin{bmatrix} \mathbf{0} & \hat{\mathbf{C}}_{\mathrm{M}}^{\Delta} & \mathbf{0} & \mathbf{0} \\ \mathbf{0} & \mathbf{0} & \mathbf{0} & \mathbf{0} \\ \mathbf{0} & \mathbf{0} & \mathbf{0} & \hat{\mathbf{C}}_{\mathrm{B}}^{\Delta} \\ \mathbf{0} & \mathbf{0} & \mathbf{0} & \mathbf{0} \end{bmatrix} \tag{A.3b}$$

$$\mathbf{C}_{\mathrm{S}}^{\circ} = \begin{bmatrix} \hat{\mathbf{C}}_{\mathrm{S}}^{\circ} & \mathbf{0} \\ \mathbf{0} & \hat{\mathbf{C}}_{\mathrm{S}}^{\circ} \end{bmatrix} \tag{A.3c}$$

$$\mathbf{C}_{\mathrm{S}}^{\Delta} = \begin{bmatrix} \mathbf{0} & \hat{\mathbf{C}}_{\mathrm{S}}^{\Delta} \\ \mathbf{0} & \mathbf{0} \end{bmatrix} \tag{A.3d}$$

The zero matrices in the Eq. (A.3a) and (A.3b) each possess three columns and rows, while the null matrices in Eq. (A.3c) und (A.3d) have only two columns and rows each. The $\mathbf{B}$ matrices for combining the approximation of local continuous kinematic measures with the discrete degrees of freedom of the element are given as follows.

$$\mathbf{B}_{\mathrm{MB}} = \begin{bmatrix} \mathbf{B}_{\mathrm{MB}_1} & \mathbf{B}_{\mathrm{MB}_2} & \dots & \mathbf{B}_{\mathrm{MB}_{\mathcal{N}}} \end{bmatrix} \qquad \mathbf{B}_{\mathrm{MB}_i} = \begin{bmatrix} \hat{\mathbf{B}}_{\mathrm{M}_i}^{\circ} & \hat{\mathbf{B}}_{\mathrm{M}_i}^{\Delta} & \hat{\mathbf{B}}_{\mathrm{B}_i}^{\circ} & \hat{\mathbf{B}}_{\mathrm{B}_i}^{\Delta} \end{bmatrix}^{\mathsf{T}} \tag{A.4a}$$

$$\mathbf{B}_{\mathrm{S}} = \begin{bmatrix} \mathbf{B}_{\mathrm{S}_1} & \mathbf{B}_{\mathrm{S}_2} & \dots & \mathbf{B}_{\mathrm{S}_{\mathcal{N}}} \end{bmatrix} \qquad \mathbf{B}_{\mathrm{S}_i} = \begin{bmatrix} \hat{\mathbf{B}}_{\mathrm{S}_i}^{\circ} & \hat{\mathbf{B}}_{\mathrm{S}_i}^{\Delta} \end{bmatrix}^{\mathsf{T}} \tag{A.4b}$$

The sub measures introduced herein are given in the following matrices.

$$\hat{\mathbf{B}}^{\circ}_{\mathrm{M}_i} = \begin{bmatrix} N^i_{,1} & 0 & 0 & 0 & 0 & 0 & 0 & 0 & 0 \\ 0 & N^i_{,2} & 0 & 0 & 0 & 0 & 0 & 0 & 0 \\ N^i_{,2} & N^i_{,1} & 0 & 0 & 0 & 0 & 0 & 0 & 0 \end{bmatrix} \tag{A.5a}$$

$$\hat{\mathbf{B}}^{\Delta}_{\mathrm{M}_i} = \begin{bmatrix} 0 & 0 & N^i_{,1} & 0 & 0 & 0 & 0 & 0 & 0 \\ 0 & 0 & 0 & N^i_{,2} & 0 & 0 & 0 & 0 & 0 \\ 0 & 0 & N^i_{,2} & N^i_{,1} & 0 & 0 & 0 & 0 & 0 \end{bmatrix} \tag{A.5b}$$

$$\hat{\mathbf{B}}^{\circ}_{\mathrm{B}_i} = \begin{bmatrix} 0 & 0 & 0 & 0 & 0 & 0 & N^i_{,1} & 0 & 0 \\ 0 & 0 & 0 & 0 & 0 & -N^i_{,2} & 0 & 0 & 0 \\ 0 & 0 & 0 & 0 & 0 & -N^i_{,1} & N^i_{,2} & 0 & 0 \end{bmatrix} \tag{A.5c}$$

$$\hat{\mathbf{B}}^{\Delta}_{\mathrm{B}_i} = \begin{bmatrix} 0 & 0 & 0 & 0 & 0 & 0 & 0 & 0 & N^i_{,1} \\ 0 & 0 & 0 & 0 & 0 & 0 & 0 & -N^i_{,2} & 0 \\ 0 & 0 & 0 & 0 & 0 & 0 & 0 & -N^i_{,1} & N^i_{,2} \end{bmatrix} \tag{A.5d}$$

$$\hat{\mathbf{B}}^{\circ}_{\mathrm{S}_i} = \begin{bmatrix} 0 & 0 & 0 & 0 & N^i_{,1} & 0 & N^i & 0 & 0 \\ 0 & 0 & 0 & 0 & N^i_{,2} & -N^i & 0 & 0 & 0 \end{bmatrix} \tag{A.5e}$$

$$\hat{\mathbf{B}}^{\Delta}_{\mathrm{S}_i} = \begin{bmatrix} 0 & 0 & 0 & 0 & 0 & 0 & 0 & 0 & N^i \\ 0 & 0 & 0 & 0 & 0 & 0 & 0 & -N^i & 0 \end{bmatrix} \tag{A.5f}$$

The differential operators for membrane, bending, and transverse shear state as well as their auxiliary matrices are structured as follows.

$$\mathbf{D}_{\mathrm{MB}} = \begin{bmatrix} \mathbf{D}^{\circ}_{\mathrm{M}} & \mathbf{D}^{\Delta}_{\mathrm{M}} & \mathbf{D}^{\circ}_{\mathrm{B}} & \mathbf{D}^{\Delta}_{\mathrm{B}} \end{bmatrix}^{\top} \tag{A.6a}$$

$$\mathbf{D}_{\mathrm{S}} = \begin{bmatrix} \mathbf{D}^{\circ}_{\mathrm{S}} & \mathbf{D}^{\Delta}_{\mathrm{S}} \end{bmatrix}^{\top} \tag{A.6b}$$

The sub operators used therein are structured as follows.

$$\mathbf{D}^{\circ}_{\mathrm{M}} = \begin{bmatrix} \frac{\partial}{\partial X_1} & 0 & 0 & 0 & 0 & 0 & 0 & 0 & 0 \\ 0 & \frac{\partial}{\partial X_2} & 0 & 0 & 0 & 0 & 0 & 0 & 0 \\ \frac{\partial}{\partial X_2} & \frac{\partial}{\partial X_1} & 0 & 0 & 0 & 0 & 0 & 0 & 0 \end{bmatrix} \tag{A.7a}$$

$$\mathbf{D}^{\Delta}_{\mathrm{M}} = \begin{bmatrix} 0 & 0 & \frac{\partial}{\partial X_1} & 0 & 0 & 0 & 0 & 0 & 0 \\ 0 & 0 & 0 & \frac{\partial}{\partial X_2} & 0 & 0 & 0 & 0 & 0 \\ 0 & 0 & \frac{\partial}{\partial X_2} & \frac{\partial}{\partial X_1} & 0 & 0 & 0 & 0 & 0 \end{bmatrix} \tag{A.7b}$$

$$\mathbf{D}^{\circ}_{\mathrm{B}} = \begin{bmatrix} 0 & 0 & 0 & 0 & 0 & \frac{\partial}{\partial X_1} & 0 & 0 & 0 \\ 0 & 0 & 0 & 0 & 0 & 0 & \frac{\partial}{\partial X_2} & 0 & 0 \\ 0 & 0 & 0 & 0 & 0 & \frac{\partial}{\partial X_2} & \frac{\partial}{\partial X_1} & 0 & 0 \end{bmatrix} \tag{A.7c}$$

$$\mathbf{D}^{\Delta}_{\mathrm{B}} = \begin{bmatrix} 0 & 0 & 0 & 0 & 0 & 0 & 0 & \frac{\partial}{\partial X_1} & 0 \\ 0 & 0 & 0 & 0 & 0 & 0 & 0 & 0 & \frac{\partial}{\partial X_2} \\ 0 & 0 & 0 & 0 & 0 & 0 & 0 & \frac{\partial}{\partial X_2} & \frac{\partial}{\partial X_1} \end{bmatrix} \tag{A.7d}$$

$$\mathbf{D}^{\circ}_{\mathrm{S}} = \begin{bmatrix} 0 & 0 & 0 & 0 & \frac{\partial}{\partial X_1} & 1 & 0 & 0 & 0 \\ 0 & 0 & 0 & 0 & \frac{\partial}{\partial X_2} & 0 & 1 & 0 & 0 \end{bmatrix} \tag{A.7e}$$

$$\mathbf{D}^{\Delta}_{\mathrm{S}} = \begin{bmatrix} 0 & 0 & 0 & 0 & 0 & 0 & 0 & 1 & 0 \\ 0 & 0 & 0 & 0 & 0 & 0 & 0 & 0 & 1 \end{bmatrix} \tag{A.7f}$$

The auxiliary matrices $\mathbf{A}_i \; \forall \; i \in \{1, \ldots, 5\}$ for transforming the terms of virtual work into the vector-matrix notation are defined as follows.

$$\mathbf{A}_1 = \frac{1}{h^c} \begin{bmatrix} 0 & 0 & -2 & 0 & 0 & -(h^\circ + h^c) & 0 & -h^\Delta & 0 \\ 0 & 0 & 0 & -2 & 0 & 0 & -(h^\circ + h^c) & 0 & -h^\Delta \end{bmatrix} \tag{A.8a}$$

$$\mathbf{A}_2 = \begin{bmatrix} 1 & 0 & 0 & 0 \\ 0 & 1 & 0 & 0 \end{bmatrix} \tag{A.8b}$$

$$\mathbf{A}_3 = \begin{bmatrix} \mathbf{I} & \mathbf{0} & \frac{1}{2} h^\Delta \mathbf{I} & \frac{1}{2} h^\circ \mathbf{I} \end{bmatrix} \tag{A.8c}$$

$$\mathbf{A}_4 = \frac{1}{h^c} \begin{bmatrix} \mathbf{0} & 2\mathbf{I} & h^\circ \mathbf{I} & h^\Delta \mathbf{I} \end{bmatrix} \tag{A.8d}$$

$$\mathbf{A}_5 = \begin{bmatrix} 1 & 0 & 0 & 0 & 0 & 0 & 0 & 0 & 0 & 0 & 0 & 0 & 0 \\ 0 & 1 & 0 & 0 & 0 & 0 & 0 & 0 & 0 & 0 & 0 & 0 & 0 \\ 0 & 0 & 1 & 0 & 0 & 0 & 0 & 0 & 0 & 0 & 0 & -\frac{2}{h^c} & 0 \\ 0 & 0 & 0 & 1 & 0 & 0 & 0 & 0 & 0 & 0 & 0 & 0 & -\frac{2}{h^c} \\ 0 & 0 & 0 & 0 & 0 & 0 & 1 & 0 & 0 & 0 & 0 & 0 & 0 \\ \frac{1}{2} h^\Delta & 0 & \frac{1}{2}(h^\circ + h^c) & 0 & 0 & 0 & 0 & 0 & -1 & 0 & 0 & -\frac{h^\circ + h^c}{h^c} & 0 \\ 0 & \frac{1}{2} h^\Delta & 0 & \frac{1}{2}(h^\circ + h^c) & 0 & 0 & 0 & 1 & 0 & 0 & 0 & 0 & -\frac{h^\circ + h^c}{h^c} \\ 0 & 0 & 0 & 0 & \frac{1}{2} h^\circ & 0 & 0 & 0 & 0 & 0 & -1 & -\frac{h^\Delta}{h^c} & 0 \\ 0 & 0 & 0 & 0 & 0 & \frac{1}{2} h^\circ & 0 & 0 & 0 & 1 & 0 & 0 & -\frac{h^\Delta}{h^c} \end{bmatrix} \tag{A.8e}$$

The unit matrix $\mathbf{I}$ and the zero matrices $\mathbf{0}$ in Eqs. (A.8c)–(A.8d) feature three columns and rows each.

References

H. Altenbach and V. Eremeyev. Thin-walled structural elements: Classification, classical and advanced theories, new applications. In H. Altenbach and V. Eremeyev, editors, *Shell-like Structures: Advanced Theories and Applications*, pages 1–62. 2017. doi: 10.1007/978-3-319-42277-0_1.

M. Aßmus. *Structural Mechanics of Anti-Sandwiches. An Introduction*. SpringerBriefs in Continuum Mechanics. Springer, Cham, 2019. doi: 10.1007/978-3-030-04354-4.

M. Aßmus, S. Bergmann, K. Naumenko, and H. Altenbach. Mechanical behaviour of photovoltaic composite structures: A parameter study on the influence of geometric dimensions and material properties under static loading. *Composites Communications*, 5(-):23–26, 2017a. doi: 10.1016/j.coco.2017.06.003.

M. Aßmus, J. Eisenträger, and H. Altenbach. Projector representation of isotropic linear elastic material laws for directed surfaces. *Zeitschrift für Angewandte Mathematik und Mechanik*, 97(-):1–10, 2017b. doi: 10.1002/zamm.201700122.

M. Aßmus, K. Naumenko, and H. Altenbach. Subclasses of mechanical problems arising from the direct approach for homogeneous plates. In H. Altenbach, J. Chróścielewski, V.A. Eremeyev, and K. Wiśniewski, editors, *Recent Developments in the Theory of Shells*, volume 110 of *Advanced Structured Materials*, pages 1–20. Springer, Singapore, 2019. doi: 10.1007/978-3-030-17747-8.

E. Carrera. Theories and finite elements for multilayered, anisotropic, composite plates and shells. *Archives of Computational Methods in Engineering*, 9(2):87–140, 2002. doi: 10.1007/BF02736649.

E. Carrera. Theories and finite elements for multilayered plates and shells: A unified compact formulation with numerical assessment and benchmarking. *Archives of Computational Methods in Engineering*, 10(3):215–296, 2003. doi: 10.1007/BF02736224.

A.-L. Cauchy. *Recherches sur l'équilibre et le mouvement intérieur des corps solides ou fluides. élastiques ou non élastiques*, volume 2 of *Cambridge Library Collection - Mathematics*, pages 300–304. Cambridge University Press, 2009. doi: 10.1017/CBO9780511702518.038.

E. Cosserat and F. Cosserat. *Théorie des corps déformables*. A. Hermann et fils, Paris, 1909. URL http://jhir.library.jhu.edu/handle/1774.2/34209.

J. Eisenträger, K. Naumenko, H. Altenbach, and J. Meenen. A user-defined finite element for laminated glass panels and photovoltaic modules based on a layer-wise theory. *Composite Structures*, 133:265–277, 2015. ISSN 0263-8223. doi: 10.1016/j.compstruct.2015.07.049.

J.-F. Ganghoffer. *Cosserat, Eugène and François*, pages 1–6. Springer, Berlin, Heidelberg, 2017. doi: 10.1007/978-3-662-53605-6_49-1.

E. Hinton, D. R. J. Owen, and G. Krause. *Finite Elemente Programme für Platten und Schalen*. Berlin · Heidelberg, 1990. doi: 10.1007/978-3-642-50182-1.

R. Hooke. *Lectures de Potentia restitutiva, or of Spring explaining the power of springing bodies*. John Martyn, London, 1678. URL http://data.onb.ac.at/rep/103F4578.

G. R. Kirchhoff. Über das Gleichgewicht und die Bewegung einer elastischen Scheibe. *Journal für die reine und angewandte Mathematik*, 40:51–88, 1850. doi: 10.1515/crll.1850.40.51.

G. Lamé. *Leçons sur la théorie mathématique de l'elasticité des corps solides*. Gauthier-Villars, Paris, 1866.

A. Libai and J. G. Simmonds. Nonlinear elastic shell theory. *Advances in Applied Mechanics*, 23:271–371, 1983. doi: 10.1016/S0065-2156(08)70245-X.

R. D. Mindlin. Influence of rotatory inertia and shear on flexural motions of isotropic, elastic plates. *Journal of Applied Mechanics*, 18:31–38, 1951.

P. M. Naghdi. The Theory of Shells and Plates. In W. Flügge, editor, *Encyclopedia of Physics - Linear Theories of Elasticity and Thermoelasticity*, volume VI, a/2 (ed. C. Truesdell), pages 425–640. Springer, Berlin · New York, 1972. doi: 10.1007/978-3-662-39776-3_5.

K. Naumenko and V. A. Eremeyev. A layer-wise theory for laminated glass and photovoltaic panels. *Composite Structures*, 112: 283–291, 2014. doi: 10.1016/j.compstruct.2014.02.009.

W. Noll. A mathematical theory of the mechanical behavior of continuous media. *Archive for Rational Mechanics and Analysis*, 2(1):197–226, 1958. doi: 10.1007/BF00277929.

E. Oñate. *Structural Analysis with the Finite Element Method Linear Statics: Volume 2. Beams, Plates and Shells*. Springer, Dordrecht, 2013. doi: 10.1007/978-1-4020-8743-1_6.

J. Rychlewski. On Hooke's law. *Priklat. Mathem. Mekhan.*, 48(3):303–314, 1984. doi: 10.1016/0021-8928(84)90137-0.

J. C. Simo and D. D. Fox. On a stress resultant geometrically exact shell model. part i: Formulation and optimal parametrization. *Computer Methods in Applied Mechanics and Engineering*, 72(3):267–304, 1989. doi: 10.1016/0045-7825(89)90002-9.

J. C. Simo, D. D. Fox, and M. S. Rifai. On a stress resultant geometrically exact shell model. part ii: The linear theory; computational aspects. *Computer Methods in Applied Mechanics and Engineering*, 73(1):53–92, 1989. doi: 10.1016/0045-7825(89)90098-4.

B. Szabó and I. Babuška. *Finite Element Analysis*. John Wiley & Sons, Inc., New York · Chichester · Brisbane · Toronto · Singapore, 1991.

S. Vlachoutsis. Shear correction factors for plates and shells. *International Journal for Numerical Methods in Engineering*, 33 (7):1537–1552, 1992. doi: 10.1002/nme.1620330712.

W. Voigt. Über die Beziehung zwischen den beiden Elasticitätskonstanten isotroper Körper. *Wiedemann´sche Annalen*, 38: 573–587, 1889. doi: 10.1002/andp.18892741206.

P. A. Zhilin. Mechanics of deformable directed surfaces. *International Journal of Solids and Structures*, 12(9):635 – 648, 1976. doi: 10.1016/0020-7683(76)90010-X.

TECHNISCHE MECHANIK
an open access journal

journal homepage: www.ovgu.de/techmech

Tech. Mech., Vol. 39, Is. 2, (2019), 220–228

Received: March 15, 2019
Accepted: April 3, 2019
Available online: April 11, 2019

Effective Coefficients of Isotropic Complex Dielectric Composites in a Hexagonal Array

David Yañez-Olmos[1], Julián Bravo-Castillero[1]*, Ariel Ramírez-Torres[2], Reinaldo Rodríguez-Ramos[3], and Federico J. Sabina[1]

[1] Universidad Nacional Autónoma de México, Instituto de Investigaciones en Matemáticas Aplicadas y en Sistemas, Alcaldía Álvaro Obregón, 01000 CDMX, México
[2] Politecnico di Torino, Dipartimento di Scienze Mathematiche "G. L. Lagrange","Dipartimento di Eccellenza 2018−2022", 10129, Torino, Italy
[3] Universidad de La Habana, Facultad de Matemática y Computación, San Lázaro y L s/n, 10400 Vedado, La Habana, Cuba

Abstract: Based on the asymptotic homogenization method, the local problems related to two-phase periodic fibrous dielectric composites with isotropic and complex constituents are solved. A hexagonal periodicity distribution of the fibers is considered. Explicit formulas for the real and imaginary parts of the effective dielectric properties are derived. Such formulas can be computed for any desired precision related to a truncation order of an infinite system of algebraic linear equations. Two simple analytical expressions are specified for the first two truncation orders. Comparisons with results via other approaches show a good concordance. Hexagonal periodic lattices of acoustic scatterers are useful structures for acoustic applications.

Keywords: Effective properties, two-phase fibrous dielectric composites, complex dielectric properties, hexagonal array.

1 Introduction

The effective conductivity tensor of two-dimensional complex dielectric composites consisting of a hexagonal periodic array of circular inclusions embedded in a matrix is studied, where both matrix and inclusions have complex dielectric properties. Perfect contact conditions at the interface between the matrix and the inclusions are considered. This problem is of interest, for instance, in acoustic applications, see e.g. Guild et al. (2014).
The solution is based on the asymptotic homogenization technique combined with series expansions of elliptic functions. A similar procedure has been used in recent works. For instance, Godin (2012) solved rigorously the problem for two-dimensional real dielectric composites using series expansions of Weierstrass' function and its derivatives depending on unknown real coefficients. Then, the problem is reduced to an infinite system and found its solution as a convergent power series allowing to obtain analytical formulas of the effective conductivity tensor for different lattice of inclusions. An analogous procedure was followed in Godin (2013) for the determination of the effective complex permittivity of a similar two-dimensional composite but with complex properties of the constituents. In that case the method of undetermined coefficients was used with complex coefficients allowing the derivation of efficient formulas for the effective properties. Unlike the real case a non-monotonic behavior of the real and imaginary parts of the effective tensor as function of area fraction of the inclusions is shown. This procedure has been extended to investigate the macroscopic behavior of periodic tubular structures in Godin (2016) and the propagation of electromagnetic waves through a two-dimensional composite material containing a periodic rectangular array of circular inclusions by Godin and Vainberg (2019). These studies have been found relevance in some applications. For instance, the results of Godin (2013) have been applied in Guild et al. (2014) to acoustics showing a good agreement with experimental data and inertial enhancement. In Ren et al. (2016), the results of Godin (2013) were used for calculating eddy current losses in soft complex magnetic composites. Recently, in Bravo-Castillero et al. (2018) the study of the effective behavior of complex dielectric composites was done by the homogenization of the equivalent system of equations with real coefficients. Closed-form formulas for the effective coefficients were obtained for a square periodic distribution of the inclusions which were employed to study gain-enhancement and loss enhancement properties of the homogenized material. This procedure offers independent models to compute the real and imaginary parts of the effective complex dielectric conductivity. In this work, based on the methodology in Bravo-Castillero et al. (2018), the effective tensor of two-dimensional complex dielectric is determined for the case of a hexagonal periodic distribution of the inclusions.
The work is organized as follows. After the Introduction, section 2 is devoted to the statement of the problem. A summary of the homogenization process, and the models for the local problems and the effective coefficients is presented in section 3. In section 4, the solution of the local problems is described and the formulas for the real and imaginary part of the effective tensor are derived. In section 5, some numerical examples are discussed. Finally, some concluding remarks are given in section 6.

2 Statement of the Problem

Let $\Omega \subset \mathbb{R}^2$ be a two-dimensional domain with infinitely smooth boundary $\partial\Omega$. The components of the complex dielectric permittivity tensor of a two-phase fibrous reinforced composite (FRC) occupying Ω are $(\alpha^{\varepsilon} + i\beta^{\varepsilon})\delta_{jl}$ $(j, l = 1, 2)$ where $i^2 = -1$, δ

* E-mail address: julian@mym.iimas.unam.mx
doi: 10.24352/UB.OVGU-2019-020

is the Kronecker's delta, ε is a small geometric parameter that characterizes the periodicity and α^ε and β^ε are the real and imaginary part, respectively. The usual global or slow coordinates $\mathbf{x} \in \Omega$ and local or fast coordinates $\mathbf{y}$ with $\mathbf{y} = \mathbf{x}/\varepsilon$ are introduced. A hexagonal array of the periodic cell Y in global coordinates is considered so that it covers the domain $\Omega = \Omega_1^\varepsilon \cup \Omega_2^\varepsilon \cup \Gamma^\varepsilon$ where $\Gamma^\varepsilon \equiv \partial\Omega_2^\varepsilon$ and $\Omega_1^\varepsilon \cap \Omega_2^\varepsilon = \emptyset$; Ω_1^ε represents the matrix or connected set, Ω_2^ε denotes the fibers or disconnected set (an ε-periodic distribution of circles of radius $R\varepsilon$) and Γ^ε is the interface between Ω_1^ε and Ω_2^ε. The boundary $\partial\Omega$ is chosen so that it does not intersect any fiber of Ω_2^ε (Fig. 1). Fig 1 also shows a blow-up of the periodic hexagonal cell cross-section $Y \subset \mathbb{R}^2$ referred as $\mathbf{y}$-coordinates with an embedded circle of radius R and boundary Γ. Therein, Y_1 denotes the matrix or connected set and Y_2 the fiber or disconnected set. The regions Ω_1^ε and Ω_2^ε are occupied with two homogeneous materials with different electric permittivity

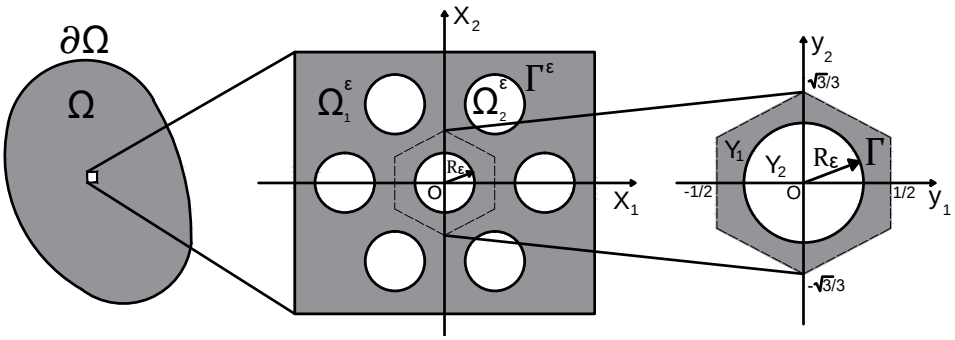

Fig. 1: (Left) Domain Ω with boundary $\partial\Omega$. (Centre) A blow-up domain contained in Ω showing a FRC type of geometry in global coordinates. (Right) Hexagonal cell in y-coordinates.

properties and the jl-components of the electric permittivity tensor are given by

$$\alpha^\varepsilon + i\beta^\varepsilon = \begin{cases} \alpha^{(1)} + i\beta^{(1)} & \text{in } \Omega_1^\varepsilon, \\ \alpha^{(2)} + i\beta^{(2)} & \text{in } \Omega_2^\varepsilon. \end{cases} \tag{1}$$

The complex electric potential $u^\varepsilon = \varphi^\varepsilon + i\psi^\varepsilon$ in Ω is sought as ε tends to zero so that Maxwell's equation in the quasi-static approximation in absence of free conduction currents are satisfied in Ω_1^ε and Ω_2^ε together with continuity of electric potential and normal component of electric displacement field across the interface Γ^ε. The Dirichlet condition "$u^\varepsilon = \tilde{u}_1 + i\tilde{u}_2$" is given on $\partial\Omega$. The related boundary value problem with complex coefficients is equivalent to the following system of two-coupled real partial differential equations

$$\frac{\partial}{\partial x_j}\left(\mathcal{A}_{jl}^\varepsilon \frac{\partial \mathbf{U}^\varepsilon}{\partial x_l}\right) = \mathbf{0} \quad \text{in } \Omega \setminus \Gamma^\varepsilon, \tag{2a}$$

$$[\![\mathbf{U}^\varepsilon]\!] = \mathbf{0} \quad \text{on } \Gamma^\varepsilon, \tag{2b}$$

$$\left[\!\!\left[\left(\mathcal{A}_{jl}^\varepsilon \frac{\partial \mathbf{U}^\varepsilon}{\partial x_l}\right) n_j\right]\!\!\right] = \mathbf{0} \quad \text{on } \Gamma^\varepsilon, \tag{2c}$$

$$\mathbf{U}^\varepsilon = \tilde{\mathbf{U}} \quad \text{on } \partial\Omega, \tag{2d}$$

where $\mathbf{U}^\varepsilon = (\varphi^\varepsilon, \psi^\varepsilon)^T$, $\tilde{\mathbf{U}} = (\tilde{u}_1, \tilde{u}_2)^T$ and $\mathbf{0} = (0,0)^T$ is the null vector of $\mathbb{R}^2$. The superscript T means transposition and the components of the 2×2 symmetric matrix-valued $\mathcal{A}^\varepsilon$ are given by

$$\mathcal{A}_{11}^\varepsilon = \boldsymbol{\alpha}^\varepsilon, \quad \mathcal{A}_{12}^\varepsilon = \mathcal{A}_{21}^\varepsilon = -\boldsymbol{\beta}^\varepsilon, \quad \mathcal{A}_{22}^\varepsilon = -\boldsymbol{\alpha}^\varepsilon, \tag{3}$$

where Einstein repeated indexes summation convention is adopted. The j-th component of unit normal vector to Γ^ε, denoted with n_j, is taken in the direction from Ω_1^ε to Ω_2^ε. The notation $[\![.]\!]$ is used to denote the jump of the enclosed function across the interface Γ^ε in the direction of the normal $\mathbf{n}$.

3 Homogenization, Effective Coefficients and Local Problems

Following Bravo-Castillero et al. (2018) a formal asymptotic solution of (2a)–(2d) can be constructed up to $O(\varepsilon^2)$ as follows

$$\mathbf{U}^\varepsilon(\mathbf{x}) = \mathbf{U}^{(0)}(\mathbf{x}) + \varepsilon \mathbf{N}_k(\mathbf{y}) \frac{\partial \mathbf{U}^{(0)}(\mathbf{x})}{\partial x_k}, \tag{4}$$

with

$$\mathbf{U}^{(0)}(\mathbf{x}) = \left(\varphi^{(0)}(\mathbf{x}), \psi^{(0)}(\mathbf{x})\right)^T \quad \text{and} \quad \mathbf{N}_k(\mathbf{y}) = \begin{pmatrix} w^k(\mathbf{y}) & g^k(\mathbf{y}) \\ \zeta^k(\mathbf{y}) & \xi^k(\mathbf{y}) \end{pmatrix},$$

where the 2×2 matrices $\mathbf{N}_k$ are Y-periodic solutions of the local problems

$$\frac{\partial}{\partial y_j}\left(\mathcal{A}_{jl}\left(\mathbf{y}\right)\frac{\partial \mathbf{N}_k(\mathbf{y})}{\partial y_l}+\mathcal{A}_{jk}(\mathbf{y})\right)=\mathbf{O} \quad \text{in } Y\setminus\Gamma, \tag{5a}$$

$$[\![\mathbf{N}_k(\mathbf{y})]\!]=\mathbf{O} \quad \text{on } \Gamma, \tag{5b}$$

$$\left[\!\!\left[\left(\mathcal{A}_{jl}\left(\mathbf{y}\right)\frac{\partial \mathbf{N}_k(\mathbf{y})}{\partial y_l}+\mathcal{A}_{jk}(\mathbf{y})\right)n_j\right]\!\!\right]=\mathbf{O} \quad \text{on } \Gamma, \tag{5c}$$

with $\langle \mathbf{N}_k(y)\rangle = \mathbf{O}$. In (5a)–(5c), $\mathbf{O}$ denotes the 2×2 null matrix.
The term $\mathbf{U}^{(0)}$ in (4) is the solution of the homogenized problem

$$\widehat{\mathcal{A}}_{jk}\frac{\partial^2 \mathbf{U}^{(0)}(\mathbf{x})}{\partial x_j \partial x_k}=\mathbf{0} \quad \text{in } \Omega, \tag{6a}$$

$$\mathbf{U}^{(0)}=\tilde{\mathbf{U}} \ \text{ in } \partial\Omega, \tag{6b}$$

where the effective coefficients $\widehat{\mathcal{A}}_{jl}$ are constants and given by

$$\widehat{\mathcal{A}}_{jk}=\left\langle \mathcal{A}_{jk}(\mathbf{y})+\mathcal{A}_{jl}(\mathbf{y})\frac{\partial N_k(\mathbf{y})}{\partial y_l}\right\rangle. \tag{7}$$

The angular brackets represent the volume average per unit length over the unit periodic cell, i.e. $\langle f(\mathbf{y})\rangle \equiv \int_Y f(y)dy$. The components of the effective coefficient $\widehat{\mathcal{A}}$ are

$$\widehat{\mathcal{A}}_{11}=\widehat{\boldsymbol{\alpha}}, \quad \widehat{\mathcal{A}}_{12}=\widehat{\mathcal{A}}_{21}=-\widehat{\boldsymbol{\beta}}, \quad \widehat{\mathcal{A}}_{22}=-\widehat{\boldsymbol{\alpha}}. \tag{8}$$

The effective coefficients $\widehat{\boldsymbol{\alpha}}$ and $\widehat{\boldsymbol{\beta}}$ can be found by using the following formulas

$$\widehat{\alpha}=\begin{cases}\langle\alpha\rangle-\frac{[\![\alpha]\!]}{|Y|}\int_\Gamma g^1 \mathrm{d}y_2-\frac{[\![\beta]\!]}{|Y|}\int_\Gamma \xi^1 \mathrm{d}y_2, & \text{for } k=1\\ \langle\alpha\rangle+\frac{[\![\alpha]\!]}{|Y|}\int_\Gamma g^2 \mathrm{d}y_1+\frac{[\![\beta]\!]}{|Y|}\int_\Gamma \xi^2 \mathrm{d}y_1, & \text{for } k=2\end{cases} \tag{9a}$$

$$\widehat{\beta}=\begin{cases}\langle\beta\rangle-\frac{[\![\beta]\!]}{|Y|}\int_\Gamma g^1 \mathrm{d}y_2+\frac{[\![\alpha]\!]}{|Y|}\int_\Gamma \xi^1 \mathrm{d}y_2, & \text{for } k=1\\ \langle\beta\rangle+\frac{[\![\beta]\!]}{|Y|}\int_\Gamma g^2 \mathrm{d}y_1-\frac{[\![\alpha]\!]}{|Y|}\int_\Gamma \xi^2 \mathrm{d}y_1, & \text{for } k=2\end{cases} \tag{9b}$$

where $\langle f\rangle = f_1|Y_1| + f_2|Y_2|$, with $|Y| = |Y_1| + |Y_2|$. The local functions g^k and ξ^k are solutions of the local problems defined as follows

Problem $\Im^k$: Find the Y-periodic functions g^k, ξ^k, such that:

$$\Delta g^k=0, \quad \Delta\xi^k=0, \qquad \text{in } Y\setminus\Gamma, \tag{10a}$$

$$[\![g^k]\!]=0, \quad [\![\xi^k]\!]=0, \qquad \text{on } \Gamma, \tag{10b}$$

$$\left[\!\!\left[\left(\alpha\frac{\partial\xi^k}{\partial y_l}+\beta\frac{\partial g^k}{\partial y_l}\right)n_j\right]\!\!\right]=-[\![\alpha]\!]\,n_k \quad \text{on } \Gamma, \tag{10c}$$

$$\left[\!\!\left[\left(\beta\frac{\partial\xi^k}{\partial y_l}-\alpha\frac{\partial g^k}{\partial y_l}\right)n_j\right]\!\!\right]=-[\![\beta]\!]\,n_k \quad \text{on } \Gamma, \tag{10d}$$

with $\left\langle g^k\right\rangle = 0$ and $\left\langle \xi^k\right\rangle = 0$. In (10a), $\Delta \equiv \frac{\partial^2}{\partial y_1^2}+\frac{\partial^2}{\partial y_2^2}$ is the two-dimensional Laplace operator in a Cartesian coordinate system.

4 Solution of the Local Problem $\Im^k$ for Hexagonal Array

In order to solve the problem (10a)–(10d), let us consider a hexagonal lattice of inclusions of radius R (see Fig. 1). Particularly, doubly-periodic harmonic functions that satisfy the given interface conditions and the null average condition over the hexagonal cell are sought. Following Guinovart-Díaz et al. (2001), for $k = 1, 2$, the solutions of the local problems are sought in the form

$$\begin{aligned} g_1^1&=\mathcal{R}e\left\{\sum_{q=1}^{\infty\, o}\left(a_q^1 z^{-q}-A_q^1 z^q\right)\right\}, \quad g_2^1=\mathcal{R}e\left\{\sum_{q=1}^{\infty\, o} c_q^1 z^q\right\}\\ g_1^2&=\mathcal{I}m\left\{\sum_{q=1}^{\infty\, o}\left(a_q^2 z^{-q}-A_q^2 z^q\right)\right\}, \quad g_2^2=\mathcal{I}m\left\{\sum_{q=1}^{\infty\, o} c_q^2 z^q\right\}\end{aligned} \tag{11}$$

and

$$\begin{aligned}\xi_1^1 &= \mathcal{R}e\left\{\sum_{q=1}^{\infty\ o}\left(b_q^1 z^{-q} - B_q^1 z^q\right)\right\}, \quad \xi_2^1 = \mathcal{R}e\left\{\sum_{q=1}^{\infty\ o} d_q^1 z^q\right\}\\ \xi_1^2 &= \mathcal{I}m\left\{\sum_{q=1}^{\infty\ o}\left(b_q^2 z^{-q} - B_q^2 z^q\right)\right\}, \quad \xi_2^2 = \mathcal{I}m\left\{\sum_{q=1}^{\infty\ o} d_q^2 z^q\right\}\end{aligned} \tag{12}$$

where $\mathcal{R}e$ and $\mathcal{I}m$ indicate the real and imaginary parts, respectively. The superscript o specifies that the sum is carried out over odd indices, the unknown coefficients a_q^k, b_q^k, c_q^k and d_q^k are real and

$$A_q^k = \sum_{p=1}^{\infty\ o} p a_p^k \eta_{pq}^k, \quad B_q^k = \sum_{p=1}^{\infty\ o} p b_p^k \eta_{pq}^k, \tag{13}$$

with

$$(k=1)\ \ \eta_{pq}^1 = \begin{cases}\frac{2\pi}{\sqrt{3}}, & p+q=2\\ \dfrac{(p+q-1)!}{p!q!}S_{p+q}, & p+q>2\end{cases} \qquad (k=2)\ \ \eta_{pq}^2 = \begin{cases}-\pi, & p+q=2\\ \dfrac{(p+q-1)!}{p!q!}S_{p+q}, & p+q>2\end{cases}$$

and S_j are the reticulate sums given by

$$S_{p+q} = \sum_{n^2+m^2\neq 0} \frac{1}{(m\omega_1 + n\omega_2)^{p+q}},$$

where $\omega_1 = 1$ and $\omega_2 = e^{\frac{\pi}{3}i}$ are the periods. As the cross-section of the inclusion is described by a circle of radius R, the interface in the unit cell is defined by $\Gamma = Re^{i\theta}$ with $0 \le \theta < 2\pi$, then substituting (11)–(12) into the interface conditions (10b)–(10d), one obtain the following infinite system of algebraic equations

$$\begin{pmatrix} \mathbf{I} + (-1)^{k+1}\chi_\alpha \mathbf{W}^k & \chi_{\beta\alpha}^+ \mathbf{I} + (-1)^{k+1}\chi_{\beta\alpha}^- \mathbf{W}^k \\ \chi_{\beta\alpha}^+ \mathbf{I} + (-1)^{k+1}\chi_{\beta\alpha}^- \mathbf{W}^k & -\left(\mathbf{I} + (-1)^{k+1}\chi_\alpha \mathbf{W}^k\right)\end{pmatrix}\begin{pmatrix}\tilde{\mathbf{A}}^k \\ \tilde{\mathbf{B}}^k\end{pmatrix} = (-1)^{k+1}\begin{pmatrix}\mathbf{V}^1 \\ \mathbf{V}^2\end{pmatrix}, \tag{14}$$

where $\mathbf{I}$ is the infinite identity matrix, $\tilde{\mathbf{A}}^k = (\tilde{a}_1^k, \tilde{a}_3^k, \ldots)^T$, $\tilde{\mathbf{B}}^k = (\tilde{b}_1^k, \tilde{b}_3^k, \ldots)^T$, $a_q^k = \tilde{a}_q^k R^q/\sqrt{q}$, $b_q^k = \tilde{b}_q^k R^q/\sqrt{q}$, $\mathbf{V}^1 = (\chi_\alpha R, 0, \ldots)^T$, $\mathbf{V}^2 = (\chi_{\beta\alpha}^- R, 0, \ldots)^T$, and

$$(k=1)\ \ \mathbf{W}^1 = \begin{cases}\frac{2\pi}{\sqrt{3}}R^2, & p+q=2\\ \sum\limits_{p=1}^{\infty\ o}\sqrt{pq}\,\eta_{pq}^1 R^{p+q}, & p+q>2.\end{cases} \qquad (k=2)\ \ \mathbf{W}^2 = \begin{cases}-\pi R^2, & p+q=2\\ \sum\limits_{p=1}^{\infty\ o}\sqrt{pq}\,\eta_{pq}^2 R^{p+q}, & p+q>2.\end{cases}$$

Furthermore,

$$\chi_\alpha = \frac{[\![\alpha]\!]}{\alpha^{(1)}+\alpha^{(2)}}, \quad \chi_{\beta\alpha}^+ = \frac{\beta^{(1)}+\beta^{(2)}}{\alpha^{(1)}+\alpha^{(2)}} \quad \text{and} \quad \chi_{\beta\alpha}^- = \frac{[\![\beta]\!]}{\alpha^{(1)}+\alpha^{(2)}}. \tag{15}$$

The matrix $\mathbf{W}^k$, $k = 1, 2$ is real, symmetric and bounded, and consequently the classical results from the theory of infinite systems Kantorovich and Krylov can be used to solve (14). In this sense, the infinite linear system can be truncated into an appropriate order $p = q = 2n_o - 1$, with $n_o \in \mathbb{N}$. In this way, (14) is transformed into a linear system of order $2n_o$. Now, the use of (11) and (12) into (9a) and (9b) leads to,

$$\widehat{\alpha} = \alpha^{(1)} - (-1)^{k+1}\frac{2\pi}{|Y|}\left(\alpha^{(1)}a_1^k + \beta^{(1)}b_1^k\right), \tag{16a}$$

$$\widehat{\beta} = \beta^{(1)} - (-1)^{k+1}\frac{2\pi}{|Y|}\left(\beta^{(1)}a_1^k - \alpha^{(1)}b_1^k\right). \tag{16b}$$

For the particular case of real dielectric composites with isotropic constituents (i.e., for $\beta^{(1)}, \beta^{(2)} = 0$), the formulas for the effective coefficients (16a)–(16b) reduce to formulas (3.15)–(3.16), p . 228 in Guinovart-Díaz et al. (2001).

5 Analytical Formulas, Numerical Examples and Some Comparisons

5.1 Analytical Formulas

Following Bravo-Castillero et al. (2018), the system (14) can also be written as follows

$$\left(\eta\mathcal{I} + (-1)^{k+1}\boldsymbol{\lambda}\mathcal{W}^k\right)\begin{pmatrix}\tilde{\mathbf{A}}^k\\ \tilde{\mathbf{B}}^k\end{pmatrix} = (-1)^{k+1}\begin{pmatrix}\mathbf{V}^1\\ \mathbf{V}^2\end{pmatrix}, \tag{17}$$

where

$$\eta = \begin{pmatrix}1 & \chi^+_{\beta\alpha}\\ \chi^+_{\beta\alpha} & -1\end{pmatrix}, \quad \boldsymbol{\lambda} = \begin{pmatrix}\chi_\alpha & \chi^-_{\beta\alpha}\\ \chi^-_{\beta\alpha} & -\chi_\alpha\end{pmatrix}, \quad \mathcal{I} = \begin{pmatrix}\mathbf{I} & \Theta\\ \Theta & \mathbf{I}\end{pmatrix} \quad \text{and} \quad \mathcal{W}^k = \begin{pmatrix}\mathbf{W}^k & \Theta\\ \Theta & \mathbf{W}^k\end{pmatrix},$$

with Θ denoting the infinite null matrix. After multiplication of (11) by $\boldsymbol{\lambda}^{-1}$ and noticing that $\boldsymbol{\lambda}^{-1}(\mathbf{V}^1, \mathbf{V}^2)^T = R\mathbf{e}_1$, where $\mathbf{e}_1$ is the infinite vector $(1, 0, 0, \ldots)^T$. Then, equation (17) becomes

$$\begin{pmatrix}\tilde{\mathbf{A}}^k_{n_o}\\ \tilde{\mathbf{B}}^k_{n_o}\end{pmatrix} = (-1)^{k+1}(\boldsymbol{\theta}\mathcal{I}_{n_o} + (-1)^{k+1}\mathcal{W}^k_{n_o})^{-1}R\mathbf{e}^T_{2n_o}, \tag{18}$$

or equivalently

$$\begin{pmatrix}\tilde{\mathbf{A}}^k_{n_o}\\ \tilde{\mathbf{B}}^k_{n_o}\end{pmatrix} = (-1)^{k+1}\begin{pmatrix}\theta_{11}\mathbf{I}_{n_o} + (-1)^{k+1}\mathbf{W}^k_{n_o} & \theta_{12}\mathbf{I}_{n_o}\\ -\theta_{12}\mathbf{I}_{n_o} & \theta_{11}\mathbf{I}_{n_o} + (-1)^{k+1}\mathbf{W}^k_{n_o}\end{pmatrix}^{-1} R\mathbf{e}^T_{2n_o}, \tag{19}$$

where the sub-index n_o represents the truncation order of the vectors $\tilde{\mathbf{A}}^k$, $\tilde{\mathbf{B}}^k$, $\mathbf{e}_1$, and the matrices $\mathcal{I}$ and $\mathcal{W}^k$. The matrix $\boldsymbol{\theta} = \boldsymbol{\lambda}^{-1}\boldsymbol{\eta}$ has the form

$$\boldsymbol{\theta} = \begin{pmatrix}\theta_{11} & \theta_{12}\\ -\theta_{12} & \theta_{11}\end{pmatrix}, \tag{20}$$

and its components are

$$\theta_{11} = \frac{\chi_\alpha + \chi^-_{\beta\alpha}\chi^+_{\beta\alpha}}{(\chi_\alpha)^2 + (\chi^-_{\beta\alpha})^2} \quad \text{and} \quad \theta_{12} = \frac{\chi_\alpha\chi^+_{\beta\alpha} - \chi^-_{\beta\alpha}}{(\chi_\alpha)^2 + (\chi^-_{\beta\alpha})^2}. \tag{21}$$

Using the finite system (19), we find the unknowns $\tilde{\mathbf{A}}^k_{n_o}$ and $\tilde{\mathbf{B}}^k_{n_o}$ for different orders of truncation, which are then substituted into the effective coefficients expressions (16a)–(16b). In this way, formula (19) is helpful in finding closed-forms for the effective coefficients.

1. If $n_o = 1$, equation (19) takes the form

$$\begin{pmatrix}\tilde{a}^k_1\\ \tilde{b}^k_1\end{pmatrix} = (-1)^{k+1}\begin{pmatrix}\theta_{11} + (-1)^{k+1}W^k_{11} & \theta_{12}\\ -\theta_{12} & \theta_{11} + (-1)^{k+1}W^k_{11}\end{pmatrix}^{-1}\begin{pmatrix}R\\ 0\end{pmatrix}, \tag{22}$$

where W^k_{pq} denote the elements of $\mathbf{W}^k$. Then,

$$\tilde{a}^k_1 = (-1)^{k+1}\frac{(\theta_{11} + (-1)^{k+1}W^k_{11})R}{(\theta_{11} + (-1)^{k+1}W^k_{11})^2 + \theta^2_{12}}, \tag{23a}$$

$$\tilde{b}^k_1 = (-1)^{k+1}\frac{\theta_{12}R}{(\theta_{11} + (-1)^{k+1}W^k_{11})^2 + \theta^2_{12}}. \tag{23b}$$

Substitution of equations (23a)–(23b) in the expressions for the effective coefficients (16a)–(16b) yields

$$\widehat{\alpha} = \alpha^{(1)} - \frac{2(\alpha^{(1)}\theta_{11} + \beta^{(1)}\theta_{12})Y_2 + 2\alpha^{(1)}Y_2^2}{(\theta_{11} + Y_2)^2 + \theta^2_{12}}, \tag{24a}$$

$$\widehat{\beta} = \beta^{(1)} - \frac{2(\beta^{(1)}\theta_{11} - \alpha^{(1)}\theta_{12})Y_2 + 2\beta^{(1)}Y_2^2}{(\theta_{11} + Y_2)^2 + \theta^2_{12}}, \tag{24b}$$

where V_γ is the volume fraction of the phase γ. Particularly, $Y_1 + Y_2 = \frac{\sqrt{3}}{2}$ with $Y_2 = \pi R^2$.

2. If $n_o = 2$, equation (19) takes the form

$$\begin{pmatrix} \tilde{a}_1^k \\ \tilde{a}_3^k \\ \tilde{b}_1^k \\ \tilde{b}_3^k \end{pmatrix} = (-1)^{k+1} \begin{pmatrix} \theta_{11} + (-1)^{k+1} w_{11} & 0 & \theta_{12} & 0 \\ 0 & \theta_{11} + (-1)^{k+1} w_{33} & 0 & \theta_{12} \\ -\theta_{12} & 0 & \theta_{11} + (-1)^{k+1} w_{11} & 0 \\ 0 & -\theta_{12} & 0 & \theta_{11} + (-1)^{k+1} w_{33} \end{pmatrix}^{-1} \begin{pmatrix} R \\ 0 \\ 0 \\ 0 \end{pmatrix}. \tag{25}$$

To find $\tilde{a}_1^1$, $\tilde{a}_3^1$, $\tilde{b}_1^1$ and $\tilde{b}_3^1$, the above linear system (25) must be solved. Then, the coefficients $\tilde{a}_1^1$ and $\tilde{b}_1^1$ are substituted into the effective coefficients expressions (16a)–(16b).

5.2 Numerical Examples

Now, we compare the effective coefficients (16a)–(16b) for successive truncation orders $n_o = 1, 2, 3, 4$. In particular, we fix

$$\kappa^{(1)} = 1 - 5i \qquad \kappa^{(2)} = 30 - 0.3i,$$

and denote by $V_p = \frac{\pi}{4}$ the percolation limit where the cylinders are in contact. Fig 2 and 3 displays the real and imaginary parts of the effective complex dielectric coefficient $\hat{\kappa}$ as a function of the inclusion volume fraction V_o. It is observed that the first approximation is a very good estimation of the complex effective dielectric coefficient for $V_o < 0.7$. Besides, the effective coefficients for a truncation order at $n_o = 3$ and 4 are quite similar. This agreement shows that the second order approximation is good enough for higher orders of approximations. Therefore, in what follows, we restrict our analysis to first, second and third approximation orders of the effective coefficients.

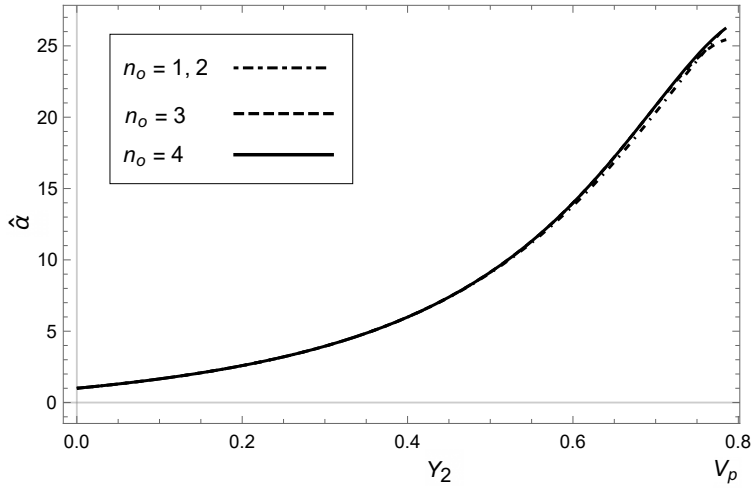

Fig. 2: The real part of the complex effective dielectric coefficient $\widehat{\kappa}$ as a function of the volume fraction Y_2 shown for successive truncation orders $n_o = 1, 2, 3, 4$.

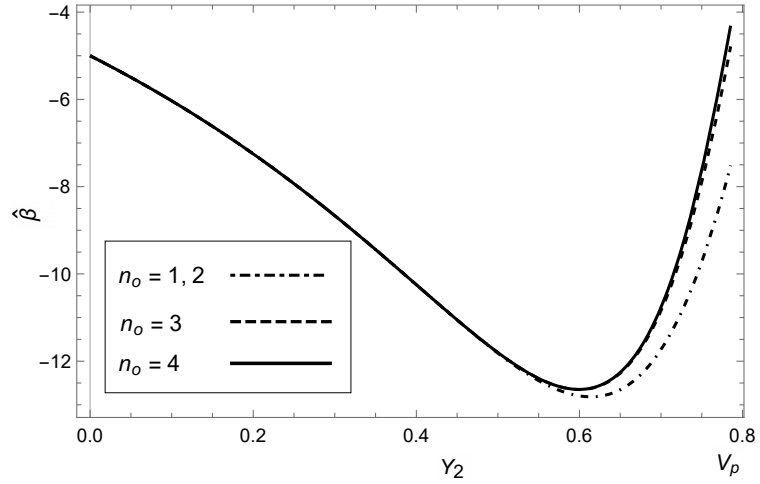

Fig. 3: The imaginary part of the complex effective dielectric coefficient $\widehat{\kappa}$ as a function of the volume fraction Y_2 shown for successive truncation orders $n_o = 1, 2, 3, 4$.

5.3 Comparisons

We compare our results with those obtained in Godin (2013) for

$$\kappa^{(1)} = 2 - 0.3i \quad \text{and} \quad \kappa^{(2)} = 1 - 8i.$$

The approximation to the real (imaginary) part of the complex effective coefficient reported in Godin (2013), are determined by

$$\widehat{\alpha} = Re\,(\varepsilon^*) \qquad \text{and} \qquad \widehat{\beta} = Im\,(\varepsilon^*), \tag{26}$$

where

$$\varepsilon^* = \kappa^{(1)} \frac{1 + \alpha\lambda f}{1 - \alpha\lambda f},$$

and

$$\alpha = \frac{\kappa^{(2)} - \kappa^{(1)}}{\kappa^{(2)} + \kappa^{(1)}}, \qquad f = \frac{2}{\sqrt{3}}\pi R^2 = \frac{2}{\sqrt{3}} Y_2, \qquad \lambda = 1 + 5\alpha^2 S_3^2 R^{12} + \alpha^2 \left(25\alpha^2 S_3^4 + 11 S_6^2\right) R^{24} + O\left(R^{36}\right)$$

and while the only non-zero real lattice sums are S_{3k}, $k = 1, 2, \ldots$, here

$$S_3 = \sum_{n^2+m^2 \neq 0} \frac{1}{\left(m + ne^{\frac{\pi}{3} i}\right)^6} \approx 5.86303 \qquad S_6 = \sum_{n^2+m^2 \neq 0} \frac{1}{\left(m + ne^{\frac{\pi}{3} i}\right)^{12}} \approx 6.00964.$$

As it was pointed out in the previous section, it is sufficient to work up to a truncation order of $n_o = 3$. Fig 4 and 5 show the comparison between the results using the present approach and those from Godin (2013). In particular, we note that the second order approximation of the effective coefficients agrees with the result in Godin (2013), whereas the results using a first order truncation is close to the data reported in Godin (2013). These comparisons assure the use of the obtained short formulas arising from (19) to investigate the complex effective dielectric coefficient.

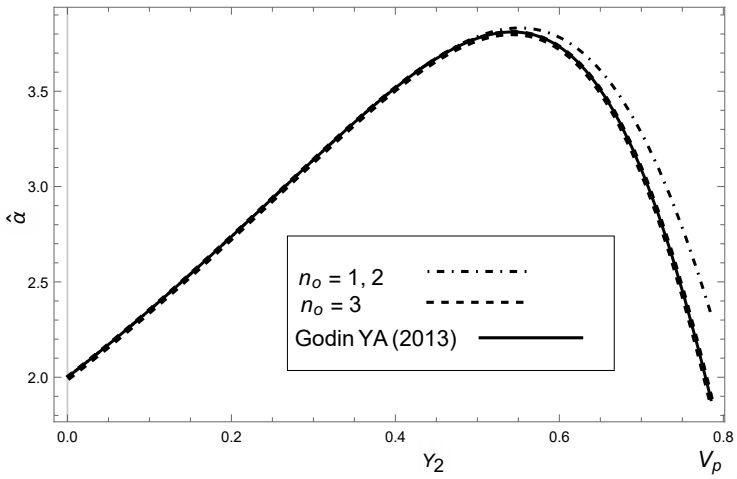

Fig. 4: Comparison of the real part of the complex effective dielectric coefficient $\widehat{\kappa}$ depending on the volume fraction Y_2 calculated using (16a)–(16b) truncated at $n_o = 1, 2, 3$. Also plotted the results from Godin (2013).

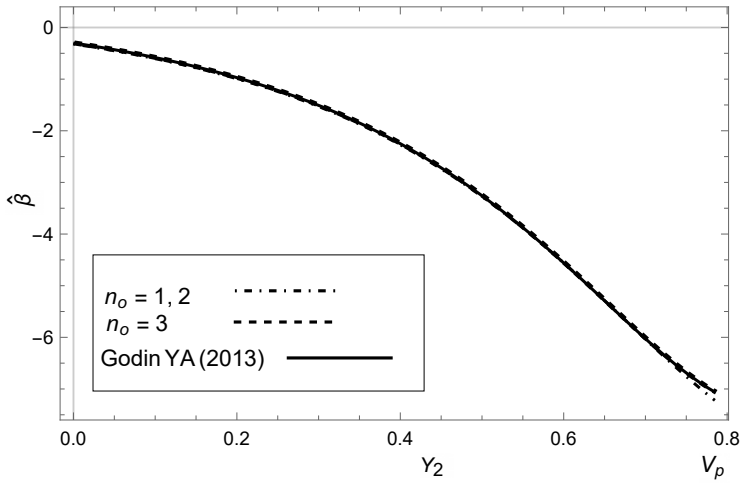

Fig. 5: Comparison of the imaginary part of the complex effective dielectric coefficient $\widehat{\kappa}$ depending on the volume fraction Y_2 calculated using (16a)–(16b) truncated at $n_o = 1, 2, 3$. Also plotted the results from Godin (2013).

6 Concluding Remarks

A system of two equations with real periodic and rapidly oscillating coefficients (2a)–(2d) is studied via asymptotic homogenization for predict the macroscopic behavior of two-phase fibrous dielectric composites wherein the constituents exhibit complex dielectric isotropy. Series expansions of complex potentials with unknown real coefficients (11)–(12) are used to solve the local problems (10a)–(10d) for a hexagonal periodic distribution of the fibers. The unknown coefficients are solutions of an infinity system of linear algebraic equations (14). An explicit solution (19) of the infinite system was derived for any truncation order. Formula (19) is useful in finding closed-forms expressions for the effective coefficients. Therefore, two simple analytical formulas (24a)–(24b) and (25) are specified for the two first truncation order. Numerical examples illustrated a very good concordance of such formulas with those reported in Godin (2013). These results could be useful for acoustic applications wherein hexagonal periodic lattices of acoustic scatterers structures are present Guild et al. (2014). Besides, these formulas can be used for estimating gain and loss enhancement properties of active and passive composites in certain volume fraction intervals as in Bravo-Castillero et al. (2018). Besides it is interesting to mention that results display for either the real part of the effective dielectric coefficient a monotonic behavior and the imaginary part a non-monotonic one, or the opposite. Some examples show gain- or loss-enhancement properties.

Acknowledgements

This work was supported by the project PAPIIT-DGAPA-UNAM IA100919. RRR would like to thank MyM-IIMAS-UNAM and PREI-DGAPA-UNAM for financial support. FJS thanks DGAPA, UNAM for funding. The authors are grateful to Ana Pérez Arteaga and Ramiro Chávez Tovar for technical assistance and ART acknowledges the Dipartimento di Scienze Matematiche (DISMA) “G. L. Lagrange” of the Politecnico di Torino, “Dipartimento di Eccellenza 2018-2022”

Bibliography

J. Bravo-Castillero, A. Ramírez-Torres, F.J. Sabina, C. García-Reimbert, R. Guinovart-Díaz, and R. Rodríguez-Ramos. Analytical formulas for complex permittivity of periodic composites. estimation of gain and loss enhancement in active and passive composites. *Waves in Random and Complex Media*, pages 1–21, 2018. doi: 10.1080/17455030.2018.1546063.

Y.A. Godin. Effective complex permittivity tensor of a periodic array of cylinders. *Journal of Mathematical Physics*, 53(6): 053505, 2012. doi: 10.1063/1.4726213.

Y.A. Godin. Effective complex permittivity tensor of a periodic array of cylinders. *Journal of Mathematical Physics*, 54(5): 053505, 2013. doi: doi: 10.1063/1.4803490.

Y.A. Godin. Effective properties of periodic tubular structures. *The Quarterly Journal of Mechanics and Applied Mathematics*, 69 (2):181–193, 2016. doi: 10.1093/qjmam/hbw003.

Y.A. Godin and B. Vainberg. Dispersive and effective properties of two-dimensional periodic media. *Proceedings of the Royal Society A*, 475(2221):20180298, 2019. doi: 10.1098/rspa.2018.0298.

M.D. Guild, V.M. García-Chocano, W. Kan, and J. Sánchez-Dehesa. Enhanced inertia from lossy effective fluids using multi-scale sonic crystals. *AIP Advances*, 4(12):124302, 2014. doi: 10.1063/1.4901880.

R. Guinovart-Díaz, J. Bravo-Castillero, R. Rodríguez-Ramos, and F. J Sabina. Closed-form expressions for the effective coefficients of fibre-reinforced composite with transversely isotropic constituents. i: Elastic and hexagonal symmetry. *Journal of the Mechanics and Physics of Solids*, 49(7):1445–1462, 2001. doi: 10.1016/S0022-5096(01)00005-9.

L.V. Kantorovich and V.I. Krylov. Approximate methods of higher analysis. *translated by C. D. Benster. XII + 681 S. m. 68 Abb. Groningen, 1958. P. Noordhoff Ltd.*

X. Ren, R. Corcolle, and L. Daniel. A homogenization technique to calculate eddy current losses in soft magnetic composites using a complex magnetic permeability. *IEEE Transactions on Magnetics*, 52(12):1–9, 2016. doi: 10.1109/TMAG.2016.2594048.

DOI: 10.24352/UB.OVGU-2019-021 TECHNISCHE MECHANIK, 39, 2, (2019), 229 – 240
submitted: November 29, 2018

Application of the Classical Beam Theory for Studying Lengthwise Fracture of Functionally Graded Beams

V. Rizov, H. Altenbach

The present paper deals with analysis of lengthwise cracks in linear-elastic functionally graded beam configurations. A general approach for deriving of the strain energy release rate is developed by applying the classical beam theory. A crack located arbitrary along the beam thickness is considered, i.e. the crack arms have different thicknesses. The approach holds for beams which are functionally graded in the thickness direction (the modulus of elasticity can be distributed arbitrary along the thickness of the beam). The approach is applied to analyze the strain energy release rate for a lengthwise crack in a functionally graded cantilever beam. The beam is loaded by one concentrated force applied at the free end of the upper crack arm. An exponential law is used to describe the continuous variation of the modulus of elasticity along the beam thickness. The solution to the strain energy release rate in the cantilever beam is verified by applying the J-integral approach. The solution is verified further by using the compliance method for deriving the strain energy release rate. The effects of crack location along the beam thickness, crack length and material gradient on the strain energy release rate in the functionally graded cantilever beam are analyzed by applying the solution derived.

1 Introduction

The quick development of engineering demands an extensive use of high performance structural materials such as functionally graded materials. The novel inhomogeneous composites known as functionally graded materials are composed of two or more constituent materials. The basic idea of the functionally graded materials is that by allowing a gradual variation of the composition of the constituent materials in one or more spatial directions, the material properties are modified to meet different material performance requirements in different parts of a structural member (Gasik, 2010; Jha *et al*., 2013; Knoppers *et al*., 2003; Mahamood and Akinlabi, 2017; Miyamoto *et al*., 1999; Nemat-Allal *et al*., 2011; Wu *et al*., 2014; Zhang *et al*., 2011). Thus, it is not surprising that application of functionally graded materials as advanced structural materials in the practical engineering has increased significantly for the last three decades.

Understanding the fracture behaviour is very important for the structural applications of functionally graded materials (Carpinteri and Pugno, 2006; Dolgov, 2005; Dolgov, 2016; Erdogan, 1995; Paulino, 2002; Rizov, 2017; Rizov, 2018; Tilbrook *et al*., 2005; Upadhyay and Simha, 2007; Uslu Uysal and Güven, 2016). The presence of cracks drastically reduces the load-bearing capacity of functionally graded structural members and components. Also, the structural integrity and reliability of functionally graded materials and structures essentially depend upon their fracture behaviour. Therefore, development of methods for fracture analyses is vital for evaluation of operational performance of functionally graded engineering structures.

The present paper aim is to develop an approach for analyzing the lengthwise fracture behaviour of functionally graded beams in terms of the strain energy release rate by applying the classical linear-elastic beam theory. Analyses of lengthwise fracture are needed since some functionally graded materials can be built-up layer by layer (Mahamood and Akinlabi, 2017) which is a premise for appearance of lengthwise cracks between layers. It should be mentioned that while the previous publications (Rizov, 2017; Rizov, 2018) are focussed on analyzing the strain energy release rate for lengthwise cracks in individual beam configurations, the present paper develops a general approach for the strain energy release rate. The beams under consideration are functionally graded in the thickness direction (it is assumed that the modulus of elasticity varies continuously along the beam thickness). The general approach developed is applicable for a lengthwise crack located arbitrary along the beam thickness.

Besides, the law that describes the distribution of the modulus of elasticity in the thickness direction is arbitrary. The approach is used to calculate the strain energy release rate for a functionally graded cantilever beam configuration containing a lengthwise crack. The *J*-integral method is applied to verify the solution to the strain energy release rates. The solution is verified also by using the compliance method. Parametric investigations are performed in order to evaluate the effects of various material and geometrical parameters on the lengthwise fracture behaviour.

2 Deriving of the Strain Energy Release Rate

A portion of a functionally graded beam containing a lengthwise crack is shown in Figure 1. The beam has a rectangular cross-section of width, b, and thickness, $2h$. The thicknesses of the lower and upper crack arms are denoted by h_1 and h_2, respectively.

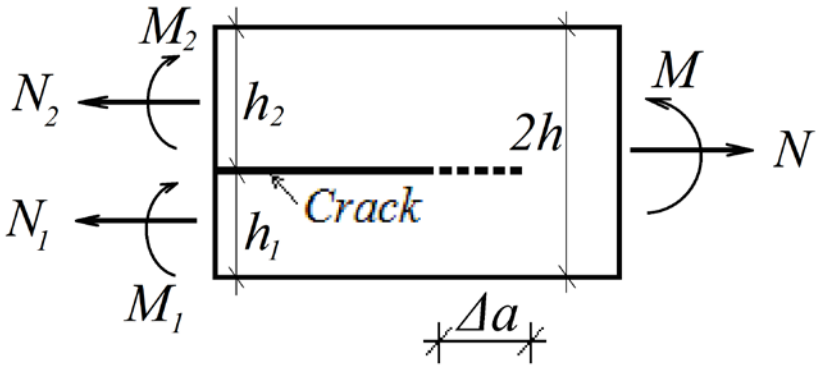

Figure 1. Portion of a functionally graded beam with a lengthwise crack (Δa is a small increase of the crack length, h_1 and h_2 are, respectively, the thicknesses of the lower and upper crack arms).

The bending moment and axial force in the beam cross-section ahead of the crack tip are denoted by M and N, respectively. In order to derive the strain energy release rate, G, a small increase, Δa, of the crack length is assumed. The strain energy release rate is written as

$$G = -\frac{\Delta U}{\Delta A}, \tag{1}$$

where ΔU is the change of the strain energy, ΔA is the increase of crack area. Since

$$\Delta A = b\Delta a, \tag{2}$$

formula (1) is re-written as

$$G = -\frac{\Delta U}{b\Delta a}. \tag{3}$$

The change of the strain energy is expressed as a difference between the strain energy cumulated in the beam portion of length, Δa, before the increase of crack and the strain energy cumulated in the portions of two crack arms of length, Δa, behind the crack tip

$$\Delta U = \Delta a\, b \int_{-h}^{h} u_{03} dz_3 - \Delta a\, b \int_{-\frac{h_1}{2}}^{\frac{h_1}{2}} u_{01} dz_1 - \Delta a\, b \int_{-\frac{h_2}{2}}^{\frac{h_2}{2}} u_{02} dz_2 \ , \tag{4}$$

where u_{01}, u_{02} and u_{03} are, respectively, the strain energy densities in the lower and upper crack arms and the un-cracked beam portion ahead of the crack tip, z_1, z_2 and z_3 are, respectively, the vertical centroidal axes of the cross-sections of lower and upper crack arms and the un-cracked beam portion. By combining of (3) and (4), one arrives at the following expression for the strain energy release rate:

$$G = \int_{-\frac{h_1}{2}}^{\frac{h_1}{2}} u_{01} dz_1 + \int_{-\frac{h_2}{2}}^{\frac{h_2}{2}} u_{02} dz_2 - \int_{-h}^{h} u_{03} dz_3 \ . \tag{5}$$

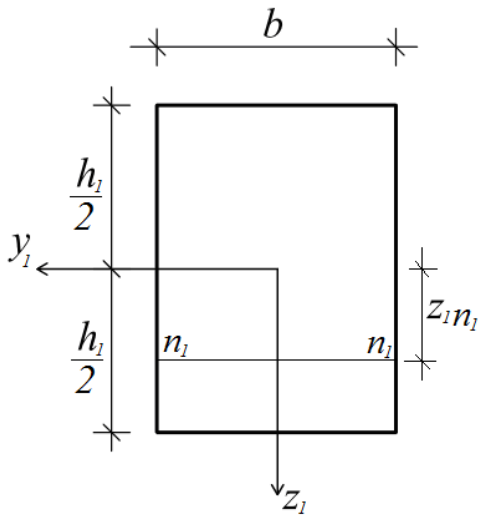

Figure 2. Cross-section of the lower crack arm ($n_1 - n_1$ is the position of the neutral axis).

The strain energy density in the cross-section of lower crack arm behind the crack tip is written as

$$u_{01} = \frac{1}{2}\sigma\varepsilon \,, \tag{6}$$

where σ is the normal stress, ε is the lengthwise strain. The normal stress is obtained by applying the Hooke's law

$$\sigma = E\varepsilon \,, \tag{7}$$

where the modulus of elasticity, E, is distributed continuously in the thickness direction

$$E = E\left(z_1\right). \tag{8}$$

Beams of high length to thickness ratio are considered in the present paper. Therefore, according to the Bernoulli's hypothesis for plane sections the lengthwise strain is distributed linearly along the thickness of the lower crack arm

$$\varepsilon = \kappa_1\left(z_1 - z_{1n_1}\right), \tag{9}$$

where κ_1 is the curvature of the lower crack arm, z_{1n_1} is the coordinate of the neutral axis (Figure 2). It should be mentioned that the neutral axis shifts from the centroid since the material is functionally graded in the thickness direction and, also, the beam is under combination of axial force and bending moment.

The curvature and the coordinate of the neutral axis of the lower crack arm are determined from the following equations for equilibrium of the cross-section:

$$N_1 = b\int_{-\frac{h_1}{2}}^{\frac{h_1}{2}} \sigma \, dz_1 , \tag{10}$$

$$M_1 = b\int_{-\frac{h_1}{2}}^{\frac{h_1}{2}} \sigma \, z_1 dz_1 , \tag{11}$$

where N_1 and M_1 are, respectively, the axial force and the bending moment in the cross-section of the lower crack arm behind the crack tip. In equations (10) and (11), σ is determined by the Hooke's law (7). Equations obtained after solving the integrals in (10) and (11) for a particular law for distribution of the modulus of elasticity along the beam thickness should be solved with respect to the curvature and the coordinate of the neutral axis.

By substituting of (7), (8) and (9) in (6), one obtains the following expression for the strain energy density in the lower crack arm:

$$u_{01} = \frac{1}{2} E\left(z_1\right)\left[\kappa_1\left(z_1 - z_{1n_1}\right)\right]^2 . \tag{12}$$

Formula (12) is applied also to calculate the strain energy density in the cross-section of the upper crack arm behind the crack tip. For this purpose, z_1 , κ_1 and z_{1n_1} are replaced, respectively, with z_2 , κ_2 and z_{2n_2} where κ_2 and z_{2n_2} are the curvature of the upper crack arm and the coordinate of neutral axis of the upper crack arm. Equilibrium equations (10) and (11) are used to determine z_{2n_2} and κ_2 . For this purpose, N_1 , M_1 , σ , $h_1/2$ and z_1 are replaced, respectively, with N_2 , M_2 , σ_g , $h_2/2$ and z_2 where N_2 and M_2 are the axial force and the bending moment in the cross-section of the upper crack arm behind the crack tip, σ_g is the normal stress in the upper crack arm. The Hooke's law (7) is applied to determine σ_g (the lengthwise strain is obtained by replacing of z_1 , κ_1 and z_{1n_1} with z_2 , κ_2 and z_{2n_2} in formula (9)).

Formula (12) is used also to determine the strain energy density in the beam cross-section ahead of the crack tip by replacing of z_1 , κ_1 and z_{1n_1} , respectively, with z_3 , κ_3 and z_{3n_3} . The curvature, κ_3 , and the coordinate of the neutral axis, z_{3n_3} , of the beam cross-section ahead of the crack tip are obtained after replacing of N_1 , M_1 , σ , $h_1/2$ and z_1 , respectively, with N , M , σ_r , h and z_3 in equilibrium equations (10) and (11). The normal stress, σ_r , in the beam cross-section ahead of the crack tip is found by (7). The distribution of lengthwise strain is determined by (9). For this purpose, z_1 , κ_1 and z_{1n_1} are replaced with z_3 , κ_3 and z_{3n_3} , respectively.

Finally, the strain energy densities in the two crack arms and in the beam cross-section ahead of the crack front are substituted in formula (5) to calculate the strain energy release rate. It should be noted that (5) is applicable for various functionally graded beam configurations, loading conditions and laws for distribution of the modulus of elasticity along the beam thickness. Besides, the lengthwise crack can be located arbitrary along the beam thickness.

3 Numerical Example

This section of the paper presents numerical results obtained by investigating the lengthwise fracture behaviour of a functionally graded cantilever beam configuration by applying the approach for analysis of the strain energy release rate developed in section 2.

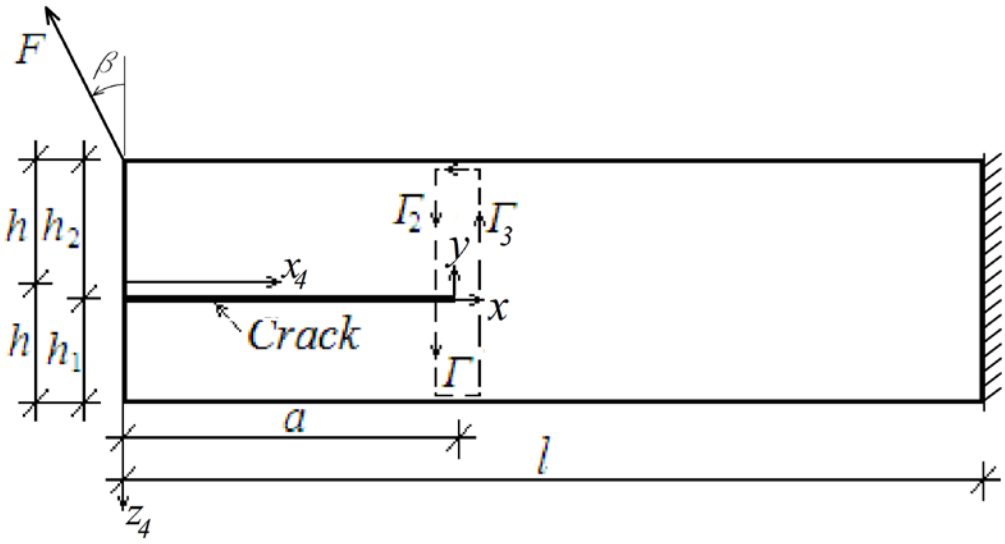

Figure 3. Functionally graded cantilever beam with a lengthwise crack of length, a.

The cantilever beam configuration shown in Figure 3 is considered. A lengthwise crack of length, a, is located arbitrary along the beam thickness. Thus, the two crack arms have different thicknesses denoted by h_1 and h_2. The length of beam is l. The cross-section of beam is a rectangle of width, b, and thickness, $2h$. The beam is clamped in its right-hand end. The beam is loaded by one concentrated force, F, applied at the free end of the upper crack arm (the angle of orientation of F is denoted by β). The lower crack arm is free of stresses. Thus,

$$u_{01} = 0. \tag{13}$$

It is assumed that the modulus of elasticity is distributed continuously along the beam thickness according to the following exponential law:

$$E(z_4) = E_0 e^{s\frac{h+z_4}{2h}}, \tag{14}$$

where

$$-h \le z_4 \le h. \tag{15}$$

Axis, z_4, is shown in Figure 3. In (14), E_0 is the value of modulus of elasticity in the upper surface of the beam, s is a material property that controls the material gradient along the beam thickness.

The fracture behaviour is analyzed in terms of the strain energy release rate by using formula (5). The strain energy density in the cross-section of the upper crack arm behind the crack tip is obtained by applying (12). Equations (10) and (11) are used to determine the curvature and the coordinate of the neutral axis. In order to carry-out the integration in (10) and (11), the modulus of elasticity has to be presented as a function of z_2. For this purpose, (14) is re-written as

$$E(z_2) = E_0 e^{s\frac{z_2+\frac{h_2}{2}}{2h}}, \tag{16}$$

where

$$-h_2/2 \le z_2 \le h_2/2. \tag{17}$$

After replacing of N_1, M_1, σ, $h_1/2$ and z_1 with N_2, M_2, σ_g, $h_2/2$ and z_2, and substituting of (7), (9) and (16) in (10) and (11), one derives the following equations:

$$N_2 = bE_0\kappa_2 e^{\eta}\left\{\frac{1}{\theta^2}\left[e^{\theta\frac{h_2}{2}}\left(\theta\frac{h_2}{2}-1\right)+e^{-\theta\frac{h_2}{2}}\left(\theta\frac{h_2}{2}+1\right)\right]-\frac{z_{2n_2}}{\theta}\left(e^{\theta\frac{h_2}{2}}-e^{-\theta\frac{h_2}{2}}\right)\right\}, \tag{18}$$

$$M_2 = bE_0\kappa_2 e^{\eta}\left\{\frac{1}{\theta^3}\left[e^{\theta\frac{h_2}{2}}\left(\theta^2\frac{h_2^2}{4}-\theta h_2+2\right)-e^{-\theta\frac{h_2}{2}}\left(\theta^2\frac{h_2^2}{4}+\theta h_2+2\right)\right]-\right.$$
$$\left.-\frac{z_{2n_2}}{\theta^2}\left[e^{\theta\frac{h_2}{2}}\left(\theta\frac{h_2}{2}-1\right)+e^{-\theta\frac{h_2}{2}}\left(\theta\frac{h_2}{2}+1\right)\right]\right\}, \tag{19}$$

where $\theta = s/(2h)$, $\eta = sh_2/(4h)$. It follows from Figure 3 that

$$N_2 = F\sin\beta, \tag{20}$$

$$M_2 = Fa\cos\beta - F\frac{h_2}{2}\sin\beta. \tag{21}$$

Equations (18) and (19) are solved with respect to κ_2 and z_{2n_2} by using the MatLab computer program. Then the strain energy density in the upper crack arm is obtained by substituting of (16), z_2, κ_2 and z_{2n_2} in (12).

Equations (18) and (19) are used also to determine κ_3 and z_{3n_3}. For this purpose, M_2, κ_2, h_2 and z_{2n_2} are replaced, respectively, with M_3, κ_3, $2h$ and z_{3n_3} where $M_3 = Fa\cos\beta - Fh\sin\beta$, and then equations (18) and (19) are solved with respect to κ_3 and z_{3n_3}. The strain energy density in the un-cracked beam portion is obtained by substituting of (14), z_3, κ_3 and z_{3n_3} in (12).

By substituting of u_{01}, u_{02} and u_{03} in (5), one derives the following expression for the strain energy release rate in the functionally graded cantilever beam configuration (Figure 3):

$$G = \frac{1}{2}E_0\kappa_2^2 e^{\eta}\left\{\frac{1}{\theta^3}\left[e^{\theta\frac{h_2}{2}}\left(\theta^2\frac{h_2^2}{4}-\theta h_2+2\right)-e^{-\theta\frac{h_2}{2}}\left(\theta^2\frac{h_2^2}{4}+\theta h_2+2\right)\right]-\right.$$

$$-\frac{2z_{2n_2}}{\theta^2}\left[e^{\theta\frac{h_2}{2}}\left(\theta\frac{h_2}{2}-1\right)+e^{-\theta\frac{h_2}{2}}\left(\theta\frac{h_2}{2}+1\right)\right]+\frac{z_{2n_2}^2}{\theta}\left(e^{\theta\frac{h_{22}}{2}}-e^{-\theta\frac{h_2}{2}}\right)\Bigg\}-$$

$$-\frac{1}{2}E_0\kappa_3^2e^{\eta_1}\Bigg\{\frac{1}{\theta^3}\left[e^{\theta h}\left(\theta^2h^2-2\theta h+2\right)-e^{-\theta h}\left(\theta^2h^2+2\theta h+2\right)\right]-$$

$$-\frac{2z_{3n_3}}{\theta^2}\left[e^{\theta h}\left(\theta h-1\right)+e^{-\theta h}\left(\theta h+1\right)\right]+\frac{z_{3n_3}^2}{\theta}\left(e^{\theta h}-e^{-\theta h}\right)\Bigg\}, \tag{22}$$

where $\eta_1 = s/2$.

The solution to the strain energy release rate (22) is verified by applying the *J*-integral method (Broek, 1986). The *J*-integral is solved along the integration contour, Γ, shown in Figure 3. The *J*-integral solution is written as

$$J = J_{\Gamma_2} + J_{\Gamma_3}, \tag{23}$$

where J_{Γ_2} and J_{Γ_3} are, respectively, the *J*-integral values in segments, Γ_2 and Γ_3, of the integration contour (Γ_2 and Γ_3 coincide with cross-sections of the upper crack arm and the un-cracked beam portion, respectively).

The *J*-integral in segment, Γ_2, is written as

$$J_{\Gamma_2} = \int_{\Gamma_2}\left[u_{02}\cos\alpha_{\Gamma_2} - \left(p_{x_{\Gamma_2}}\frac{\partial u}{\partial x} + p_{y_{\Gamma_2}}\frac{\partial v}{\partial x}\right)\right]ds_{\Gamma_2}, \tag{24}$$

where α_{Γ_2} is the angle between the outwards normal vector to the contour of integration in segment, Γ_2, and the crack direction, $p_{x_{\Gamma_2}}$ and $p_{y_{\Gamma_2}}$ are the components of the stress vector, *u* and *v* are the components of the displacement vector with respect to the coordinate system *xy*, and ds_{Γ_2} is a differential element along the contour of integration. The components of (24) are written as

$$p_{x_{\Gamma_2}} = -\sigma_g = -E\varepsilon_g, \tag{25}$$

$$p_{y_{\Gamma_2}} = 0, \tag{26}$$

$$ds_{\Gamma_2} = dz_2 , \tag{27}$$

$$\frac{\partial u}{\partial x} = \varepsilon_g , \tag{28}$$

$$\cos\alpha_{\Gamma_2} = -1. \tag{29}$$

In (25) and (28), the longitudinal strain, ε_g, is determined by replacing of z_1 , κ_1 and z_{1n_1} with z_2 , κ_2 and z_{2n_2} in formula (9) where the coordinate, z_2, varies in the interval $[-h_2/2; h_2/2]$.

By substituting of u_{02}, (25) – (29) in (24), one derives

$$J_{\Gamma_2}=\frac{1}{2}E_0\kappa_2^2e^{\eta}\left\{\ \frac{1}{\theta^3}\left[e^{\theta\frac{h_2}{2}}\left(\theta^2\frac{h_2^2}{4}-\theta h_2+2\right)-e^{-\theta\frac{h_2}{2}}\left(\theta^2\frac{h_2^2}{4}+\theta h_2+2\right)\right]-\right.$$
$$\left.-\frac{2z_{2n_2}}{\theta^2}\left[e^{\theta\frac{h_2}{2}}\left(\theta\frac{h_2}{2}-1\right)+e^{-\theta\frac{h_2}{2}}\left(\theta\frac{h_2}{2}+1\right)\right]+\frac{z_{2n_2}^2}{\theta}\left(e^{\theta\frac{h_{22}}{2}}-e^{-\theta\frac{h_2}{2}}\right)\ \right\}. \tag{30}$$

The solution of the *J*-integral in segment, Γ_3, of the integration contour (Figure 3) is obtained also by (30). For this purpose, h_2 , κ_2 , η and z_{2n_2} are replaced with $2h$, κ_3 , η_1 and z_{3n_3} , respectively. Also, the sign of (30) is set to „minus" because the integration contour is directed upwards in segment, Γ_3.

It should be noted that the *J*-integral solution obtained by substituting of J_{Γ_2} and J_{Γ_3} in (23) is exact match of the solution to the strain energy release rate (22). This fact is a verification of the analysis developed in the present paper.

The solution to the strain energy release rate (22) is verified further by applying the compliance method. According to this method, the strain energy release rate is expressed as

$$G=\frac{F^2}{2b}\frac{dC}{da}, \tag{31}$$

where C is the compliance. For the cantilever beam configuration shown in Figure 3 the compliance is written as

$$C=\frac{w}{F}, \tag{32}$$

where w is the projection of the displacement of the application point of the force, F , on the direction of F . By applying the integrals of Maxwell-Mohr, w is obtained as

$$w=\int_0^a\left(x_4\cos\beta-\frac{h_1}{2}\sin\beta\ \right)\kappa_2(x_4)dx_4+\int_a^l\left(x_4\cos\beta-h\sin\beta\ \right)\kappa_3(x_4)dx_4, \tag{33}$$

where the lengthwise axis, x_4 , is shown in Figure 3. By substituting of (32) and (33) in (31), one derives

$$G=\frac{F}{2b}\left[\left(a\cos\beta-\frac{h_2}{2}\sin\beta\ \right)\kappa_2(a)-\left(a\cos\beta-h\sin\beta\ \right)\kappa_3(a)\right], \tag{34}$$

where κ_2 and κ_3 are determined from equations (18) and (19).

The strain energy release rates obtained by (34) are exact matches of these calculated by (22) which is a conformation for the correctness of the present analysis.

Influence of different factors such as the crack location along the beam thickness, orientatrion of F , material gradient and crack length on the lengthwise fracture behaviour of the functionally graded cantilever beam is evaluated. For this purpose, calculations of the strain energy release rate are performed by applying solution (22). The strain energy release rates obtained are presented in non-dimensional form by using the formula $G_N=G/(E_0b)$. The calculations are carried-out assuming that $F=10$ N, $b=0.005$ m and $l=0.100$ m.

The inluence of the orientation of F on the fracture is investigated. For this purpose, the strain energy release rate is calculated assuming that $0^o \le \beta \le 90^o$. The strain energy release rate is plotted in non-dimensional form against β in Figure 4 at three $2h/b$ ratios. Figure 4 shows that the strain energy release rate decreases with increasing of β. The increase of $2h/b$ ratio leads also to decrease of the strain energy release rate (Figure 4).

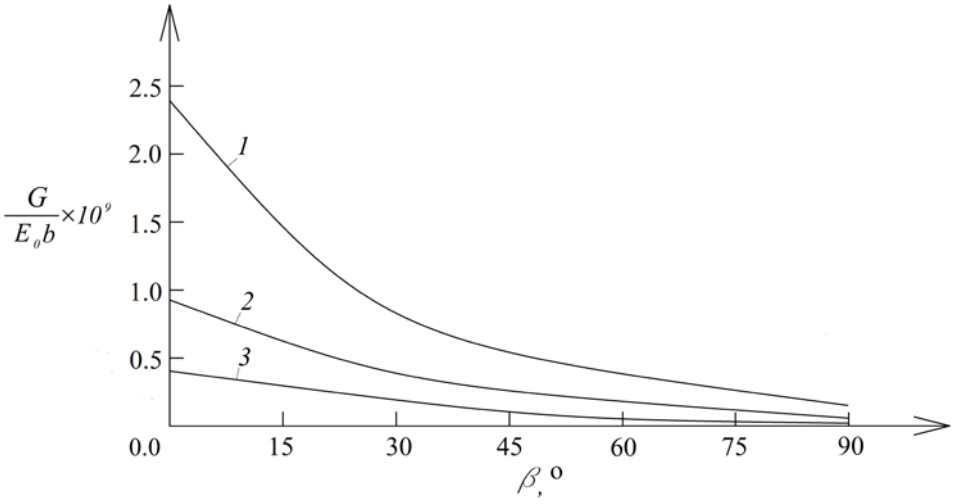

Figure 4. The strain energy release rate in non-dimensional form plotted against β (curve 1 - at $2h/b = 0.6$, curve 2 - at $2h/b = 0.8$ and curve 3 - at $2h/b = 1.0$).

The effects of the crack location along the beam thickness and the crack length on the fracture behaviour are analyzed.

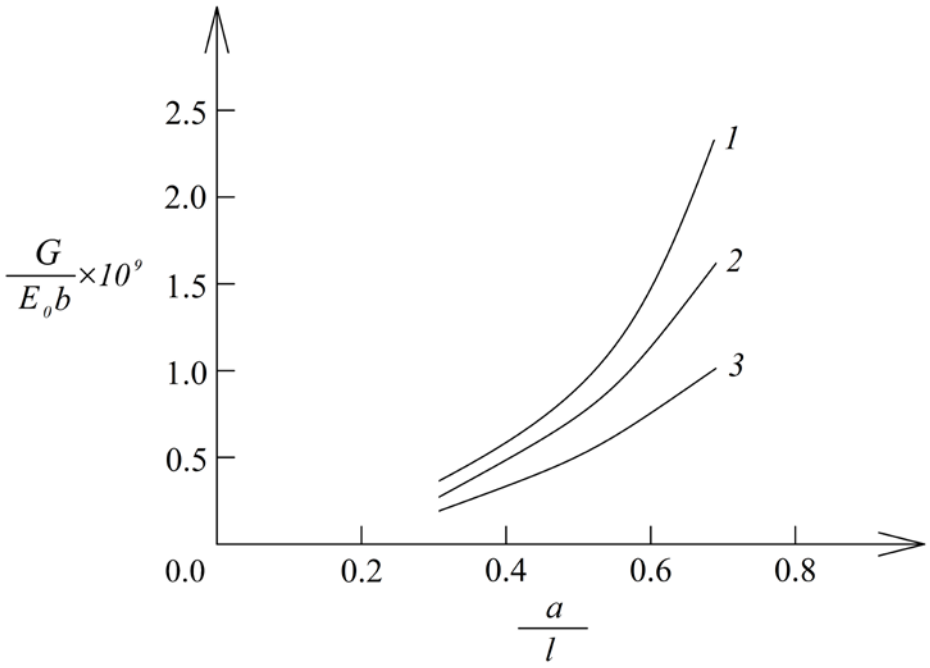

Figure 5. The strain energy release rate in non-dimensional form plotted against a/l ratio (curve 1 - at $h_2/2h = 0.3$, curve 2 - at $h_2/2h = 0.5$ and curve 3 - at $h_2/2h = 0.7$).

The crack location along the beam thickness is characterized by $h_2/2h$ ratio. The ratio, a/l, characterizes the crack length. The strain energy release rate is calculated at three $h_2/2h$ ratios for various a/l ratios. The effects of crack location and the crack thickness on the lengthwise fracture are illustrated in Figure 5 where the

strain energy release rate in non-dimensional form is plotted against a/l ratio at three $h_2/2h$ ratios for $s=0.2$ and $\beta=0$. The curves in Figure 5 indicate that the strain energy release rate increases with increasing of a/l ratio. Concerning the effect of crack location along the beam thickness, Figure 5 shows that the strain energy release rate decreases with increasing $h_2/2h$ ratio (this behaviour is due to the increase of the stiffness of the upper crack arm with increasing of $h_2/2h$ ratio).

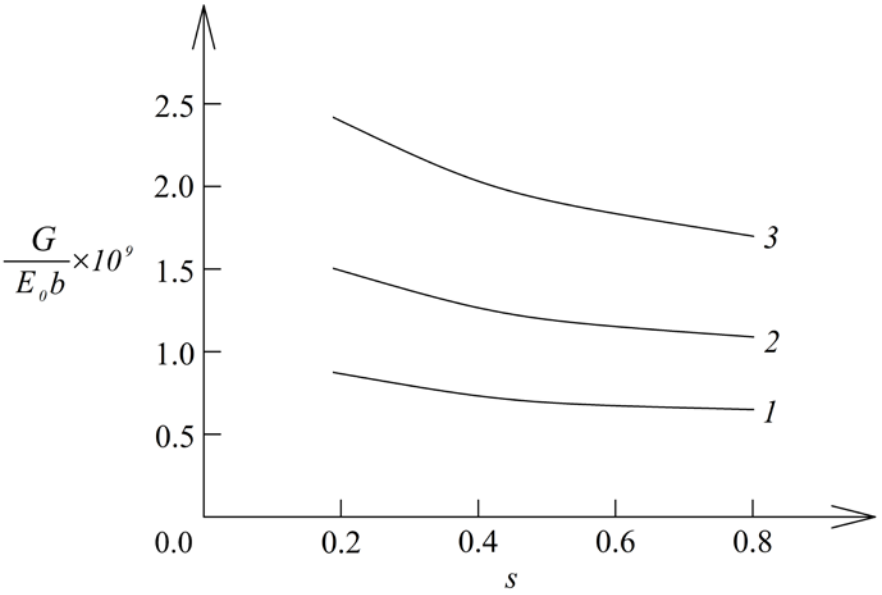

Figure 6. The strain energy release rate in non-dimensional form plotted against s (curve 1 - at $F=6$ N, curve 2 - at $F=8$ N and curve 3 - at $F=10$ N).

The effect of the material gradient along the beam thickness on the fracture is analyzed too. The material gradient is characterized by the parameter, s.

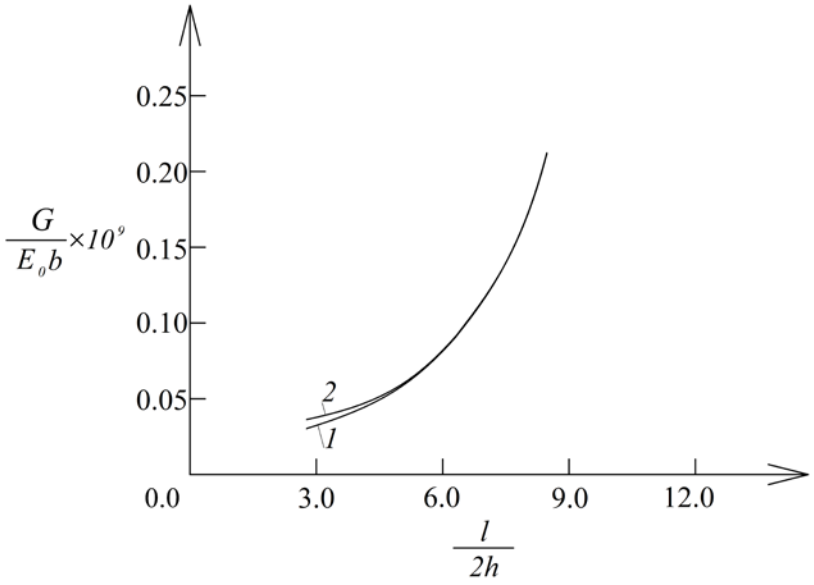

Figure 7. The strain energy release rate in non-dimensional form plotted against $l/2h$ ratio (curve 1 – by applying the classical beam theory, curve 2 – by applying the asymptotically exact beam theory).

The strain energy release rate is calculated at various s for three values of the external force, F. Figure 6 shows the strain energy release rate plotted in non-dimensional form against s at three values of F for

$h_2 / 2h = 0.3$. One can observe in Figure 6 that the strain energy release rate decreases with increasing of s. This behaviour is attributed to the increase of the beam stiffness. The increase of the external force leads also to increase of the strain energy release rate (Figure 6).

The strain energy release rate is calculated also by applying the asymptotically exact beam theory (Le, 2017) and the results obtained are compared with the strain energy release rate derived by solution (22) that is based on the classical beam theory which uses the Bernoulli's hypothesis. The functionally graded linear-elastic cantilever beam configuration shown in Figure 3 is considered. In order to evaluate the effects of the length to thickness ratio of the beam on the lengthwise fracture behaviour, the strain energy release rate calculated by formula (22) and the exact asymptotic beam theory is plotted in non-dimensional form against $l / 2h$ ratio in Figure 7. The curves in Figure 7 indicate that the strain energy release rate increases with increasing of $l / 2h$ ratio. Also, it is evident from Figure 7 that the strain energy release rate derived by using the classical beam theory is in a very good agreement with the results obtained by applying the asymptotically exact beam theory at $l / 2h \geq 5$.

4 Conclusions

A lengthwise fracture in functionally graded beams is analyzed in terms of the strain energy release rate. The beams under consideration are functionally graded in the thickness direction (the modulus of elasticity varies continuously along the beam thickness). It is assumed that the material has linear-elastic behaviour. A general approach for analysis of the strain energy release rate is developed by applying the classical linear-elastic beam theory. The approach is applicable for a crack that is located arbitrary along the beam thickness (the two crack arms have different thicknesses). Thus, the approach can be used to investigate the effect of the crack location on the strain energy release rate for lengthwise cracks in functionally graded beam configurations. Also, the approach is applicable for arbitrary distribution of the modulus of elasticity in the thickness direction of the beam. The strain energy release rate for a lengthwise crack in a functionally graded cantilever beam is analyzed by using the general approach. The cantilever beam is loaded by one force applied at the free end of the upper crack arm. The crack is located arbitrary along the beam thickness. The continuous variation of the modulus of elasticity along the beam thickness is described by applying an exponential law. The *J*-integral approach is used to verify the solution to the strain energy release rate in the cantilever beam. A further check of the solution is carried-out by applying the compliance method. The influence of the crack location along the beam thickness, the orientation of F, the crack length and the material gradient on the strain energy release rate in the cantilever beam is analyzed by using the solution. The calculations show that the strain energy release rate decreaeses with increasing of β. The increase of $2h/b$ ratio leads also to decrease of the strain energy release rate. The analysis reveals that the strain energy release rate decreases with increasing the thickness of the upper crack arm. It is found that increase of the crack length leads to increase of the strain energy release rate. The material gradient in the thickness direction is characterized by the parameter, s. The investigation shows that the strain energy release rate decreases with increasing of s.

Acknowledgments

Rizov gratefully acknowledges the financial support by DAAD for his research stay in Department of Technical Mechanics, Institute of Mechanics, Otto-von-Guericke-University, Magdeburg, Germany.

References

Broek, D.: *Elementary engineering fracture mechanics*. Springer (1986).

Carpinteri, A.; Pugno, N.: Cracks in re-entrant corners in functionally graded materials. *Engineering Fracture Mechanics*, 73, (2006), 1279-1291.

Dolgov, N.A.: Determination of Stresses in a Two-Layer Coating. *Strength of Materials* 37, (2005), 422-431.

Dolgov, N.A.: Analytical Methods to Determine the Stress State in the Substrate–Coating System Under Mechanical Loads. *Strength of Materials* 48, (2016), 658-667.

Erdogan, F.: Fracture mechanics of functionally graded materials. *Comp. Eng.*, 5, (1995), 753-770.

Gasik, M.M.: Functionally graded materials: bulk processing techniques. *International Journal of Materials and Product Technology*, 39, (2010), 20-29.

Jha, D.K.; Kant, T.; Singh, R.K.: A critical review of recent research on functionally graded plates. *Compos. Struct*., 96, (2013), 833–849.

Knoppers, J.W.; Gunnink, J.; den Hout, Van; Van Vliet, W.: *The reality of functionally graded material products*, *TNO Science and Industry*, The Netherlands (2003), 38–43.

Le, K.C.: An asymptotically exact theory of functionally graded piezoelectric shells. *Int. J. Eng. Sci*., 112C, (2017), 42-62.

Mahamood, R.M.; Akinlabi, E.T.: *Functionally Graded Materials*. Springer (2017).

Miyamoto, Y.; Kaysser, W.A.; Rabin, B.H.; Kawasaki, A.; Ford, R.G.: *Functionally Graded Materials: Design, Processing and Applications*. Kluwer Academic Publishers, Dordrecht/London/Boston (1999).

Nemat-Allal, M.M.; Ata, M.H.; Bayoumi, M.R,; Khair-Eldeen, W.: Powder metallurgical fabrication and microstructural investigations of Aluminum/Steel functionally graded material. *Materials Sciences and Applications*, 2, (2011), 1708-1718.

Paulino, G.C.: Fracture in functionally graded materials. *Engng. Fract. Mech*., 69, (2002), 1519-1530.

Rizov, V.: Lengthwise Fracture of Two-Dimensional Functionally Graded Non-Linear Elastic Beam. *Technische Mechanik*, 37, (2017), 48-61.

Rizov, V.: Multilayered Functionally Graded Non-linear Elastic Beams with Logarithmic Material Gradient: A Delamination Analysis. *Technische Mechanik*, 38, (2018), 203-219.

Tilbrook, M.T.; Moon, R.J.; Hoffman, M.: Crack propagation in graded composites. *Composite Science and Technology*, 65, (2005), 201-220.

Upadhyay, A.K.; Simha, K.R.Y.: Equivalent homogeneous variable depth beams for cracked FGM beams; compliance approach. *Int. J. Fract*., 144, (2007), 209-213.

Uslu Uysal, M.; Kremzer, M.: Buckling Behaviour of Short Cylindrical Functionally Gradient Polymeric Materials. *Acta Physica Polonica* A, 127, (2015), 1355-1357, DOI:10.12693/APhysPolA.127.1355.

Uslu Uysal, M.: Buckling behaviours of functionally graded polymeric thin-walled hemispherical shells. *Steel and Composite Structures, An International Journal*, 21, (2016), 849-862.

Uslu Uysal, M.; Güven, U.: A Bonded Plate Having Orthotropic Inclusion in Adhesive Layer under In-Plane Shear Loading. *The Journal of Adhesion*, 92, (2016), 214-235, DOI:10.1080/00218464.2015.1019064.

Wu, X.L., Jiang, P., Chen, L., Zhang, J.F., Yuan, F.P., Zhu, Y.T.: Synergetic strengthening by gradient structure. *Mater. Res. Lett*., 2, 185–191 (2014).

Zhang, Y.; Sun, M.J.; Zhang, D.: Designing functionally graded materials with superior load-bearing properties. *Acta Biomater*, 8, (2011), 1101–1108.

Addresses: Prof. Dr. Victor Rizov, Department of Technical Mechanics, University of Architecture, Civil Engineering and Geodesy, 1 Chr. Smirnensky blvd., 1046 – Sofia, Bulgaria, email: V_RIZOV_FHE@UACG.BG
Prof. Dr.-Ing. habil. Dr.h.c.mult. Holm Altenbach, Lehrstuhl für Technische Mechanik und Geschäftsführender Leiter Institut für Mechanik G10/58, Fakultät für Maschinenbau, Otto-von-Guericke-Universität Magdeburg, Universitätsplatz 2, 39106 Magdeburg, Deutschland, email: holm.altenbach@ovgu.de

TECHNISCHE MECHANIK

Scientific Journal for Fundamentals and Applications of Engineering Mechanics
Wissenschaftliche Zeitschrift für Grundlagen und Anwendungen der Technischen Mechanik

Instructions for Authors

TECHNISCHE MECHANIK publishes articles in all fields of mechanics, theoretical as well as applied, including related disciplines, and in particular also articles demonstrating practical applications. The journal publishes full length papers, as well as discussions on papers which have appeared in the journal.
TECHNISCHE MECHANIK is a non-profit (open-access) journal, founded by the Otto-von-Guericke-University. It can be freely downloaded from the website.

Manuscripts have to be written with LaTeX. The most important features of the style guidelines are implemented in the files contained in **tm-article.zip** (download from http://www.ovgu.de/techmech/).

Each submitted paper runs through a standard peer review process. Please suggest three international well known reviewers for your paper when you submit it.

Please submit your paper in electronic form by email.

Hinweise für Autoren

Die Zeitschrift TECHNISCHE MECHANIK veröffentlicht Forschungsarbeiten aus dem Gesamtgebiet der Mechanik, d. h. allen Zweigen der theoretischen und angewandten Mechanik einschließlich angrenzender Fachgebiete sowie Diskussionsbeiträge zu in dieser Zeitschrift erschienenen Arbeiten. Die Zeitschrift ist ein open-access Journal das 1980 von der Otto-von-Guericke-Universität gegründet wurde. Alle Artikel können kostenfrei von unserer Webseite herunter geladen werden.

Artikel werden ausschließlich in englischer Sprache veröffentlicht.

Die Manuskripte müssen in LaTeX geschrieben werden. Die wichtigsten Stil-Richtlinien sind in den Dateien umgesetzt, die in **tm-article.zip** (bereit gestellt unter http://www.ovgu.de/techmech/) enthalten sind.

Jeder eingereichte Beitrag durchläuft einen standardmäßigen Begutachtungsprozess. Bitte schlagen Sie bei Einreichung des Artikels drei mögliche, international renommierte Gutachter vor.

Bitte reichen Sie Ihren Beitrag elektronisch per E-Mail ein.

Internetadresse / website	http://www.ovgu.de/techmech
E-Mail / email	Technische.Mechanik@ovgu.de

Address of the editor:
Institut für Mechanik
Otto-von-Guericke-Universität
Postfach 4120

D-39016 Magdeburg

Tel.: +49-391-67-52459
Sekretariat -58608
Fax: +49-391-67-12439
-12863
e-mail: Technische.Mechanik@ovgu.de
http://www.ovgu.de/techmech/

Inhalt / Contents

ISSN 0232-3869 (print)
ISSN 2199-9244 (online)